NEURAL MECHANISMS OF TEMPERATURE COMPENSATION IN AN INSECT AUDITORY SYSTEM

DISSERTATION

zur Erlangung des akademischen Grades
Doctor rerum naturalium (Dr. rer. nat.)
im Fach Biophysik

eingereicht an der
Lebenswissenschaftlichen Fakultät
der Humboldt-Universität zu Berlin

von

Dipl.-Phys. Frederic Alexander Römschied

Präsidentin der Humboldt-Universität zu Berlin
Prof. Dr.-Ing. Dr. Sabine Kunst

Dekan der Lebenswissenschaftlichen Fakultät
Prof. Dr. Richard Lucius

Gutachter/-innen: 1. Prof. Dr. Susanne Schreiber
2. Prof. Dr. Bernhard Ronacher
3. Prof. Dr. Jan Benda

Eingereicht am 1. Juli 2016
Tag der mündlichen Prüfung: 23. September 2016

Zusammenfassung

Das menschliche Gehirn funktioniert weitgehend zuverlässig – egal ob man im Schneegestöber nach einer schützenden Unterkunft sucht oder im Hochsommer einen Marathon läuft. Der Grund hierfür liegt im Erhalt einer nahezu konstanten Körpertemperatur, der für den menschlichen Organismus einen hohen Energieaufwand darstellt. Dadurch verliert die Temperaturabhängigkeit chemischer Prozesse auf mikroskopischer Ebene für den Menschen an Bedeutung – im Gegensatz zu allen wechselwarmen Lebewesen, deren Körpertemperatur sich der Umgebungstemperatur umgehend anpasst. Dass lebenswichtige Körper- und Gehirnfunktionen vieler Wechselwarmer dennoch über einen breiten Temperaturbereich funktionieren, legt nahe, dass sich diese Tiere Mechanismen zu Nutze machen, die die Temperaturabhängigkeit auf mikroskopischer Ebene ausgleichen.

Die vorliegende Arbeit beschreibt Möglichkeiten der so genannten *Temperaturkompensation* am Beispiel des Hörsystems der Heuschrecke. Für einige Heuschreckenarten ermöglicht das Hörsystem die Lokalisierung und Identifizierung möglicher Partner anhand von Werbegesang, auch bei schlechten Sichtverhältnissen in hoher Vegetation. Insbesondere funktioniert die akustische Kommunikation über eine Temperaturspanne von bis zu 15°C.

Diese Doktorarbeit erklärt zum einen, wie einzelne Nervenzellen mit temperaturabhängigen Ionenkanälen eine temperaturkompensierte Stimulusrepräsentation erzeugen können. Weiterhin wird gezeigt, dass der zugrundeliegende zell-intrinsische Kompensationsmechanismus nicht den neuronalen Energieverbrauch beeinträchtigen muss. Zum anderen wird belegt, dass die Schallverarbeitung auf höheren Verarbeitungsstufen selbst *nicht* temperaturkompensiert ist. Anhand mathematischer und computergestützter Modelle wird erläutert wie dennoch mit der gemessenen Temperaturabhängigkeit der neuronalen Verarbeitung temperaturkompensierte Gesangserkennung ermöglicht wird.

Die vorgeschlagenen Mechanismen können auf alle wechselwarmen Organismen verallgemeinert werden.

Abstract

The human brain largely remains functional regardless of whether one is searching for the shortest path to a warming shelter in a snowstorm or running a marathon on a summer's day. This robustness of brain functionality can be attributed to the maintenance of a constant body temperature, which requires a large investment of energy. Due to homeothermy, the temperature dependence of all chemical reactions, including those inside the body, loses relevance as a constraint for humans. For poikilotherms, in contrast, a rise in ambient temperature translates to an increase in body temperature, which speeds up all chemical processes. Yet, many poikilotherms exhibit robustness of vital behaviors across a broad range of temperatures, which suggests the existence of mechanisms that compensate for temperature dependencies at the microscopic level.

The present thesis proposes mechanisms for such *temperature compensation*, using the auditory system of the grasshopper as a model system. For various grasshopper species, the auditory system facilitates localization and recognition of conspecifics under conditions of low visibility. In particular, communication and recognition remain functional across a temperature range of up to 15°C.

Here, we show on the one hand how single nerve cells with temperature-dependent ion channels can generate a temperature-compensated stimulus representation. Importantly, we reveal that the underlying cell-intrinsic compensation mechanism need not impair neuronal energy efficiency. On the other hand, we show that sound processing in higher-order neurons does *not* exhibit the degree of compensation that is found at the input level. Using a combination of mathematical modeling and simulations we show how temperature compensation of song recognition can be achieved at the network level, with temperature-dependent neural filters.

In principle the proposed mechanisms are applicable to all poikilothermic species.

Die Benennung der Poikilothermen mit "Spielball der Umgebung" ist sprachlich und sachlich in die physiologische Literatur übergegangen. Wir möchten nun im Folgenden klarzulegen versuchen, wie gegenüber den physikalischen Kräften der Umgebung der Körper des Kaltblüters keineswegs lediglich das Verhalten eines leblosen physikalischen Objects zeigt, und wie auch bei ihm schon Vorrichtungen bestehen, die den Organismus von den Launen der Umgebung zu emancipiren suchen.

—Ludolf von Krehl & Franz Soetbeer, 1899

Contents

Illustrations

Figures

Tables

Abbreviations

AP	Action Potential
CI	Confidence Interval
FWHMax	Full Width at Half-Maximum
FWHMin	Full Width at Half-Minimum
IPSP	Inhibitory Post-Synaptic Potential
L-N	Linear-Nonlinear
MAD	Median Absolute Deviation
MoG	Mix-of-Gaussians
MTEO	Multiresolution Teager Energy Operator
NL	Nonlinearity
RAM	Randomly Amplitude-Modulated
RMSD	Root Mean Squared Distance
RoG	Ratio-of-Gaussians
SPL	Sound Pressure Level
STA	Spike-Triggered Average
TWIPR	Time-Warp Invariant Pattern Recognition

1 Introduction

If you ever lay in a meadow on a warm summer evening, surrounded by a plethora of chirps and rustling noises, you might have realized that *hearing* the insect residents of the meadow is much easier than actually *seeing* them. Being invisible is highly useful if predators are around. But at the same time, it forces insects, such as grasshoppers, to use acoustic communication to find a partner. In that sense, grasshopper courtship is comparable to human courtship in TV shows like *Blind Date* or *Herzblatt*, in which an opaque wall forces a bachelorette to use acoustic communication to assess the attractivity of three male candidates on the other side of the wall.

What complicates courtship for grasshoppers is the fact that they are poikilotherms. Their body temperature follows the ambient temperature, such that the speed of all physico-chemical processes inside their body changes whenever their surroundings heat up or cool down. Due to the resulting temperature dependence of muscle activity, the speed of courtship song produced at two temperatures 10°C apart can differ by a factor of two.[1]

For grasshoppers this is an everyday problem. The fact that they have not gone extinct suggests that, first, their nervous systems are able to recognize the right partner regardless of song speed, and second, that their nervous systems remain functional at different temperatures, despite being based on temperature-dependent processes.

The existence of such *compensation for temperature* in poikilotherms has been known for a long time (Bullock, 1955), but knowledge about possible underlying mechanisms has been scarce (Robertson and Money, 2012). This thesis attempts to uncover mechanisms of temperature compensation specifically at the level of single nerve cells, or small networks of neurons. The model system of choice is the auditory system of grasshoppers, which is used by various species for mate recognition and sexual selection (Faber, 1953; Ragge, 1986, 1987; Stumpner and

[1] Imagine the male candidates on *Blind Date* were asked to sing a ballad by the bachelorette's favorite artist. If a candidate sang the ballad at twice the original speed, this could signify the premature end of any romantic feeling in the bachelorette.

von Helversen, 1994). Notably, for the species considered here, *Chorthippus biguttulus*, acoustic communication remains functional between 25 and 40°C (von Helversen, 1972).

The remainder of this chapter is devoted to a more general motivation of the research subject. Chapter 2 introduces the grasshopper as a model system.[2] Chapter 3 outlines the experiments that formed the basis of the analyses and models outlined in later chapters. The main modeling formalisms that will be applied in this thesis are introduced in Chapter 4.[3]

Chapter 5 first summarizes empirical evidence[4] for temperature compensation of spike rate in auditory receptor neurons of the grasshopper, and second, proposes a mechanism to achieve the observed degree of compensation in single nerve cells with temperature-dependent ion-channel kinetics. Chapter 6 shows that the proposed mechanism of temperature compensation does not compromise neuronal energy efficiency. The results of Chapters 5 and 6 were published in Roemschied et al. (2014).

Chapter 7 summarizes experimental findings[5] which suggest that the degree of temperature compensation found at the level of receptor neurons is lost at the level of ascending neurons, two synapses downstream. Ascending neurons constitute a bottleneck in the processing of sound information, therefore their temperature dependence contrasts the temperature robustness of song recognition observed at the behavioral level. This apparent mismatch is resolved in Chapter 8: a mathematical model of song recognition is introduced, which, incorporating the experimentally observed temperature dependence of ascending neurons, reproduces robustness of song recognition across temperatures. A manuscript based on Chapters 7 and 8 is currently in preparation.

Chapter 9 provides a general summary of all results and an outlook.

What is temperature? According to classical kinetic theory, *temperature* is a measure of the average energy of motion of particles in a system.[6] Therefore, if the temperature of a gas is increased, the particles in it move faster, which increases the rate of encounters between particles. If at impact the particle energy exceeds the *activation energy*, E_a, an encounter leads to a chemical

[2] This can be skipped by readers with a background in biology.

[3] This can be skipped by readers with a background in computational neuroscience.

[4] from joint work with Monika Eberhard and Bernhard Ronacher at Humboldt-Universität zu Berlin

[5] from joint work with Sarah Wirtssohn and Bernhard Ronacher at Humboldt-Universität zu Berlin

[6] $\frac{m}{2}\bar{v}^2 = \frac{3}{2}k_B T$, with the *Boltzmann constant* k_B, the particle mass m, the average velocity $\bar{v}$, and the absolute temperature T.

reaction. This is described by the *Arrhenius equation*, which also formalizes the dependence of chemical reaction rates on temperature,

$$k = A \cdot \exp\left(\frac{-E_a}{RT}\right). \tag{1.1}$$

Equation 1.1 states that the rate k of a chemical reaction is proportional to the fraction of molecules in a system with energies at least equal to the activation energy at temperature T.[7] Hence, the higher the temperature, the faster the reaction rate. But how does this affect organisms and their behavior?

The role of temperature regarding life on earth. Life on earth requires liquid water to facilitate intracellular transport, solution of ions and nutrients, or enzymatic reactions (Koshland, 2002; McKay, 2004; Ball, 2015). Considering that enzymes denaturate at high temperatures and that cellular membranes can be destroyed by ice crystals at low temperatures, clear limits are imposed on the range of temperatures at which life is possible (with the exception of *extremophiles*; Rothschild and Mancinelli, 2001).[8] Further, all cellular chemical reactions follow Equation 1.1, which instantly shows that temperature affects terrestrial life at the very basic level. Importantly, just as enzymes have an optimal operating temperature[9], every organism has an optimal temperature at which its fitness is maximal, and a range of temperatures over which it thrives and performs (Huey and Stevenson, 1979). Then, how can a complex organism, that is based on an immense and highly orchestrated set of biochemical processes, remain functional in an environment of *changing* temperatures? In particular, how can a nervous system consisting of thousands to billions of neurons reliably generate behavior across temperatures?

Ways to maintain nervous system function in changing ambient temperatures. There are multiple strategies for an organism to prevent temperature from impairing functionality of the nervous system, at the cellular, systemic, or

[7] More specifically, the kinetic energies E of particles at a given temperature follow a *Maxwell-Boltzmann* distribution $f(E) \sim \sqrt{E} \cdot (RT)^{-3/2} \cdot \exp\left(\frac{-E}{RT}\right)$. The fraction of particles that is able to react, that is, with kinetic energies above the activation energy, is obtained by integrating the probability density correspondingly, $\int_{E_a}^{\infty} f(E)dE$.

[8] Recent evidence suggests that even the synthesis of amino acids, the building blocks of life, from abiotic compounds during the development of life on the young earth required comparatively mild temperatures (Galtier et al., 1999; Bada, 2013).

[9] Enzymes are proteins that act as biological catalysts. An optimal temperature emerges because the increase in reaction rate with heating is opposed by enzyme denaturation above a critical temperature.

behavioral level. Strategies at the behavioral level include avoidance of pathological temperatures, for example, using thermoreceptors, as found in a large variety of organisms (Venkatachalam and Montell, 2007; Garrity et al., 2010; Klein et al., 2015), or the choice of a habitat of constant temperature (e.g., caves: Barr and Holsinger, 1985; Culver and Pipan, 2009).

Homeothermy, that is, the investment of energy to achieve a constant body temperature, constitutes a reasonable yet costly systemic strategy that allows for optimization of bodily functions to this temperature (Yu et al., 2012). At the level of nervous systems, central pattern generators involved in locust flight and crab chewing exhibit temperature compensation of wingbeat frequency, and the phase relationship between neurons in the circuit, respectively (Xu and Robertson, 1996; Tang et al., 2010). In the former case, heating increases hyperpolarization of flight neurons, which compensates for a heating-induced increase in rhythm frequency, leading to a robust flight pattern across a temperature range of 18°C. In the latter case, the specific temperature dependence of opposing cellular mechanisms enables robustness of phase across a range of 10°C.

While these examples illustrate mechanisms of temperature compensation in complex interconnected neural circuits (Marder and Bucher, 2001), it is largely unknown how temperature robustness is achieved in the sensory periphery, or in individual neurons without network input. Experimental evidence from mollusc neurons suggests that a cancellation of temperature effects on different properties of ionic conductances[10] can result in cellular temperature compensation of action potential frequency(Partridge and Connor, 1978). This finding consititutes an important starting point of the present thesis.

This thesis: temperature compensation of sensory computations in a small nervous system. Various grasshopper species utilize acoustic communication as a means of locating potential partners in dense vegetation that prevents visual detection. Remarkably, communication of the species *Chorthippus biguttulus* is robust to independent variations of the temperature of the male and female (von Helversen, 1972). In particular, females are able to ignore the temperature dependence of male song, even when their own temperature is changed. Whether this example of temperature robustness is due to compensatory mechanisms at the cellular or network level has been unclear, also because the influence of temperature on neuronal sound processing has not been fully characterized. Yet, grasshoppers possess comparatively few neurons

[10] here: rate constants and peak conductances

involved in song recognition, their identitiy is well-known, and we begin to understand the neuronal basis of song recognition (cf. Chapter 2 for a review).

The aim of the present thesis is hence, first, to quantify the effects of temperature on neuronal sound processing in the grasshopper, second, to identify candidate mechanisms to explain temperature robustness at both the cellular and the network level, and third, to discuss the implementation of these neural mechanisms of temperature compensation in the comparatively small auditory system of the grasshopper. The employed methods comprise data analysis, mathematical analysis, and computational modeling.

2 The grasshopper as a model system

If one wants to understand the *computations* that a brain is capable of doing, it seems much more feasible to start with a *small* brain and comparatively few nerve cells rather than a brain consisting of a network of billions of nerve cells. Likewise, profound knowledge of the *behaviors* that a brain can generate, and of the organization of the nervous system and its sensory inputs, greatly aid in understanding brain function. Therefore, the grasshopper lends itself as a model system: Its nervous system is comparatively small[1], parts of it are conserved across different species, and single neurons can be identified across different animals (Meier and Reichert, 1995; Neuhofer et al., 2008). Further, grasshoppers exhibit a plethora of interesting and well-characterized behaviors, including acoustic communication, phonotaxis, predator avoidance, and swarming (Nattier et al., 2011; Bidau, 2014).

2.1 Acoustic communication and temperature robustness

The auditory system of grasshoppers likely evolved first to detect sounds of approaching predators (such as broadband noise of approaching lizards, or ultrasound echolocation signals of bats) and later for partner selection (Stumpner and von Helversen, 2001). Among grasshoppers, gomphocerine species stand out because they developed bidirectional communication for courtship (Faber, 1953; Elsner, 1974; von Helversen and von Helversen, 1994). Males initiate courtship-song production by rubbing their hindlegs against the wings (cf. Figure 2.1*A*). This produces amplitude-modulated acoustic noise that, for various species, exhibits a characteristic structure of alternating segments of high and low amplitudes in the sound envelope, termed *syllables* and *pauses*, respectively (cf. Figure 2.1*A*,*B*). A female evaluates the song by

[1] that is, on the order of $10^5 - 10^6$ neurons in the central nervous system, and $10^2 - 10^3$ in individual ganglia (Boyan and Ball, 1993)

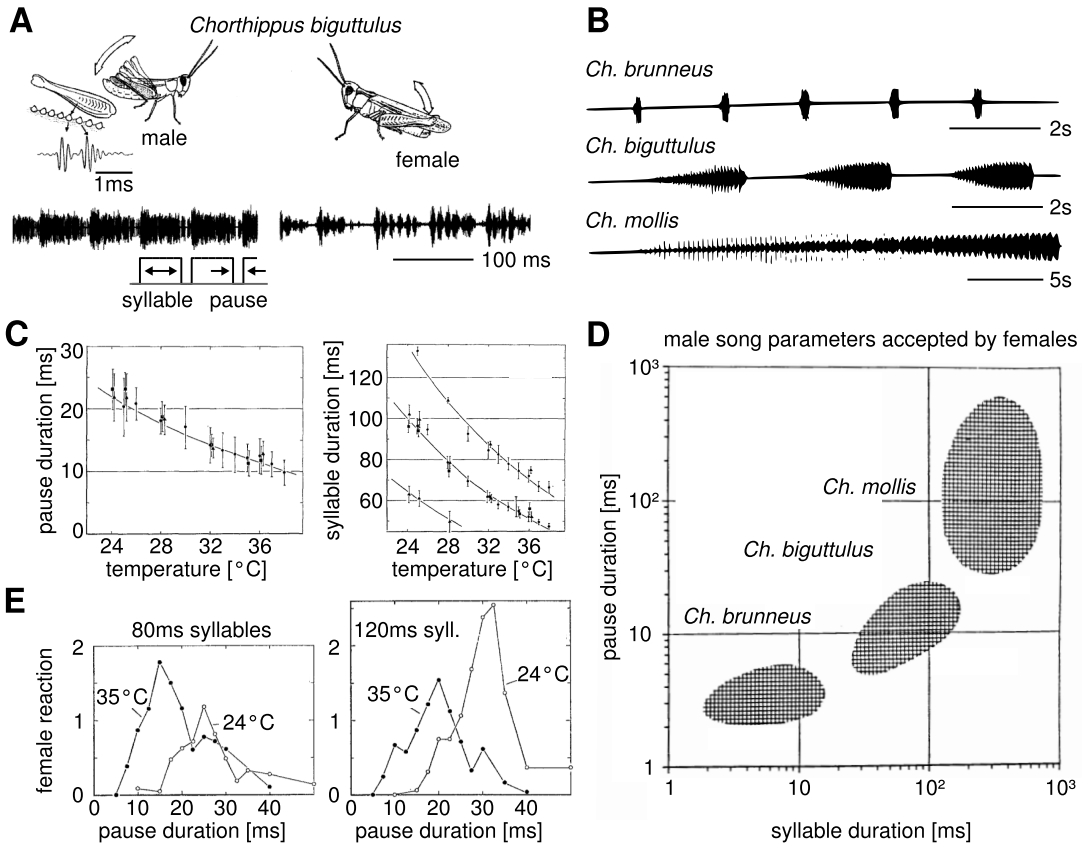

Figure 2.1 Various grasshopper species use acoustic communication for partner selection. **A:** Duetting grasshoppers (*Chorthippus biguttulus*). Modified from Figure 2a in von Helversen and von Helversen (1997). Song consisting of amplitude-modulated sound is generated through rapid rubbing of the hindlegs against the wings. Songs consists of alternating segments of high and low sound amplitudes, termed *syllables* and *pauses*. **B:** Songs of different species (*Ch. biguttulus*, *Ch. mollis*, *Ch. brunneus*) can be distinguished based on their amplitude modulation pattern. Modified from Figure 6 in von Helversen and von Helversen (1994). **C:** Syllable and pause durations of male song decrease with increasing temperature. Modified from Figures 6 and 7 in von Helversen (1972). **D:** Females of three grasshopper species prefer male songs of different time scales. Female preferences cover the relevant range of male temperatures. Modified from Figure 7 in von Helversen and von Helversen (1994). **E:** Females at different temperatures exhibit broad tuning for syllables and pauses of male song, enabling acceptance of males singing at various temperatures. Modified from Figure 20 in von Helversen (1972).

extracting information that is indicative of the sender's identity and quality (Ronacher et al., 2004). If the evaluation is positive, it initiates a response song, which allows the male to use phonotaxis to find the female. When they meet, mating begins after a final mutual assessment that is potentially based on chemical cues (Ritchie, 1990; Finck et al., 2016).

Songs of different grasshopper species have similar frequency spectra (between 5 and 40 kHz), but differ in their amplitude modulations (von Helversen and von Helversen, 1994, 1997; Figure 2.1*B*). The song of *Chorthippus biguttulus* males and females can reach peak sound intensities of around 80 and 70 dB Sound Pressure Level (SPL), respectively, recorded at a distance of 15 cm, but rapidly attenuates with distance, limiting the acoustic communication distance to around 2 m (Lang, 2000).

European grasshopper species can experience a broad range of ambient temperatures during their mating season. Since grasshoppers are poikilotherms and temperature affects basic chemical and physiological rates (Hille, 2001), song production is temperature dependent (Faber, 1932). As a result, the duration of syllables and pauses decreases with heating (von Helversen, 1972;Figure 2.1C). This temperature-induced variability of song features exerted selective pressure on grasshoppers to broaden their range of accepted syllable-pause combinations (von Helversen and von Helversen, 1994; Figure 2.1*D*,*E*). Remarkably, females accept songs of males singing at a broad range of temperatures even if their own temperature is changed (von Helversen, 1972; Figure 2.1*E*). How this robustness to independent temperature variations of the sender and the receiver of sound is achieved at the neural level in the receiver is to date unclear, and will be topic of this thesis.

2.2 Structure of the auditory system

The early stages of auditory processing in the grasshopper are considered conserved across species (Römer et al., 1988; Ronacher and Stumpner, 1988; Sokoliuk et al., 1989; Neuhofer et al., 2008). Consequently, the migratory locust has become an established model system for the singing grasshopper *Chorthippus biguttulus* (Figure 2.2*A*), due to its superior electrophysiological accessibility. This is also exploited in the interpretation of the results of this thesis.

Sound processing starts as soon as sound-pressure waves elicit vibrations of the tympanum, which in turn activate stretch-sensitive ion channels in the membranes of receptor neurons (Gray, 1960; Meyer and Hedwig, 1995; cf. Figure 2.2*B*,*C*). Receptor neurons constitute the primary processing stage for

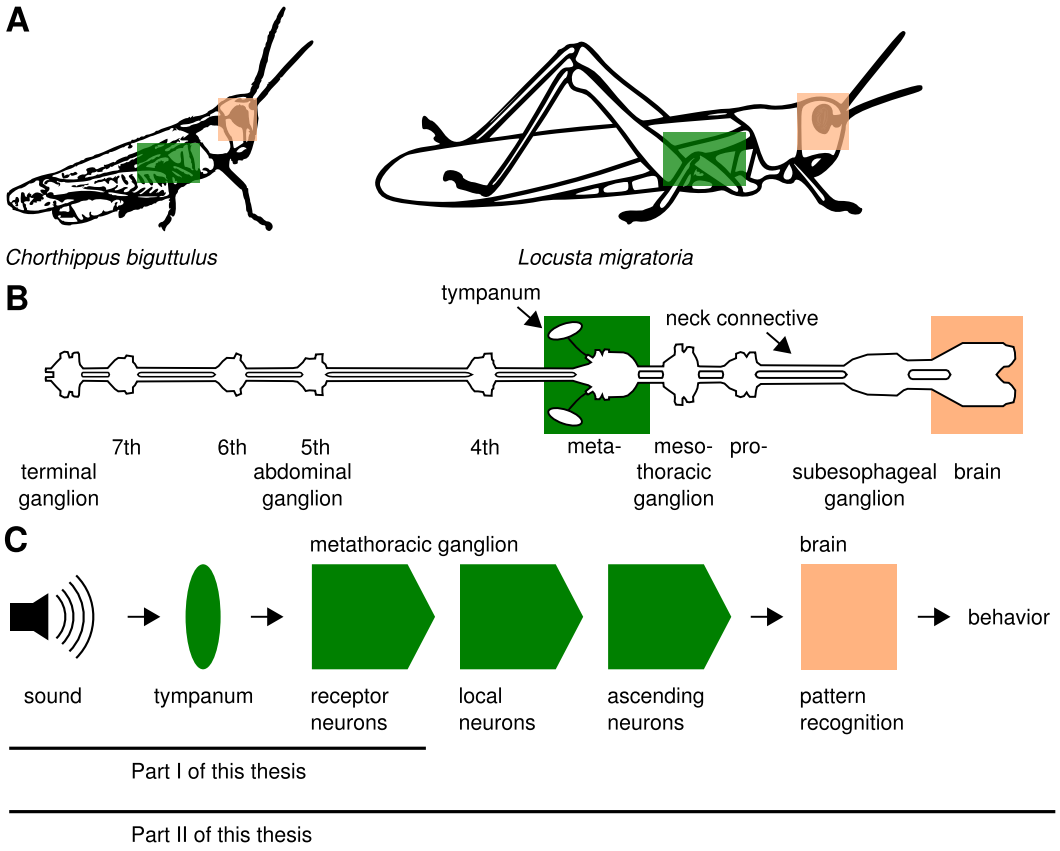

Figure 2.2 The structure of the auditory system is conserved across grasshopper species. **A:** Different grasshoppers with ear and brain location. *Chorthippus biguttulus* modified from von Helversen and von Helversen (1997), *Locusta migratoria* modified from Hildebrandt (2010). **B:** Ganglion structure, modified from Hildebrandt (2010). The auditory nerve guides auditory signals from the tympanum to the metathoracic ganglion (green box), where the first steps of auditory processing take place for various grasshopper species. **C:** Functional architecture of the early auditory system. Within the metathoracic ganglion, sound information is processed by three layers of neurons (receptor, local, and ascending), which are organized in a feed-forward network. Ascending neurons project the processed sound information to the brain (orange box), where further evaluation takes place.

incoming sound. They exhibit a characteristic sigmoidal dependence of spike rate on sound intensity (e.g., Benda, 2002; Gollisch et al., 2002). Also, receptor neurons form the bottom layer of a *feed-forward* network that resides in the metathoracic ganglion. In other words, receptor neurons only receive *input* from the tympanum, not from the network, which will be important for the interpretation of the experimental results in Chapter 5. Local neurons and ascending neurons form the second and third layer, respectively, in which a transformation from a population-based representation of sound at receptor level to a sparse, labeled-line representation is achieved (Clemens et al., 2011). This abstracted sound representation is forwarded by ascending neurons to the brain, where pattern recognition and sound source localization take place, and where command neurons trigger response behavior via activation of motor neurons (Stumpner and von Helversen, 2001). Hence, ascending neurons constitute a *bottleneck* for auditory information on the way to the brain (Gerhardt and Huber, 2002). As such, ascending neurons are an ideal target for a comparison of temperature effects on sound processing at the neural level to the temperature robustness of song recognition at the behavioral level, which will be the subject of Chapters 7 and 8.

2.3 Electrophysiology

The term *electrophysiology* refers to studying the electrical properties and signals of biological cells, such as neurons or heart cells. In particular, measurable signals that form the basis of electrophysiological research are those that are due to the movement of ions, such as the membrane voltage (i.e., the potential difference between the medium inside and outside a cell), the current that flows through an ion channel if a fixed voltage is applied, or the potential difference between cutaneous electrodes generated by a heart muscle contractions during a heart beat. While the latter signal can be obtained non-invasively, the former examples require the use of invasive techniques, namely *intracellular* or *extracellular recordings*, using *electrodes*.

Famous classical studies that pioneered in using intra- and extracellular recordings were the description of action potential generation in the squid giant axon by Hodgkin and Huxley (1952), and the description of receptive fields[2] of neurons in the visual cortex of cats (Hubel and Wiesel, 1959, 1962).

Popular stimulus paradigms used in combination with intracellular recordings include the *current clamp* (intracellular only), in which the membrane

[2] that is, the parts of the visual field that, when stimulated with light, elicit action potentials in the recorded neuron

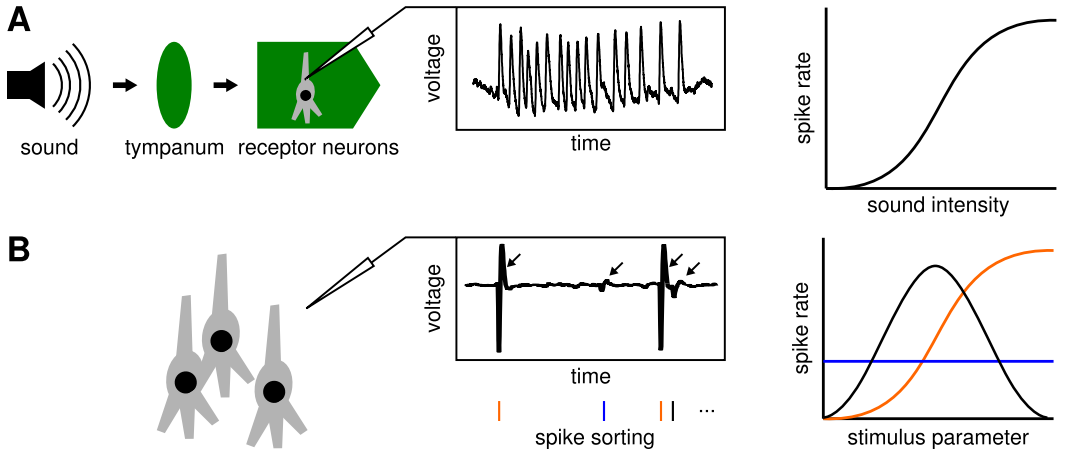

Figure 2.3 Electrophysiology as a window to nervous system function. **A:** Intracellular voltage trace. Because the electrode is *inside* a single neuron, all recorded spikes can be uniquely assigned to that neuron. The presentation of a stimulus during the recording can reveal the function of a neuron. Here, the hypothetical neuron increases its spike rate with increasing sound intensity. The sigmoidal shape of the response curve is typical for auditory receptor neurons in the grasshopper. **B:** Extracellular voltage trace. Here, the electrode records from the extracellular space. All neurons in the vicinity of the electrode can contribute to the recorded signal. Hence, the assignment of spikes to individual neurons constitutes a non-trivial problem. The approach to tackle this problem is termed *spike sorting*. Typically, different neurons exhibit differences in the shape of their extracellular spikes, which can be used for sorting. Once spikes are sorted, response curves can be computed from the individual spike trains just as for an intracellular recording.

voltage is measured for an applied current of a fixed amplitude, the *voltage clamp* (intracellular only), in which the transmembrane current for a fixed membrane voltage is measured, or the *dynamic clamp*, in which a dynamically applied current mimics the ionic conductance of one or more ion channels or the synaptic input of a population of neurons (for an overview, see Prinz et al., 2004). These techniques are highly useful to assess a neuron's excitability or the composition of its conductances. Further, determining the number of action potentials in response to an applied external stimulus of varied intensity can provide insights to the recorded neuron's function (cf. Figure 2.3*A*; here, the fictive neuron exhibits a sigmoidal dependence of spike rate on sound intensity, which can easily be computed from the recorded voltage trace). An important advantage of intracellular recordings is that the recorded cell can be labeled for subsequent identification[3], but it is more difficult to hold a recording over long time periods, as opposed to an extracellular recording. For extracellular

[3] for example, by applying a fluorescent dye at the end of the recording

recordings, the number and identity of recorded neurons is mostly unknown *per se*.[4] Yet, the shape of the extracellular action potential differs between neurons, which can be exploited to assign different labels to action potentials, based on their shape. This approach is referred to as *spike sorting*.[5] After spike sorting, spike trains of individual extracellular neurons (also referred to as *units*) can be used for functional characterization just as the spike trains obtained from intracellular recordings (cf. Figure 2.3). While studies using simultaneous intra- and extracellular recordings have shown that spike sorting *can* accurately separate contributions of different neurons to the extracellular voltage (Harris et al., 2000), there is no guarantee that the estimated number indeed corresponds to the number of neurons that contributed to the recorded signal. Further, the extracellular action potential of all neurons depends on the distance of the recording electrode to each neuron (Pettersen and Einevoll, 2008), which can change throughout the recording (e.g., due to respiratory movements) and hence can impair spike sorting results.

Both intra- and extracellular recordings have been widely used to characterize neuronal function in grasshoppers (for reviews, see Boyan and Ball, 1993; Ronacher et al., 2004). For example, important insights have been gained on the neuronal circuitry underlying jumping and flight (Pearson et al., 1980; Robertson and Pearson, 1983; Pearson et al., 1985), olfaction (Laurent and Davidowitz, 1994; Wehr and Laurent, 1996), or collision avoidance (Gabbiani et al., 1999, 2004). Further, increasing evidence has elucidated the role of the three first layers of auditory processing, and the role of spike-frequency adaptation in auditory processing (Stumpner and Ronacher, 1994; Benda et al., 2001; Hildebrandt et al., 2009, 2015). Extracellular hook electrodes have been used to record from multiple auditory receptor neurons simultaneously, and from auditory interneurons in freely moving grasshoppers (Stumpner and Ronacher, 1994; Wolf, 1986), as well as the data that Chapter 7 of this thesis is based on (see Chapter 3). For the latter, an additional challenge for spike sorting arises due to the effect of temperature on the neuronal action potential. More specifically, action potential generation speeds up with heating (Hille, 2001; Thompson et al., 1985; Bestmann and Dippold, 1989), which can lead to confusion of neuronal identities if spike sorting is applied once for an entire voltage trace that was recorded during a change of temperature. In Chapter 7, an approach is proposed to track neuronal identity across temperatures.

[4] But with the recent advent of the *juxtacellular* recording technique (Pinault, 2011), it became possible to label neurons in extracellular recordings.

[5] For a review, see Lewicki (1998).

3 Experiments

This chapter summarizes the experiments from which all data originated that motivated the analyses and model development outlined in the subsequent chapters. I am immensely grateful to Monika Eberhard (currently at Ernst-Moritz-Arndt-Universität Greifswald) and Sarah Wirtssohn, who performed all experiments, and who obtained intracellular and extracellular recordings, respectively. The following sections largely correspond to the experimental procedures described in Roemschied et al. (2014) and Wirtssohn (2015), which were drafted by M. Eberhard and S. Wirtssohn, respectively. I edited, compiled, and reproduced them here solely to facilitate reading of the thesis.

3.1 Experimental animals

Adult female migratory locusts (*Locusta migratoria*) were used in the present experiments. Due to the high degree of conservation between the auditory systems of the *Locusta migratoria* and *Chorthippus biguttulus*, the electrophysiologically more accessible locust constitutes a well established model system for the singing grasshopper (Ronacher and Stumpner, 1988; Sokoliuk et al., 1989; Neuhofer et al., 2008). The locusts were obtained from commercial suppliers and housed at room temperature with *ad libitum* food and water supply.

3.2 Animal preparation and data acquisition

Neuronal signals from the auditory pathway of the locust were obtained by electrophysiological recordings.

3.2.1 Intracellular recordings

Intracellular recordings from auditory neurons within the metathoracic ganglion were conventionally conducted as described elsewhere (Franz and Ronacher,

2002; Wohlgemuth and Ronacher, 2007), using glass microelectrodes filled with a 3-5% solution of Lucifer yellow in 0.5 M LiCl. Neuronal responses were amplified (BRAMP-01; npi electronic GmbH, Tamm, Germany) and recorded by a data-acquisition board (BNC-2090A; National Instruments, Austin, TX) with 20 kHz sampling rate. To control for temperature, the preparation was placed directly on a Peltier element connected to a 2 V battery and a potentiometer. Temperature was monitored and recorded with a digital thermometer (GMH 3210, Greisinger electronic GmbH, Regenstauf, Germany) connected to a NiCr-Ni-thermoelement (GTF 300, Type K, Greisinger electronic GmbH, Regenstauf, Germany). For each experiment, recordings were conducted first at a fixed higher tissue temperature (in the range of 28-29°C), then the preparation was cooled down to a lower temperature (in the range of 21-23°C) and recordings were repeated.

After completion of the recordings, Lucifer yellow was injected into the recorded cell by applying a hyperpolarizing current. Subsequently, the thoracic ganglia were removed, fixed in 4% paraformaldehyde, dehydrated, and cleared in methylsalicylate. The stained cells were identified under a fluorescent microscope according to their characteristic morphology. Altogether, nine receptor neurons were recorded in eight preparations.

3.2.2 Extracellular recordings

The antennae, legs and wings were removed. Animals were waxed with the dorsal side down on a Peltier element glued to an animal holder. Three small cuts were made into the cuticle of the first abdominal segment, such that a cuticle flap was formed. Special attention was paid to not damage the hearing structures. The flap was pulled aside to form a window in the abdominal cuticle. Through this window, the descending connectives from the first three abdominal ganglia were cut. The window in the abdomen was closed by replacing the cuticle flap and sealing it with wax resin. The maxillae were removed, the labium was lifted and the gut was cut below the esophagus. The thin neck cuticle and the labial structure were removed to assess the connectives ascending from the prothoracic ganglion (in the following also referred to as *neck connectives*, cf. Figure 2.2*B*). The tip of the abdomen was removed and the gut pulled out through the hole, such that the cavity below the connectives could be filled with a mixture of vaseline and mineral oil (Carl Roth). Two hook electrodes made from tungsten wire were placed in parallel around one of the connectives. To reduce noise, the connective was then cut below the subesophageal ganglion. The hook electrodes and the connectives were coated

with vaseline for electrical isolation and to prevent the preparation from drying out.

Signals recorded with the electrodes were differentially amplified (EXT-10C, npi electronic) and band-pass filtered with cut-off frequencies of 0.3 and 3 kHz (DPA-2FX, npi electronic) before digitization with a sampling rate of 20 kHz (PCI-MIO-16E-1, National Instruments) and storage on a personal computer.

Data from nine units were obtained at several temperatures. The data from all units, including those for which the Spike-Triggered Average (STA) filter[1] was determined at one temperature only, were pooled for population analysis, rendering a total of 177 units. Data from a total of 12 specimens were included in this study; of these, one specimen was recorded from at one temperature, two specimens at three temperatures, and the other specimens at two temperatures with $5°C \leq \Delta T \leq 10°C$.

3.3 Acoustic stimulation

3.3.1 Estimation of response curves

To obtain spike rate vs. sound intensity curves (response curves) during the intracellular recordings, we used acoustic broad band stimuli (100 ms duration, 1-40 kHz bandwidth) repeated five times each at 8 intensities, rising from 32 to 88 dB SPL. Acoustic stimuli were stored digitally and delivered by a custom-made program (LabView 7 Express, National Instruments, Austin, TX). Following a 100 kHz D/A conversion (BNC-2090A; National Instruments, Austin, TX), the stimulus was routed through a computer-controlled attenuator (ATN-01M; npi electronic GmbH, Tamm, Germany) and an audio amplifier (Pioneer stereo amplifier A-207R, Pioneer Electronics Inc., USA). Acoustic stimuli were broadcast unilaterally by speakers (D2905/970000; Scan-Speak, Videbæk, Denmark) located at ±90° and 30 cm from the preparation. Sound intensity was calibrated with a half inch microphone (type 4133; Brüel & Kjær, Nærum, Denmark) and a measuring amplifier (type 2209; Brüel & Kjær, Nærum, Denmark), positioned at the site of the preparation.

3.3.2 Estimation of neural filters and temperature tracking

Acoustic stimulation during the extracellular recordings consisted of a broad-band carrier (5-40 kHz), with a signal envelope which was amplitude-modulated with low-pass Gaussian noise with a cutoff frequency of 200 Hz. The mean

[1] see Section 4.2 and Chapter 7 for details

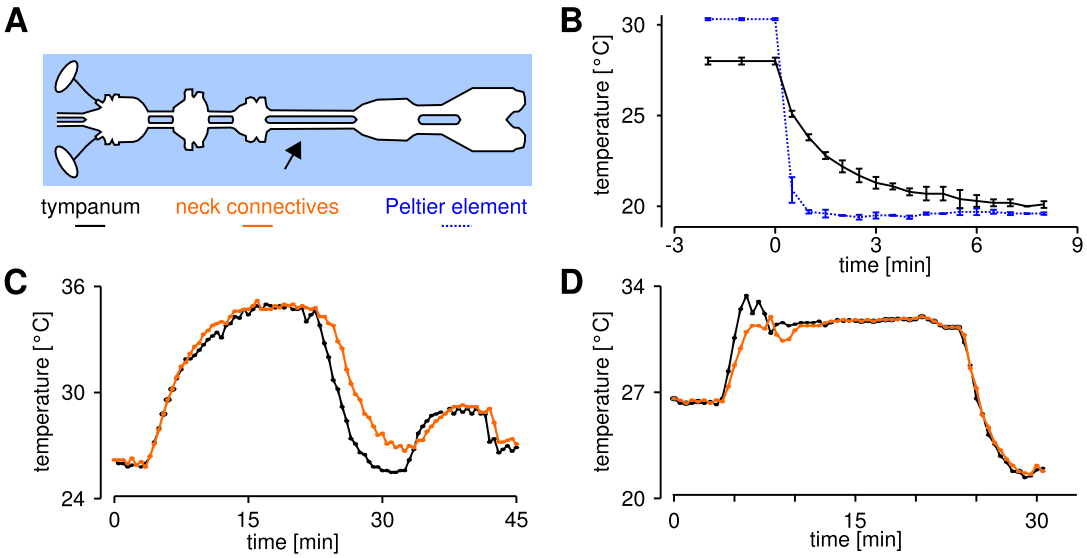

Figure 3.1 Control of the physiological temperature while recording. **A:** During electrophysiological recordings, the ganglion preparation was placed on a Peltier element, which allowed to change the temperature of the preparation. Intracellular recordings were obtained from auditory receptor neurons in the metathoracic ganglion, whose appendages connect to the tympanum. Extracellular recordings were obtained from ascending neurons, using hook electrodes around the neck connectives. **B:** Intracellular recordings were performed first at a higher temperature, followed by cooling and subsequent recording at the cooler temperature. Due to the evident lag between Peltier cooling and cooling at the tympanum, only data recorded at least 3 minutes after the cooling were used for subsequent analysis. **C, D:** Time course of the temperature at the neck connectives and the tympanum for two different locusts, adapted from Wirtssohn (2015). During extracellular recordings, temperature differences between the neck connectives (i.e., the recording site) and the tympanum were small and transient.

intensity was set to 60 dB in order to cover the intensity range most ascending neurons are sensitive to (Stumpner and Ronacher, 1991). The intensity modulations had a standard deviation of 6 dB. To estimate the STA filters, the noise stimulus was presented for 6 to 18 min. To evaluate the performance of the corresponding Linear-Nonlinear (L-N) model (see Footnote 1), a 6 s-segment was repeated at least 18 times. This protocol was applied at 1-3 constant temperatures (ranging from around 20 to 32°C) within the same animal. The order of temperatures (from cold to warm or vice versa) was randomized to rule out a serial effect. During the experimental manipulation of the animal's body temperature, 50 ms-noise pulses were presented at an intensity of 50 dB, to enable a tracking of single unit spike waveforms which gradually changed with temperature.

3.4 Temperature control and monitoring

3.4.1 Temperature during intracellular recordings

To control for differences between the temperatures of the Peltier element and the tissue at the inner side of the tympanal membrane at the attachment site of receptor neurons, the dependence between those variables was measured directly and used for calibration (Figure 3.1*A,B*). The calibration showed that at the higher Peltier temperature (30°C) tissue temperature only reached 28°C (in the steady state) due to heat dissipation. After the cooling process the difference between Peltier and tissue temperature in the steady-state was less than 0.5°C. Moreover, cooling down proved to be slower in the tissue than at the Peltier element.

In order not to underestimate neuronal temperature dependence (i.e., Q_{10} values[2]), we took a conservative approach: Electrophysiological recordings started 3-5 min after induction of the temperature change. Tissue temperature was derived from the calibration curve at the onset of a recording (lasting 40 s). Although temperature may still have been subject to small changes during the recording, this procedure ensured that temperature changes (i.e., the difference between high and low temperature) were, at most, slightly underestimated, favoring larger Q_{10} values. Consequently, the Q_{10} values estimated in Chapter 5 constitute an upper bound. Thus, we cannot rule out that real temperature dependence is even lower, that is, neurons are more temperature compensated.

3.4.2 Temperature during extracellular recordings

The temperature of the preparation was controlled by means of a Peltier element. In four recording sessions, the temperature was measured with two thermocouples. One was placed in the abdomen in the vicinity of the ear, and the other in the vicinity of the neck connectives, close to the recording site. Each thermocouple was connected to a thermometer with a measuring resolution of 0.5°C (Greisinger, type GTH 1150). Of the four specimens, three were recorded at cold and warm temperature, with a temperature difference above 5°C. In eight recording sessions, the temperature was measured with one thermocouple in the thorax, close to the recording site, with a thermometer with a resolution of 0.05°C (Greisinger, type GMH 3210). In these sessions,

[2] In biological sciences, the temperature dependence of an observable is often reported using the Q_{10} coefficient, which quantifies the relative change in the observable with a temperature increase of 10°C. Q_{10} values smaller/larger than, or equal to unity characterize a decrease/increase in the observable with heating, or temperature invariance, respectively.

the recording temperature was maintained constant with a median standard deviation < 0.11°C. Control experiments showed that while maintaining a stable temperature, the temperature difference between the recording site and the ear was negligible (cf. Figure 3.1*C,D*). After a drastic temperature change a temperature equilibrium between the abdomen and the thorax was established after a few minutes. It was therefore sufficient to measure temperature only in the thorax close to the recording site during the experiments. Acoustic stimulation was started after waiting several minutes when the target temperature was reached.

4 Computational models of neurons and networks

Hypothesis-driven experimental research requires rigorous control of an oftentimes large amount of parameters, which elucidates the important role of mathematical or computational modeling: Hypotheses can be tested in models before starting an experiment, in particular when experiments are costly or labor intensive. Further, models can be used to generate predictions, which in turn motivate new experiments. Models can be arbitrarily complex, and hence the number of parameters can approach that of the real system of consideration. Yet, the modeler has full control and knowledge about the parameters that are varied and those that are kept constant in a simulation.

In the neurosciences, models are developed at a multitude of abstraction levels – from morphologically accurate models of single neurons with detailed dynamics of the membrane potential and neurotransmitters, to the most abstract models that treat entire brain regions as processing units (Herz et al., 2006; Horwitz et al., 2000; MacGregor, 2012).

In this thesis, two types of models will be used to identify mechanisms that allow poikilothermic animals to maintain functional nervous systems across a broad range of temperatures: first, *conductance-based neuron models*, and second, *Linear-Nonlinear (L-N) models*. Both will be briefly introduced in the following (cf. introductory Figure 4.1).

4.1 Conductance-based neuron models

The first and presumably best-known conductance-based model is the Hodgkin-Huxley model of action potential generation in the squid giant axon (Hodgkin and Huxley, 1952). Here, the dynamics of the membrane potential V are governed by voltage-dependent changes in the permeability of the membrane for sodium and potassium ions. The authors made the simplifying assumptions that, first, the neuron has no spatial extent, and therefore there is no need

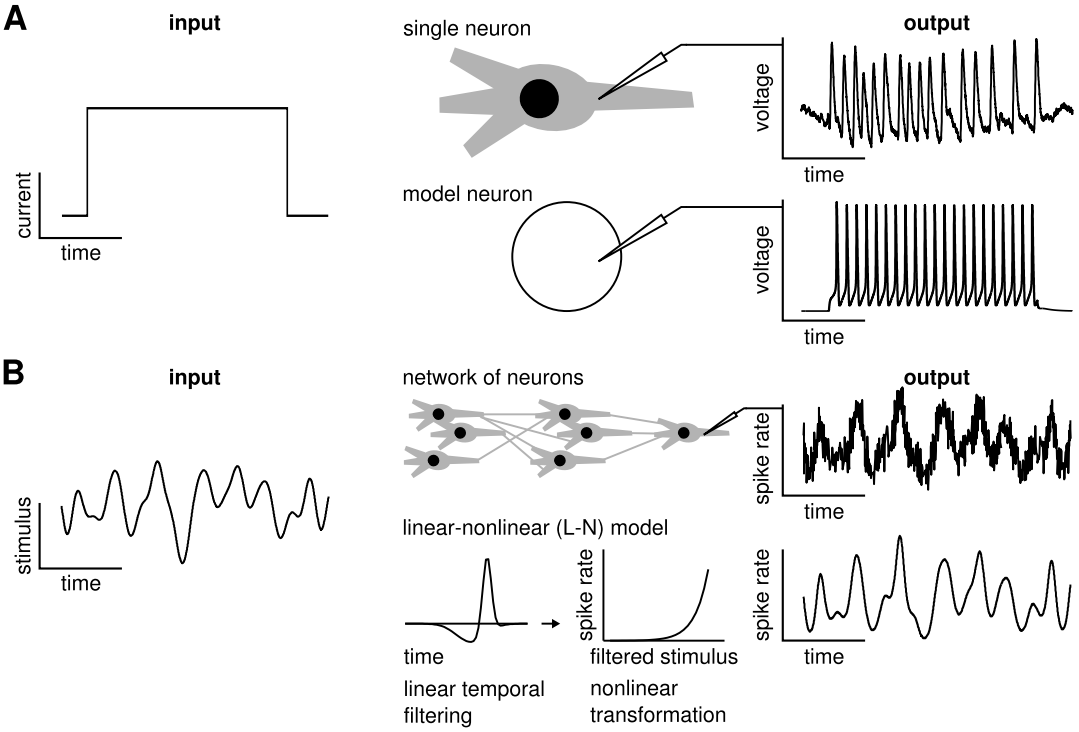

Figure 4.1 Computational models of neural function, as used in this thesis. **A:** Single-neuron models capture the membrane voltage dynamics – here in response to a current injection. **B:** L-N models approximate the response to a time-varying stimulus of an arbitrary system, such as a network of neurons, as a cascade of two processing steps: first, linear temporal filtering of the stimulus, and second, transformation of the filtered stimulus using a static nonlinearity.

to account for the propagation of the action potential through the axon, and second, there are no individual ion channels in the model but *conductances* that describe the average activity of a large number of channels for each type of ion. The membrane is treated as a *capacitor*, such that the total current across the membrane, I_m, can be described using Kirchhoff's current law as the sum of the capacitive current and the ionic currents:

$$\begin{aligned} I_\mathrm{m} &= C_\mathrm{m}\frac{dV}{dt} + I_\mathrm{ionic} \\ &= C_\mathrm{m}\frac{dV}{dt} + I_\mathrm{K} + I_\mathrm{Na} + I_\mathrm{L}. \end{aligned}$$

Here, C_m is the capacitance of the membrane, and the ionic current for this particular model comprises potassium (K), sodium (Na), and leak (L) components. Hodgkin and Huxley described each ionic current as the product of the conductance and the *driving force* for that particular ion,

$$I_i = g_i \cdot (V - E_i),$$

where the driving force is the difference between the membrane potential and the *Nernst potential* E_i for ion i.[1] Hodgkin and Huxley found that the sodium and potassium conductances could be described using *gating variables* that quantified the proportion p_i of open channels,

$$g_i = \bar{g}_i \cdot p_i = \bar{g}_i \cdot m_i^{a_i} h_i^{b_i}.$$

Here, $\bar{g}$ denotes the *peak conductance*. m and h denote *activation* and *inactivation* gating variables on the unit interval, that could be raised to positive powers a and b. Hodgkin and Huxley determined these powers from fits to data of *voltage clamp* experiments (cf. Section 2.3), which led to the equation

$$C_\mathrm{m}\frac{dV}{dt} = I_\mathrm{m} - \bar{g}_\mathrm{K} \cdot n^4 \cdot (V - E_\mathrm{K}) - \bar{g}_\mathrm{Na} \cdot m^3 h \cdot (V - E_\mathrm{Na}) - g_\mathrm{L} \cdot (V - E_\mathrm{L})$$

[1] The Nernst (or reversal) potential describes the potential of a specific ion across the membrane, and it depends on the ratio of the concentrations of the ion inside and outside of the cell: $E = \frac{RT}{zF} \ln \frac{[\text{ion outside}]}{[\text{ion inside}]}$, with the universal gas constant R, the absolute temperature T, the ionic valence z and the Faraday constant F.

The gating variables were found to depend on voltage and were well described by first-order kinetics,

$$\frac{dx}{dt} = \alpha_x(V) \cdot (1 - x) - \beta_x(V) \cdot x, \quad x \in \{n, m, h\},$$

with the voltage dependent opening and closing rates α and β, which were also determined from fits to the data. A common alternative formulation of the gating variable dynamics is based on the *steady-state value* x_∞ and the *time constant* τ_x of the gating variable, which relate to the opening and closing rates via

$$x_\infty(V) = \frac{\alpha_x}{\alpha_x + \beta_x} \quad \text{and} \quad \tau_x(V) = \frac{1}{\alpha_x + \beta_x}, \tag{4.1}$$
$$\Rightarrow \frac{dx}{dt} = \frac{x_\infty - x}{\tau_x}.$$

The framework of conductance-based modeling pioneered by Hodgkin and Huxley can be extended by an arbitrary set of ionic currents, and it is widely used also in multi-compartment neuron models (e.g., Alle et al., 2009; Taylor et al., 2009, or within the *NEURON* modeling framework, Hines and Carnevale, 1997). Compared to more abstract models, conductance-based models are analytically less tractable. However, this is compensated for by the higher degree of biophysical realism, which allows for the experimental fitting of parameters. This, in particular, makes conductance-based models highly attractive for interdisciplinary research on the verge of theory and experiments. In practice, dynamics of the membrane voltage and the (in-) activation variables are typically computed numerically.

Conductance-based neuron models will be used in Part I of this thesis, first, to determine how single neurons with temperature-dependent ionic conductances can generate spike-rate output that is independent of temperature (i.e., temperature compensated), and second, to show that temperature compensation of spike rate need not impair neuronal energy efficiency.

4.2 Linear-nonlinear models of neurons and networks

While the biophysical detail of a conductance-based neuron model facilitates identification of its parameters with actual cellular properties, L-N models (Hunter and Korenberg, 1986) are purely phenomenological, in that they approximate the input-output relation of any system as a cascade of a *linear filtering* of the input, and a *nonlinear transformation* of the filtered input to the

output variable (cf. Figure 4.1*B*). More specifically, the transformation of a time dependent stimulus $s(t)$ to an output $r(t)$ in a L-N model is given by

$$r(t) = D(f * s) = D\left(\int_0^\infty d\tau f(\tau) \cdot s(t-\tau)\right).$$

Here, f is a linear temporal filter, the asterisk denotes convolution, and D is a static nonlinearity.

Both stages of the L-N model can be readily estimated if the input to and output of a system are known. In the following this is illustrated using the response of a neuron to a known stimulus as an example, based on Schwartz et al. (2006). First, the linear stage is estimated by averaging the stimulus segments $\vec{s}_i$ preceding each of n neuronal spikes,

$$\vec{f}_{\mathrm{STA}} = \frac{1}{n}\sum_{i=1}^{n} \vec{s}_i.$$

$\vec{f}_{\mathrm{STA}}$ is referred to as the Spike-Triggered Average (STA). The vector representation is due to the choice of finite-length stimulus segments. Once the STA is estimated, the *projection* of the filter onto an arbitrary stimulus segment, $\vec{f}_{\mathrm{STA}} \cdot \vec{s}$, corresponds to the *linear response* of the filter to that stimulus segment, that is, the discrete equivalent to the convolution. While the distribution of linear responses to all stimulus segments corresponds to the probability of the stimulus, $P(\vec{s})$, the distribution of linear responses to only those stimuli that elicited a spike[2] corresponds to the *conditional probability* of finding the stimulus given a spike, $P(\vec{s}|\mathrm{spike})$. Now, the static nonlinearity ought to assign an instantaneous spike rate to a given stimulus segment. This can be interpreted as the conditional probability of observing a spike given a stimulus, which can be computed using Bayes' rule,

$$P(\mathrm{spike}|\vec{s}) = \frac{P(\mathrm{spike}) \cdot P(\vec{s}|\mathrm{spike})}{P(\vec{s})}.$$

In practice, the estimation of the nonlinear stage of the L-N model hence corresponds to computing the division of two histograms, $P(\vec{s}|\mathrm{spike})$ and $P(\vec{s})$, while $P(\mathrm{spike})$ is estimated from the neuronal spike rate. If the stimulus

[2] This is also termed the *Spike-Triggered Ensemble* of stimuli.

is chosen such that it follows a Gaussian distribution[3], and if $P(\vec{s}|\text{spike})$ is approximated as Gaussian, the shape of the nonlinearity is fully parametrized once the STA is determined. This is known as the Ratio-of-Gaussians (RoG) approach to computing the static nonlinearity (Pillow and Simoncelli, 2006), which will be used in Chapter 7.

Spike-triggered analysis and the L-N model framework have been widely used to describe the responses of single neurons as well as networks of neurons, for example to characterize neural computations in the retina and visual cortex from amphibians to non-human primates (e.g., Chichilnisky, 2001; Baccus and Meister, 2002; Schwartz et al., 2006), auditory spatial processing in ferrets (Dahmen et al., 2010), or olfactory coding in fruit flies (Nagel and Wilson, 2011). More recently, the L-N framework has been applied to characterize the computational features of auditory neurons in the grasshopper (Clemens et al., 2011, 2012), to model behavioral song preferences of crickets (Clemens and Hennig, 2013), and to describe the emergence of firing-rate resonances in the auditory system of crickets (Rau et al., 2015). In Chapter 8 of this thesis, this general approach is adopted, but on the one hand *extended* to link neural filters and their temperature dependence to robust song recognition across temperatures, as observed in the grasshopper (von Helversen, 1972), and on the other hand *simplified* to facilitate mathematical analysis and identification of model parameters with specific roles in song recognition.

[3] Until recently, a Gaussian stimulus was considered the gold standard for estimation of L-N model components, because it was shown to lead to convergence of the model parameters to the true values (Paninski, 2003).

Part I

Mechanistic models of nerve cell function

5 Cell-intrinsic temperature compensation of neuronal spike rate

We now turn towards the original results of this thesis, and present first experimental evidence for temperature robustness of sound processing at the primary processing stage in the grasshopper. The specific network structure present in the auditory system of the grasshopper implies that the underlying mechanisms is cell-intrinsic. Hence, a candidate mechanism for cell-intrinsic temperature compensation is identified using computational modeling. Large parts of this chapter were published in Roemschied et al. (2014). I am particularly grateful to Monika Eberhard (University of Greifswald) who performed the electrophysiological recordings.

5.1 Introduction

Changes in temperature considerably modulate physico-chemical processes and, consequently, also affect neural processing (Schmidt-Nielsen, 1997; Robertson and Money, 2012). As introduced in Chapter 1, the dependence of neural activity on temperature poses a particular challenge for animals without central heat regulation, like insects, who are permanently subject to temperature fluctuations. These animals must have evolved intrinsic mechanisms at the behavioral, systems, or cellular level that help to circumvent temperature-induced behavioral modulations. Such compensatory mechanisms, however, may also come into play for homeothermic animals under pathological conditions, like fever or hypothermia in mammals.

Nevertheless, our understanding of generic design principles that enhance robustness to temperature fluctuations remains limited. The goal of this study is to identify mechanisms and limitations of cellular temperature compensation on the level of firing rates. To this end, we characterize the temperature dependence of neural responses in an insect auditory system, which we find to be surprisingly low. We use mathematical modeling to show how the observed

low temperature dependence can be explained by cell-intrinsic properties. Temperature dependence is usually quantified by the so-called Q_{10} value, which characterizes the relative change of a variable when temperature rises by 10°C. Several invertebrate species were found to have firing-rate Q_{10} values above 2 (i.e., to double their neurons' firing rate), which is in line with the fact that many underlying biochemical processes also exhibit Q_{10} values of two or more (French and Kuster, 1982; Pfau et al., 1989; Warzecha et al., 1999; Hille, 2001). In contrast, we found that grasshopper auditory receptor neurons on average increased their firing rate by only around 40-50% (corresponding to a Q_{10} value of 1.4-1.5). The absence of network inputs to receptor neurons (Vogel and Ronacher, 2007; Clemens et al., 2011) suggests that a cellular mechanism underlies the observed temperature compensation. Receptor responses are shaped by a cascade of two major steps (Gollisch and Herz, 2005, cf. Section 2.2) – first, auditory transduction, which translates the vibrations of the tympanal membrane into receptor currents, and second, spike generation. Temperature compensation of the response must be achieved by compensatory mechanisms in these individual components or their combined output.

We hence first investigate how cellular spike generation, in terms of the translation from input current to firing rate can be temperature compensated and identify ionic conductances whose temperature dependence favors robustness. Second, we predict properties of the temperature dependence of mechanotransduction that would allow for an efficient compensation in firing rates in agreement with our experimental data.

Moreover, we show that information transfer via spike rates is fostered by temperature increments. As our model-based approach generalizes beyond the grasshopper system, our findings can be expected to reflect principles that could be implemented in many invertebrate and vertebrate species.

5.2 Methods

For a description of the experimental methods, see Chapter 3.

5.2.1 Analysis of experimental data

Experimental spike times were extracted from the digitized recordings by applying a voltage threshold above background noise level. Mean spike rates were calculated for each intensity to obtain response curves (spike rate r vs.

sound intensity I_{dB}) per neuron, stimulation side, and temperature. We fit a three-parameter sigmoid to each response curve,

$$r = \rho(I_{\mathrm{dB}}) = r_{\mathrm{sat}} \Big/ \left(1 + \exp\left(-\frac{I_{\mathrm{dB}} - I_{50,\rho}}{w_\rho}\right)\right), \tag{5.1}$$

with saturation spike rate r_{sat}, half-maximum sound intensity $I_{50,\rho}$, and dynamic-range width w_ρ.

5.2.2 Quantification of temperature effects

Unless noted otherwise, temperature dependence of a given observable x was quantified by the temperature coefficient

$$Q_{10}(x) = \left(\frac{x(T_0 + \Delta T)}{x(T_0)}\right)^{10/\Delta T} \tag{5.2}$$

$Q_{10}(x)$ is the factor by which x changes after a temperature increase of 10°C relative to a reference temperature T_0. $Q_{10} > 1$ and $Q_{10} < 1$ indicate an increase or decrease, respectively, of x with heating, while $Q_{10} = 1$ indicates perfect temperature invariance. For plots of Q_{10} values, data points were presented as outliers when they fell outside the interval $[q_1 - 1.5 \cdot \mathrm{iqr}, q_3 + 1.5 \cdot \mathrm{iqr}]$, with the 25th and the 75th percentile defining q_1 and q_3 and an interquartile range $\mathrm{iqr} = q_3 - q_1$.

5.2.3 Temperature dependence of action-potential width

We also quantified the temperature dependence of action-potential (AP) width at half-maximum amplitude, Q_{10}(AP width), for every neuron during the stimulus period, separately at each stimulus. Figure 5.1*D* shows the distribution of Q_{10}(AP width) pooled across all stimulus amplitudes (median 0.66). Our results qualitatively agree with the finding of broader action potentials at lower temperatures reported for various vertebrate and invertebrate neurons (Thompson et al., 1985; Bestmann and Dippold, 1989; Janssen, 1992; Gabbiani et al., 1999). Further, our results agree quantitatively with those reported for locust motor neurons and locust L-neurons (Burrows, 1989; Simmons, 1990).

5.2.4 Adaptation

We checked that our results on the temperature dependence of firing rate were not compromised by the effects of adaptation. To this end, we re-analyzed

the experimental data, separately focusing on the early phase of stimulus presentation (10-40 ms post stimulus onset), and the late phase (70-100 ms post stimulus onset). Effects of adaptation were reflected in a ratio of the respective parameter values (early-versus-late phase) that differed from one. While individual characteristics of experimentally measured firing-rate curves were subject to adaptation (e.g., the slope at half-maximum sound level was steeper early on and shallower in the later part), the early-to-late ratios did not significantly change with temperature.

5.2.5 Single-neuron models

We performed simulations of the membrane potential dynamics using a single-compartment Connor-Stevens model (original model described in Connor et al., 1977; parameters taken from Dayan and Abbott, 2005). The structure of this model is identical to that of the Hodgkin-Huxley model introduced in Section 4.1, except for an additional A-type potassium current, $I_\mathrm{A} = \bar{g}_\mathrm{A} a^3 b (V - E_\mathrm{A})$, and different (in-)activation dynamics (see Appendix A.1). The original model was defined at a temperature of 18°C, where the parameters take the values given in Table 5.1. All simulations were performed in Matlab, using the variable order solver ode15s (Shampine and Reichelt, 1997) with a time step of 0.01 ms.

5.2.6 Temperature dependence of the model

Dependence on temperature T (°C) was introduced to the model at the level of reversal potentials $E(T)$, peak conductances $\bar{g}(T)$, and time constants of (in-) activation $\tau_x(T)$. The Nernst equation defined the temperature dependence of reversal potentials:

$$E = \frac{RT}{zF} \ln \frac{[\text{ion outside}]}{[\text{ion inside}]} \Rightarrow E(T_0 + \Delta T) = E(T_0) \cdot \left(1 + \frac{\Delta T}{T_0 + 273.15}\right)$$

R is the universal gas constant, z is the valence of the considered ion and F is the Faraday constant. $T_0 = 18$°C sets the reference temperature, ΔT temperature differences. Temperature dependence of $\bar{g}_\mathrm{X}(T)$ is determined by the choice of the parameter $Q_{10,\bar{g}_\mathrm{X}}$:

$$\bar{g}_\mathrm{X} \rightarrow \bar{g}_\mathrm{X}(T) = \bar{g}_\mathrm{X} \cdot Q_{10,\bar{g}_\mathrm{X}}{}^{\frac{T-T_0}{10}}, \quad \mathrm{X} \in \{\mathrm{Na}, \mathrm{K}, \mathrm{L}, \mathrm{A}\}.$$

For $\Delta T = 0$, each $\bar{g}_X(T)$ takes the value of its original definition at 18°C. For a given gating variable, temperature dependence of its opening and closing rates are identical and read:

$$\alpha_x \to \alpha_x(T) = \alpha_x \cdot Q_{10,x}^{\frac{T-T_0}{10}},$$
$$\beta_x \to \beta_x(T) = \beta_x \cdot Q_{10,x}^{\frac{T-T_0}{10}}, \quad x \in \{n, m, h, a, b\}.$$

Consequently, following Equation 4.1,

$$\tau_x \to \tau_x(T) = \tau_x / Q_{10,x}^{10/\Delta T}.$$

Exploration of parameter space

The model totals nine temperature-dependence parameters which span the explored parameter range:

$$Q_{10,\bar{g}_X}, \quad X \in \{\text{L, Na, K, A}\},$$
$$Q_{10,x}, \quad x \in \{n, m, h, a, b\}.$$

Each parameter was sampled in four steps within realistic intervals (Partridge and Connor, 1978; Hille, 2001; Tang et al., 2010), as indicated in Table 5.1, resulting in a total number of $4^9 = 262144$ models. Step currents of different amplitudes (Table 5.1) and 100 ms duration served as stimulus to the model neurons. Preceding and following a stimulus, periods of 50 ms were simulated without current stimulation. For each model, simulations were performed at 28°C and referenced with model behavior at 18°C to derive the temperature dependence.

5.2.7 Quantification of f-I curve temperature dependence

Spike rates f in response to $N = 12$ different current amplitudes I_C defined the f-I curve for a given temperature (spike detection threshold: -30 mV). Temperature dependence of the f-I curve was quantified as the Root Mean Squared Distance (RMSD) between firing rates at the two temperatures across

Table 5.1 Parameters of the Connor-Stevens model.

Parameter	Symbol	Range	Unit
Temperature	T	18.0-28.0	°C
Membrane capacitance	C_m	0.01	$\mu\mathrm{F\,mm^{-2}}$
Potassium peak conductance	$\bar{g}_\mathrm{K}$	0.2	$\mathrm{mS\,mm^{-2}}$
A-type peak conductance	$\bar{g}_\mathrm{A}$	0.477	$\mathrm{mS\,mm^{-2}}$
Sodium peak conductance	$\bar{g}_\mathrm{Na}$	1.2	$\mathrm{mS\,mm^{-2}}$
Leak peak conductance	$\bar{g}_\mathrm{L}$	0.003	$\mathrm{mS\,mm^{-2}}$
Potassium reversal potential	E_K	−72.0	mV
A-type reversal potential	E_A	−75.0	mV
Sodium reversal potential	E_Na	55.0	mV
Leak reversal potential	E_L	−17.0	mV
Input current (amplitude)	I_C	0.05-0.6	$\mu\mathrm{A\,mm^{-2}}$
Temperature dependence (peak conductance)	$Q_{10}(\bar{g})$	1.2-2.0	—
Temperature dependence (transition rates)	$Q_{10}(\alpha, \beta)$	2.0-4.0	—

input currents, normalized by the average spike rate elicited at the lower temperature:

$$\mathrm{RMSD} = \frac{\sqrt{\mathrm{mean}_I(f(T_1) - f(T_2))^2}}{\mathrm{mean}_I(f(T_\mathrm{min}))}.$$

Here, $T_1 = T_\mathrm{min} = 18°\mathrm{C}$, $T_2 = 28°\mathrm{C}$. In agreement with the functional shape of type I spiking (Ermentrout, 1996), f-I curves for each Q_{10} parameter combination were fit to a square root model,

$$r = \phi(I) = A \cdot \mathrm{Re}\left(\sqrt{I - I_0}\right),$$

where A denotes the gain and I_0 the firing threshold of the f-I curve (goodness of fit: $R^2 > 0.97$ for 99% of the models).

5.2.8 Sensitivity analysis

Sensitivity analysis was performed in the parameter space spanned by the nine temperature-dependence parameters (each dimension sampled by four values). To quantify global *impact* of one parameter on a given observable (like the RMSD), we evaluated the distribution of point-wise changes in the observable along the dimension of a specific parameter. In total, for each parameter,

$3 \cdot 4^8$ changes between neighboring points along the corresponding dimension need to be considered. These define a distribution of changes, whose median is indicative of the global impact of this parameter on the observable. The distribution's 25th and 75th percentiles are indicated as error bars (see, e.g., Figure 5.4*B*,*E*,*H*). For each observable, impact values were normalized to give unity when summed across all nine parameters. The sign of the impact provides an estimate of the qualitative influence of the parameter on the observable, that is whether an increase in the parameter value leads to an increase or decrease in the observable. We considered an impact reliable if both percentiles (25th and 75th) had the same sign as the impact.

Note that our impact evaluation constitutes a global sensitivity analysis, comparable to the Morris one-at-a-time method (Morris, 1991). In contrast to the latter approach, we use a full factorial (grid) set of inputs instead of a random one. Moreover, our measure is based on the median instead of the mean of a distribution of differences in the observable. Yet, the interpretation of a high absolute impact is comparable to that of a high (absolute) mean *elementary effect* (the sensitivity measure in Morris, 1991), as is the interpretation of a large interquartile range of the difference distributions to that of a large standard deviation of the elementary effect.

5.2.9 RMSD minimization with a genetic algorithm

Alternatively to the coarse parameter grid search, we also used optimization by a genetic algorithm (Mitchell, 1998) to validate the minimum RMSD. To this end, the turboGA function was used (Matlab file exchange; settings: population size 1000, 150 generations, 8 bit discretization, initial conditions uniformly random). For the Q_{10} parameter range used here, the minimum RMSD identified by the genetic algorithm was very close to the minimum value on the grid (0.21 for the genetic algorithm, 0.22 on the grid). On average the coordinates of the grid-based minimum deviated 5% from the coordinates of the genetic algorithm-based minimum.

5.2.10 Dimensional stacking

Dimensional stacking is a method to visualize high-dimensional data, that is, an observable f as a function of N parameters, $p_1, ..., p_N$, evaluated at a discrete set of parameter values. The method is described in detail, for categoric observables, in LeBlanc et al. (1990) and Taylor et al. (2006). Mainly, the method maps the N-dimensional data to a two-dimensional representation by iteratively slicing the data in one dimension and stacking the slices in 2D (Figure 5.4*C*;

also see introductory Figure A.1*A*). In this representation, the position of each pixel in the two-dimensional image corresponds to one parameter combination, and its color encodes the value of the observable. The image has N axes of different scales, each associated with one parameter. Visual informativeness of a dimensional stacking image crucially depends on the order in which the dimensions are stacked, that is, the *axes order*. The parameter dimensions associated with larger variability in the observable should be assigned larger-scale axes; those with lowest variability the small-scale axes. Sorting the axes with respect to their impact on the observable prior to dimensional stacking hence leads to a visually informative image, where color changes can be easily related to changes of the observable with individual parameters. In this thesis, we used the ranking of absolute impact scores (described above) to define the optimal stack order, extending the optimization method described in LeBlanc et al. (1990) and Taylor et al. (2006).

5.2.11 Model robustness

The sensitivity analysis was performed with the Connor–Stevens model with original parameters for peak conductances at the colder temperature (Dayan and Abbott, 2005). To test that our results are robust and do not strongly depend on this specific parameter choice, we additionally performed the whole sensitivity analysis on the RMSD and the f-I gain and threshold for 24 models with peak conductances of the reference model perturbed by ±20% (8 models with one individual peak conductance lowered or raised by 20%, and 16 models with all combinations of the four conductances either lowered or raised by 20%). Comparisons of the impacts for unperturbed and perturbed models are summarized in Figure 5.5*B-D* (individual changes in peak conductances represented by black symbols, combined changes by gray ones). Note that for computational efficiency only three values per parameter (instead of four) were taken. The fraction of model Q_{10} parameter combinations resulting in RMSD < 0.5 was 18% in the original Connor-Stevens model. Variations in peak conductances did not change this finding much: for each perturbed model 15-19% of its temperature dependence combinations gave RMSD < 0.5.

For completeness, we also checked that a structurally different vertebrate model with type I dynamics (Traub-Miles, Traub et al., 1991, as defined in Benda, 2002) was able to display temperature compensation despite a substantial temperature dependence of individual conductances[1] (Figure A.2).

[1] that is, the same range of temperature dependencies as used for the parameters of the Connor-Stevens model

The search for the lowest temperature dependence within the parameter space[2] was performed based on the genetic algorithm described above. As the model operates at 32°C, we checked both heating and cooling the model by 10°C.

5.2.12 Reverse-engineering the mechanosensory transduction and its temperature dependence

For a given pair of a receptor neuron response $r = \rho(I_{\mathrm{dB}})$ (Equation 5.1) and a spike generation model $r = \phi(I_C)$, the transduction function (i.e., current I_C vs. sound intensity I_{dB}) can be inferred. We assumed a sigmoidal shape of the transduction function,

$$I_C = \Theta(I_{\mathrm{dB}}) = I_{C,\mathrm{sat}} / \left(1 + \exp\left(-\frac{I_{\mathrm{dB}} - I_{50,\Theta}}{w_\Theta}\right)\right),$$

with transduction saturation current $I_{C,\mathrm{sat}}$, half-maximum sound intensity $I_{50,\Theta}$, and dynamic-range width w_Θ. Further, we chose representative parameters of a receptor neuron response. To this end, the median cold temperature, $\bar{T}_{\mathrm{c}}$, the median receptor neuron response parameters at cold temperature, $\bar{p}_\rho \in \{\bar{r}_{\mathrm{sat}}, \bar{I}_{50,\rho}, \bar{w}_\rho\}$, and the median temperature dependencies of the three receptor neuron response parameters, $\bar{Q}_{10}(p_\rho)$, were determined from the experimental data. Using these, receptor neuron response parameters were inferred for temperatures of 18 and 28°C (the temperatures at which spike generation simulations were performed), according to

$$p_{\rho,T} = \bar{p}_\rho \cdot \left(\bar{Q}_{10}(p_\rho)\right)^{\frac{T-\bar{T}_{\mathrm{c}}}{10}}.$$

The two resulting representative receptor neuron response functions were used as objective functions for reverse engineering of the transduction curve.

To infer the three parameters characterizing the optimal transduction curve for a given spike generation model $r = \phi(I_C)$, we computed

$$r = \phi(\Theta(I_{\mathrm{dB}})) = A \cdot \mathrm{Re}\sqrt{I_{C,\mathrm{sat}} / \left(1 + \exp\left(-\frac{I_{\mathrm{dB}} - I_{50,\Theta}}{w_\Theta}\right)\right) - I_0}\,.$$

[2] spanned by the temperature dependencies of the sodium and potassium kinetics, $Q_{10}(m)$, $Q_{10}(h)$, $Q_{10}(n)$, and of the peak sodium, potassium, and leak conductances, $Q_{10}(\bar{g}_{\mathrm{Na}})$, $Q_{10}(\bar{g}_{\mathrm{K}})$, $Q_{10}(\bar{g}_{\mathrm{L}})$

The transduction parameters were chosen such that they minimized the root mean squared error between $\phi(\Theta(I_{\mathrm{dB}}))$ and the representative receptor neuron response $\rho(I_{\mathrm{dB}})$:

$$\Theta(I_{\mathrm{dB}}, \text{optimal}) = \underset{\Theta(I_{\mathrm{dB}})}{\arg\min}\{\int |\rho(I_{\mathrm{dB}}) - \phi(\Theta(I_{\mathrm{dB}}))|^2 dI_{\mathrm{dB}}\}$$

This fitting procedure was repeated for all hot and cold spike generation processes, and the temperature coefficients for the three transduction parameters were computed. Since the spike generation at 18°C was unique, there was also just one set of corresponding transduction parameters:

$$I_{C,\mathrm{cold}}(I_{\mathrm{dB}}) = 0.40\mu\mathrm{A\,mm^{-2}}/\left(1 + \exp\left(-\frac{I_{\mathrm{dB}} - 57.91\mathrm{dB}}{2.69\mathrm{dB}}\right)\right).$$

5.3 Results

5.3.1 Temperature dependence of receptor neuron spike rates

Based on recordings of auditory receptor neurons in the metathoracic ganglion of the grasshopper *Locusta migratoria*, we quantified the dependence of the firing rate on temperature. Figure 5.1*A* shows voltage responses to stimulation at three different sound intensities and two different temperatures, as well as spike shapes. Interestingly, spike rates at a given sound intensity did not differ much between the low and high temperatures and mildly increased from low to high temperature, while spike width decreased. In general, firing rates of grasshopper receptor neurons are relatively high, saturating only at several hundreds of Hz. At a given temperature, the transfer function, that is the firing rate as a function of sound intensity, has a sigmoidal shape (Figure 5.1*B*). Three parameters (*saturation rate*, *half-max sound level*, and *dynamic-range width*) are sufficient to capture the experimental transfer functions (coefficient of determination $R^2 > 0.95$ for all response curves). Comparing transfer functions at the two different temperatures revealed that their temperature dependence was surprisingly low (Figure 5.1*C*): all corresponding median Q_{10} values were below 1.5; the sound intensity at half-maximal response (half-max sound level) remained almost unchanged, as did the median of the slope at half-max sound level. The width of action potentials, in contrast, was lower at the higher temperature.

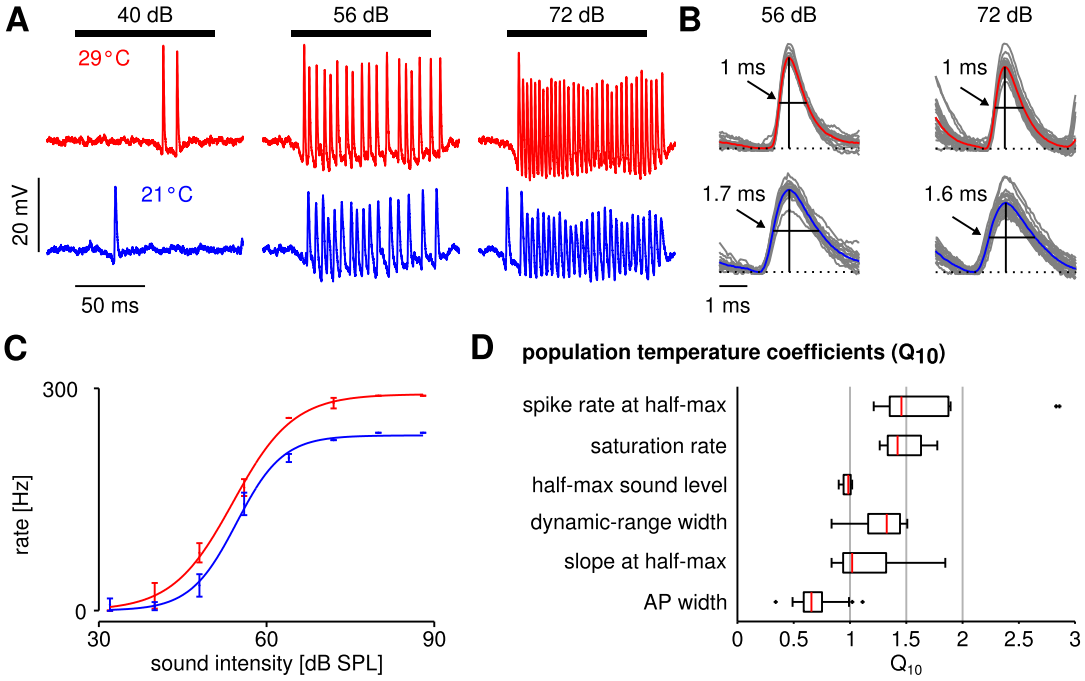

Figure 5.1 Cooling mildly affected electrophysiologically recorded firing rates generated by auditory receptor neurons in response to sound. **A:** Voltage traces at 29°C and 21°C for one neuron (red and blue lines, respectively). Black horizontal lines mark time intervals of stimulus presentation; stimulus intensity as indicated. **B:** Action potentials (grey) and average spike waveforms from *A* (red and blue, respectively). **C:** Firing-rate as a function of sound intensity was well described by sigmoidal functions at both temperatures (same neuron as in *A*). The three sigmoidal parameters (saturation rate, sound level at half-maximum, and dynamic-range width) were extracted from fits to the experimental data. **D:** Statistics of the measured temperature dependence, $Q_{10}(x) = \left(\frac{x(T+\Delta T)}{x(T)}\right)^{10/\Delta T}$, were computed for several quantities x. For a population of nine receptor neurons all three parameters of the sigmoidal function, as well as the spike rate and slope at the cold half-maximum were temperature compensated (median $Q_{10} \in [1, 1.5]$)

Compared to the temperature dependencies previously observed in other species like moth auditory receptor neurons, locust stretch receptors, and fly H1 neurons and photoreceptors (Q_{10}(spike rate) $\approx$ 2, Pfau et al., 1989; Coro and Perez, 1990; Warzecha et al., 1999; Tatler et al., 2000), the grasshopper responses were temperature compensated; the dependence was similar to what has been referred to as *warm-insensitive* in hypothalamic neurons of the rat (Q_{10}(spike rate) $\approx$ 1.3, Curras and Boulant, 1989). To understand this low dependence of receptor neuron firing rate on temperature, we next turned to mathematical modeling.

5.3.2 Mechanisms underlying temperature compensation of spike rates in conductance-based neuron models

The grasshopper auditory periphery consists of a relatively simple feed-forward network, in which the receptor neurons constitute the first layer (see Section 2.2 and Figure 2.2*B*,*C*). Receptor neurons are known to respond to vibrations of the tympanal membrane, but they do not receive input from the neuronal network. Mechanisms of temperature compensation must hence be cell-intrinsic. Since two intrinsic processes, that is, mechanosensory transduction and spike generation, shape the receptor neuron response (cf. Figure 5.2*A*), there are two candidate mechanisms to account for temperature compensation of the response curve: Either, transduction and spike generation are temperature compensated themselves. Then the response curve would be temperature compensated as well (Figure 5.2*B*). Or, transduction and spike generation are both temperature dependent, in a way that results in temperature compensation at the level of the response curve (cf. Figure 5.2*C*). To resolve which intrinsic processes can be sufficient to account for the observed degree of temperature compensation, we first focused on spike generation, to return to mechanotransduction at a later point. We analyzed in generic model neurons how the temperature dependence of ionic conductances mediating spike generation can reduce the dependence of firing rate on temperature.

We used the Connor–Stevens model (Connor et al., 1977; Dayan and Abbott, 2005) to simulate a type I spike generation process (Izhikevich, 2007) as it is assumed for grasshopper receptor neurons (Benda, 2002). Besides a sodium and a leak conductance (g_{Na} and g_{L}), this model comprises a delayed-rectifier and an A-type potassium conductance (g_{K} and g_{A}), which are both known to be present in the grasshopper nervous system (Ramirez et al., 1999). Temperature dependence was assumed to affect the opening and closing rates of all gates of the three ion channel types (i.e., the m and h gates for g_{Na}, n gates for g_{K}, a and

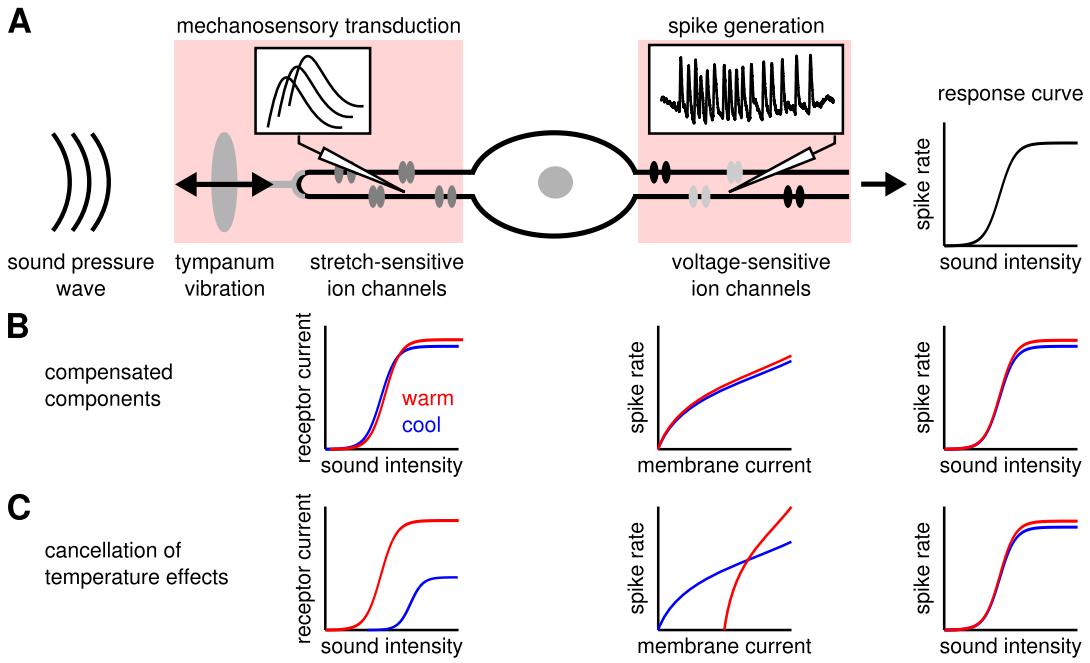

Figure 5.2 Two hypotheses to explain cell-intrinsic temperature compensation. **A:** The experimentally recorded spike rate vs. sound intensity curves of receptor neurons result from two cellular processes: first, mechanosensory transduction via stretch-sensitive ion channels, which converts vibrations of the tympanum to receptor current, and second, spike generation via voltage-sensitive ion channels, which converts membrane current to action potentials. Hence, temperature compensation of the receptor neuron response curve can either be due to **B:** individual compensation of mechanosensory transduction and spike generation, or **C:** cancellation of opposing temperature effects on transduction and spike generation.

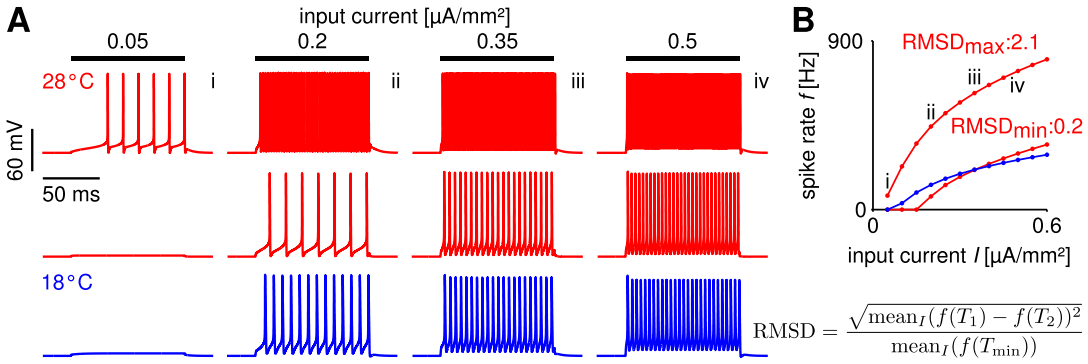

Figure 5.3 Temperature compensation of spike generation in a conductance-based neuron model. **A:** Voltage responses to step current stimuli of different amplitudes; blue: 18°C (the reference temperature), red: 28°C. Top trace corresponds to a model with strongly temperature-dependent firing rate, middle trace to a temperature-compensated model. **B:** f-I curves at both temperatures, corresponding to the examples shown in *A*. Overall temperature dependence of the f-I curve was quantified as the Root Mean Squared Distance (RMSD) between hot and cold f-I curves, normalized by the average spike rate elicited at colder temperature.

b gates for g_A), as well as their peak conductances ($\bar{g}_{Na}$, $\bar{g}_K$, $\bar{g}_A$) and that of the leak conductance, $\bar{g}_L$. For a systematic analysis[3], we independently varied the temperature dependence of these parameters[4] within physiologically realistic ranges (see Table 5.1 for values; Partridge and Connor, 1978; Hille, 2001). For each combination of parameters, the transfer function[5] was computed at two temperatures: 18 and 28°C (Figure 5.3*A,B*).

To estimate the temperature dependence of a whole f-I curve, Q_{10} values are not ideal, as they are defined as the ratio of firing rates at two different temperatures, which will be infinitely large for inputs that only elicit spikes at the higher, but not the lower temperature. To circumvent this bias, we assessed the temperature dependence of a model neuron as the Root Mean Squared Distance (RMSD) between the firing rates at the two temperatures[6], normalized by the mean rate elicited at the colder temperature. The RMSD reflects the average relative change in firing rate with temperature. Note that a Q_{10} value of 1.5 is hence comparable to an RMSD of 0.5 (50% relative change). Across all model combinations, the RMSD was distributed between 0.22 and 2.14, with a median of 0.68 (Figure 5.4*A*). This means that, intuitively, the median of the average change in firing rate of an f-I curve was 68%. The analysis showed that the effect of temperature on spike generation depended strongly

[3] cf. Prinz et al. (2003)
[4] comprising a total of nine
[5] input current to firing rate; that is, the f-I curve
[6] mean taken across input currents

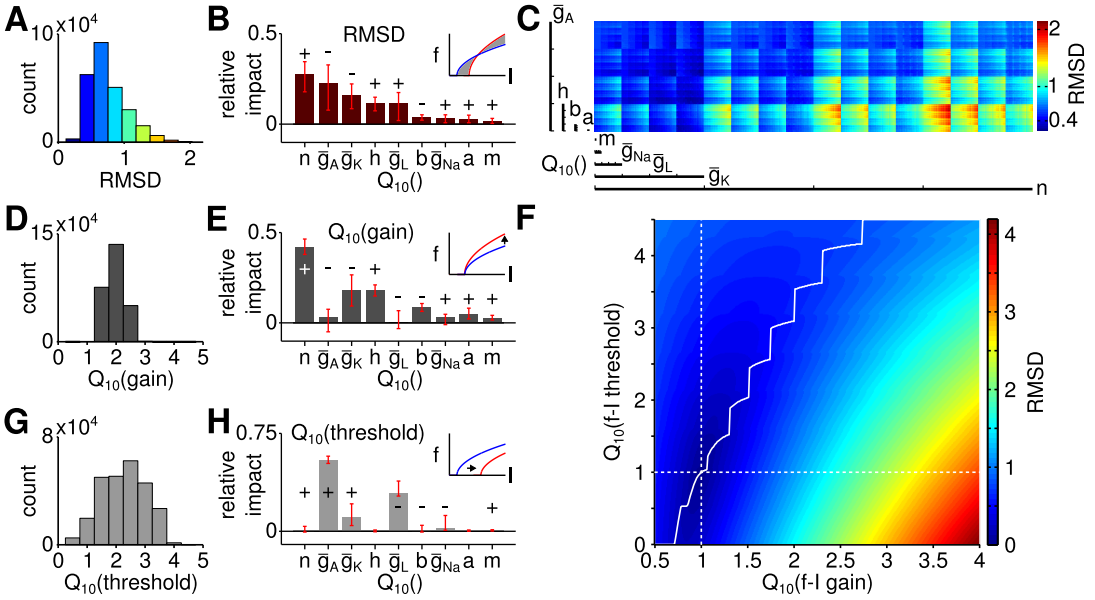

Figure 5.4 Sensitivity analysis revealed crucial parameters for temperature compensation. **A:** Temperature dependence of the f-I curve (RMSD) varied strongly, depending on the temperature dependencies of the ionic conductances. **B:** Sensitivity analysis identified parameters of the potassium conductances as key players in determining the RMSD. **C:** Visualization of the RMSD as function of the nine temperature dependence parameters, using dimensional stacking according to Taylor et al. (2006). The order of the axes was optimized using the parameter impact ranking in *B*. **E, H:** Temperature could affect the gain and the threshold of the f-I curve. To attribute conductance parameter impacts on the RMSD to impacts on f-I gain and threshold, sensitivity analysis was performed for these two f-I parameters. f-I gain exclusively increased with heating (**D**), while f-I threshold could both increase or decrease (**G**). **F:** Analytical evaluation of the RMSD as function of Q_{10}(f-I gain) and Q_{10}(f-I threshold). To minimize the RMSD for an increase in f-I gain, f-I threshold had to increase as well. Solid white line marks the values of Q_{10}(f-I threshold) that minimize a given Q_{10}(f-I gain).

on the specific temperature dependence of the ionic conductances. A fraction of models (18%) exhibited temperature compensation with relative changes in firing rate comparable to those found experimentally (RMSD < 0.5). This result shows that a low dependence of firing rate on temperature is feasible despite a substantial (and hence realistic) dependence of the individual conductances on temperature.

Next, we asked which of the nine parameters (i.e., the temperature dependence of peak conductances and transition rates) most affected the dependence of firing rate on temperature. To this end, we performed a systematic sensitivity analysis in the nine-dimensional space of all possible parameter combinations. We created – for each parameter – a distribution of local changes in RMSD

induced by changes in that parameter. Specifically, this distribution captured changes in RMSD between all neighboring points along a specific parameter's dimension. Each distribution sampled the whole parameter space (i.e., all possible combinations of the other parameters; see Section 5.2). The impact of a given parameter on the temperature dependence of the f-I curve was then defined as the median of its specific distribution, directly relating the impact of a parameter to its quantitative effect on RMSD. Figure 5.4*B* depicts the impact values of all Q_{10} parameters on the RMSD. The sum of all absolute values of impacts is normalized to unity. The impact sign, that is whether an increase in a parameter on average led to an increase or decrease in the observable, is indicated by + and -, respectively. The analysis revealed that the largest impact on the RMSD was exerted by three parameters related to potassium channels: temperature dependence of the delayed-rectifier potassium kinetics, $Q_{10}(n)$, and the A-type and delayed-rectifier potassium peak conductances, $Q_{10}(\bar{g}_{\mathrm{A}})$ and $Q_{10}(\bar{g}_{\mathrm{K}})$, respectively. The impacts of both potassium channel peak conductances were negative (i.e., increases in their Q_{10} values decreased the RMSD), while the potassium activation $Q_{10}(n)$ had a positive impact (i.e., increases in its temperature dependence increased the RMSD).

To confirm that the results did not strongly depend on the specific choice of peak conductances in the Connor-Stevens model, we tested 24 alternative models with changes of ±20% in the peak conductances of sodium, both potassium, and leak channels (see illustration in Figure 5.5*A*). The impact ranking across those models was highly similar to the ranking in the original Connor-Stevens model (Figure 5.5*B*) and we conclude that our results are robust. Moreover, we note that our results are not unique to the Connor-Stevens model. An analysis of a structurally different Traub-Miles model (Traub et al., 1991; Benda, 2002) showed that an equally low temperature dependence is possible (Figure A.2).

On a side note, a visualization of the RMSD across the complete nine-dimensional parameter space based on dimensional stacking (LeBlanc et al., 1990; Taylor et al., 2006; see Section 5.2 for details and Figure A.1 for an introductory illustration) is shown in Figure 5.4*C*. Dimensional stacking maps the nine-dimensional space onto a two-dimensional representation with nine axes. Ordering of the axes is arbitrary and hence requires optimization to maximize visual information Taylor et al. (2006). Here, we introduce a new way to determine optimal axes order, defined directly by the ranking of impact scores. Parameters with highest impact on the RMSD are depicted on large-scale axes and parameters with low impact on small-scale axes. The success of the ordering is reflected in the visually structured areas of equal RMSD. As only a subset of all parameters had relevant influence on the RMSD, optimal

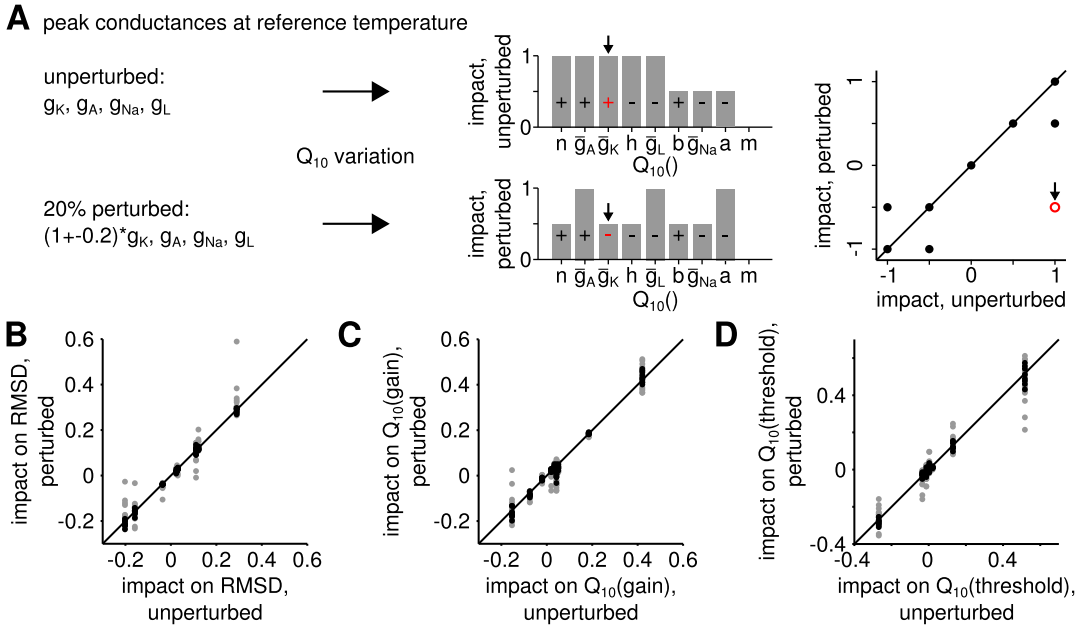

Figure 5.5 Sensitvity analysis results were robust against conductance perturbations at the reference temperature. **A:** Illustration of the perturbation method. Sensitivity analysis was repeated for ±20% perturbations of the peak conductances at 18°C, and the resulting parameter impacts were compared by means of correlation. Either single peak conductances were perturbed, or all possible combinations of all four peak conductances. **B-D:** Parameter impacts for perturbed and unperturbed conductances were highly correlated for the RMSD, Q_{10}(f-I gain), and Q_{10}(f-I threshold). Black dots denote perturbations of single conductances, grey dots mark combined perturbations.

axes ordering led to a clear visual structure. In contrast, for arbitrary axes ordering visual structure would be hard to recognize (cf. Figure A.1).

Temperature effects on f-I threshold and gain

As we saw, the temperature dependence of potassium channels plays a crucial role for temperature compensation. For a more detailed and intuitive understanding of the underlying mechanism, we next analyzed the transformation of the shape of f-I curves with changes in temperature. Type I f-I curves, as they are found in the grasshopper, can be described by a square root function $f(I) = A \cdot \mathrm{Re}\left(\sqrt{I - I_0}\right)$ (Izhikevich, 2007). Here, I_0 denotes the threshold current (or rheobase), that is, the minimum current to drive the neuron suprathreshold, and A is the gain. Temperature can hence change the f-I curve via affecting the threshold or the gain. We fitted a square root model to f-I curves at both temperatures and found that with heating, the gain always increased (Fig-

ure 5.4*D*), while the threshold could either decrease or increase with heating (Figure 5.4*G*).

Temperature dependencies of the A-type potassium and leak peak conductances had the strongest influence on the threshold (Figure 5.4*H*). In contrast, the gain was most sensitive to the temperature dependence of the delayed-rectifier potassium channel, $Q_{10}(n)$ and $Q_{10}(\bar{g}_{\mathrm{K}})$, and the sodium channel inactivation, $Q_{10}(h)$ (Figure 5.4*E*). Beyond clarifying the specific effect of the aforementioned parameters on changes to the f-I curve, the analysis shows that temperature compensation (i.e., low RMSD values) was usually achieved by modest increases in threshold balancing the effects of an increase in gain (Figure 5.4*F*). Note that these results were robust against 20% perturbations of the conductances at 18°C (Figure 5.5*C*,*D*).

Changes in gain also have direct implications for the ability to infer information about the sound intensity from the firing-rate output of receptor neurons. We hence quantified how the capacity to transmit information from input I to firing rate f changes with temperature. To this end we used Fisher information. Considering the average information transferred for a given interval of firing rates $[f_{\mathrm{min}}, f_{\mathrm{max}}]$, information transfer scales with the gain of the f-I curve and its temperature dependence hence with $Q_{10}(A)^4$ (see Appendix A.2 for details). Consequently, the same parameters that had the largest impact on the gain – potassium channel activation ($Q_{10}(n)$) and peak conductances ($Q_{10}(\bar{g}_{\mathrm{K}})$, $Q_{10}(\bar{g}_{\mathrm{A}})$), and sodium channel inactivation ($Q_{10}(h)$) – also influenced information transfer most. Overall, heating was hence advantageous for information transfer.

Model-based inference of the mechanosensory transduction function

In the previous paragraphs, we have shown that spike generation by itself can achieve a remarkable level of robustness to temperature changes. The receptor neurons, however, have an additional processing stage involved in transferring the external input signal to a firing-rate response: the so-called transduction mediated by the mechanosensitive channels in the vicinity of the tympanal membrane (Figure 5.2*A*). Transduction precedes spike generation and translates vibrations of the tympanal membrane caused by the sound pressure wave into receptor currents through these channels, which in turn drive spike generation (Gollisch and Herz, 2005). This mechanism may also contribute to temperature compensation. We therefore explored how temperature compensation can benefit from linking spike generation with the transduction process.

Little is known about the temperature dependence of transduction in the grasshopper. Here, we combined the computational analysis of spike generation

with the experimental findings for the sound-intensity to firing-rate relation in order to predict on a phenomenological level which features of the auditory transduction and its temperature dependence would improve temperature compensation. The experimentally measured receptor neuron responses to sound stimuli $r = \rho(I_{\mathrm{dB}})$ can be expressed as a cascade of mechanosensory transduction ($I_{\mathrm{C}} = \Theta(I_{\mathrm{dB}})$, with current I_{C} and sound intensity I_{dB}) and spike generation $\phi(I_{\mathrm{C}})$:

$$r = \phi(I_{\mathrm{C}}) = \phi(\Theta(I_{\mathrm{dB}})).$$

Now consider the Connor-Stevens spike generation model at the colder temperature (illustrated in Figure 5.6*A*, blue curve). When combined with an (upstream) nonlinear translation of sound intensity to current (Figure 5.6*B*, blue curve), it yields the full sound-intensity to firing-rate relation (Figure 5.6*C*, blue curve), which corresponds to the experimentally measured response curve. Hence, if the receptor neuron response as a function of sound intensity is known from experimental data and we assume a specific spike generation model (i.e., a specific f-I curve), we can mathematically infer the transduction nonlinearity that gives the best match to the experimentally recorded sound-intensity to firing-rate relation by nonlinear regression (Figure 5.6*C*, blue curves). We use the term *reverse engineering* for this approach. It can be used at the higher temperature as well and enables us to derive for each of the more than 260.000 spike generation models the corresponding ideal transduction curve that best matches the experimentally recorded sound-intensity to firing-rate relation at this higher temperature (Figure 5.6*B*,*C*, red curves). Comparing the reverse-engineered transduction curve at the colder temperature to the reverse-engineered curve at the higher temperature (for each spike generation model), allows us to identify trends in the temperature dependence of mechanotransduction, which would foster a temperature robustness of the firing rate.

Specifically, we exploited the fact that experimental response curves (firing rate to sound intensity) were well fitted by a sigmoidal function (Figure 5.1*C*) and also assumed a sigmoidal shape for the transduction curves (Hudspeth et al., 2000; Fisch et al., 2012). Accordingly, we reverse-engineered the ideal transduction sigmoid at the warmer temperature for each spike generation model (e.g., those contributing to Figure 5.4*A*-*C*), so that the resulting sound-intensity to firing-rate relation best matched a representative receptor neuron response (Figure 5.6*C*; for details on representative receptor neuron response, see Section 5.2). The model response curves $r = \phi(\Theta(I_{\mathrm{dB}}))$ matched the experimental representative response curve very well ($R^2 > 0.98$ for 99.5% of all

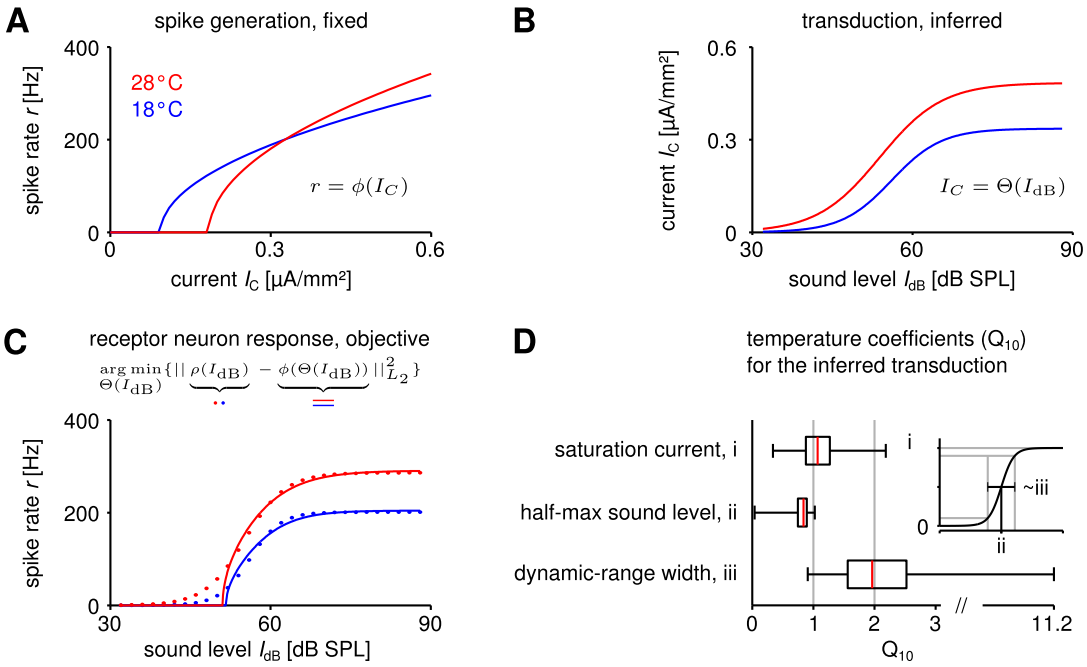

Figure 5.6 Reverse engineering mechanosensory transduction functions that favor temperature compensation of firing rate. **A:** Example of a model-based f-I curve, denoted $r = \phi(I_C)$, at two temperatures. **B:** Example of a sigmoidal transduction function converting sound intensity to current, $I_C = \Theta(I_{dB})$. **C:** Representative receptor neuron responses, $r = \rho(I_{dB})$, at two temperatures (dotted lines), as well as a receptor neuron response, $r = \phi(\Theta(I_{dB}))$, constructed from the f-I curve in *A* and the transduction function in *B*. For each model of spike generation, the optimal transduction function, $I_C = \Theta(I_{dB})$, minimizing the error between the corresponding constructed receptor neuron response and the representative receptor neuron response (dotted line in *C*) was derived. **D:** The statistics of temperature dependence of the optimal transduction functions, $\Theta(I_{dB})$, across all models. The width of the dynamic range depended most on temperature and increased with heating for nearly all optimized transduction functions. But the temperature dependence of the saturation current and the half-maximum sound intensity (mainly when decreasing with temperature) were also found to contribute to temperature compensation. Note that the ranges marked by the whiskers cover all data (including outliers) in this plot.

models). Temperature dependence of the reverse-engineered transduction was then quantified based on the Q_{10} values (i.e., the relative changes with temperature) of the three parameters that define each transduction sigmoid: *saturation current*, *half-maximum sound intensity*, and *dynamic-range width* (Figure 5.6*D*).

Evaluating the distribution of changes of the ideal transduction curves with temperature across all spike generation models, we found that the largest temperature dependence of these *matching* transduction curves was to be expected for their dynamic-range width (median $Q_{10} \approx 2$). In addition, changes in saturation current and half-maximum sound level also contributed to fostering temperature compensation of firing rate (Figure 5.6*D*). These results show in particular that a suitable temperature dependence of the transduction process can support temperature compensation, even in cases where spike generation is less robust to changes in temperature (nb.: this mechanism corresponds to a *cancellation of temperature effects* on transduction and spike generation as outlined in Figure 5.2*C*).

5.4 Discussion

We studied the temperature sensitivity of firing rate in individual neurons of the grasshopper auditory periphery and found responses to auditory stimulation to be surprisingly temperature compensated. Based on biophysically-motivated neuron models, we identified mechanisms that account for the experimentally observed cell-intrinsic temperature compensation. Our theoretical analysis suggests that spike generation itself can be relatively temperature insensitive, even though the conductances involved are affected by temperature changes. In general, the capacity to transmit rate-based information of sound intensity moderately increased with temperature due to the increase in steepness of the f-I curve. We also predict optimal temperature dependencies of the tympanum-mediated transduction process from sound to receptor current that contribute to temperature compensation. On a side note, we introduced a computationally efficient way to optimize visualization of model-derived observables in a high-dimensional parameter space in the context of dimensional stacking (LeBlanc et al., 1990; Taylor et al., 2006).

5.4.1 Temperature dependence of firing rate in single neurons

Neuronal processing is significantly challenged by variation in temperature due to the associated changes in chemical and physical processes. In many neurons across invertebrates and vertebrates, firing rate has been observed to at

least double with increases of temperature, corresponding to Q_{10} values of two or above (French and Kuster, 1982; Coro and Perez, 1990; Warzecha et al., 1999). It was hence surprising to observe that neurons in the auditory periphery of grasshoppers show Q_{10} values on the order of 1.5 and consequently are remarkably temperature compensated (Hazel and Prosser, 1974; Boulant and Dean, 1986). The temperature robustness of these neurons is hence comparable to that of *warm-insensitive* neurons in the mammalian brain (Curras and Boulant, 1989).

Temperature compensation has been studied in the context of neurons embedded in a network in a variety of systems (see, e.g., Wechselberger et al., 2006; Tang et al., 2010; Robertson and Money, 2012). Temperature compensation in grasshopper receptor neurons, by comparison, must be based on cell-intrinsic processes. A similar temperature compensation that must be based on a single-cell mechanism has so far – to our knowledge – only been described experimentally for tarsal hairs in the locust (Miles, 1985).

The cell-intrinsic mechanisms identified in our computational study attribute the observed robustness to a balancing of opposing processes. Phenomenologically, a rise in gain (consistent throughout the explored parameter range) is compensated for by an increase in the threshold of the f-I curve, minimizing the effect of temperature across a broader range of inputs. While alterations in threshold can be produced by changes in peak conductances of ion channels, they have also been described experimentally by heating in invertebrate systems (Burkhardt, 1959; Abrams and Pearson, 1982; Kispersky et al., 2012) in agreement with our observations. Biophysically, a heating-induced increase in the speed of repolarizing gating kinetics is opposed by an increase in peak potassium conductances which promote a more negative resting potential (as can be derived from Equation 6.1). Although the balancing is not perfect, average deviations on the order of not more than 50% can be easily achieved with strongly temperature-dependent conductances[7] for around 18% of the models. The temperature dependence of both delayed-rectifier and A-type potassium channels has a particularly large impact on temperature compensation. This matches experimental observations in neurons of the pancreas of mice (Xu et al., 2006) and molluscan neurons as well as previous simulations of an extended Hodgkin-Huxley model (Rush and Rinzel, 1995) and is consistent with the effect of peak conductances on firing rate, for example (Schreiber et al., 2004). Our results also hold for reference models quantitatively different from the original Connor-Stevens model – both for the total fraction of temperature-compensated models (RMSD <0.5) and the strong influence of potassium channel dynamics

[7] in particular, $Q_{10} \in [2;4]$ for all activation- and inactivation rates

on the temperature dependence of firing rate (Figure 5.5). These findings show that our results generalize beyond the specific quantitative choice of peak conductance parameters of the Connor-Stevens model. This is further supported by the fact that a structurally different Traub-Miles model could also exhibit a temperature dependence of firing rate as low as that described for the Connor-Stevens model.

5.4.2 Benefits of temperature compensation at the receptor neuron level

Auditory receptor neurons in the grasshopper constitute the bottom layer of a feedforward network: approximately 80 receptor neurons converge to around 15 local neurons, which in turn project to approximately 20 ascending neurons (Vogel and Ronacher, 2007). All auditory input passes through this peripheral network, which preprocesses information and extracts behaviorally-relevant features (Clemens et al., 2011). The large investment into high firing rates and a comparatively high redundancy between neurons in this layer (Machens et al., 2001) also increases the need for energy-efficient spike generation. Optimization of receptor neurons in terms of temperature compensation hence seems a reasonable strategy, as all effects of temperature on receptor neurons will be passed on to downstream neurons, where they may multiply. Although we currently do not know to which extent other parts of the auditory system are compensated, constraining the effects of temperature in the initial stages is likely to pay off. Downstream neurons, in contrast, may be expected to adopt different strategies, as they can make use of different mechanisms: balancing of inhibition and excitation for robustness to temperature changes (Robertson and Money, 2012) as well as an increase in population and temporal sparseness for energy efficiency and information transfer (Clemens et al., 2012). This will be addressed in Part II of this thesis.

6 What is the cost of cell-intrinsic temperature compensation?

[1] The results presented in the preceding Chapter 5 suggest that the encoding of sound intensity in the spike rates of auditory receptor neurons in the grasshopper is robust against temperature changes. Such robustness is important, because it allows the grasshopper to utilize the neuronal representation of sound intensity for computations related to courtship or predator avoidance. We proposed that temperature robustness of spike generation can be achieved at single-neuron level, exclusively due to cell-intrinsic effects. Specifically, robustness was achieved in simulated neurons via balancing the realistic temperature dependencies of different ionic conductances. As a result, we identified a parameter region of distinct ionic conductances that produced a similar spiking phenotype in different models after a change in temperature.

The *net* membrane current that underlies the neuronal action potential can be realized with an infinite amount of superpositions of different currents. Different realizations, however, consume different amounts of energy via using the sodium-potassium pump[2] to expel the sodium that entered the neuron during an action potential. Energy consumption is an established constraint for neural function (Attwell and Laughlin, 2001; Niven and Laughlin, 2008), therefore we next asked to what extent a tuning of ionic conductances for temperature compensation of spike rates impairs neuronal energy efficiency.

6.1 Measures of energy consumption and efficiency

6.1.1 Spiking regime

Energy consumption per spike was quantified as the total sodium current (also termed sodium load; Hasenstaub et al., 2010; Sengupta et al., 2010) between

[1] This chapter is based on Roemschied et al. (2014).
[2] also referred to as Na-K-ATPase

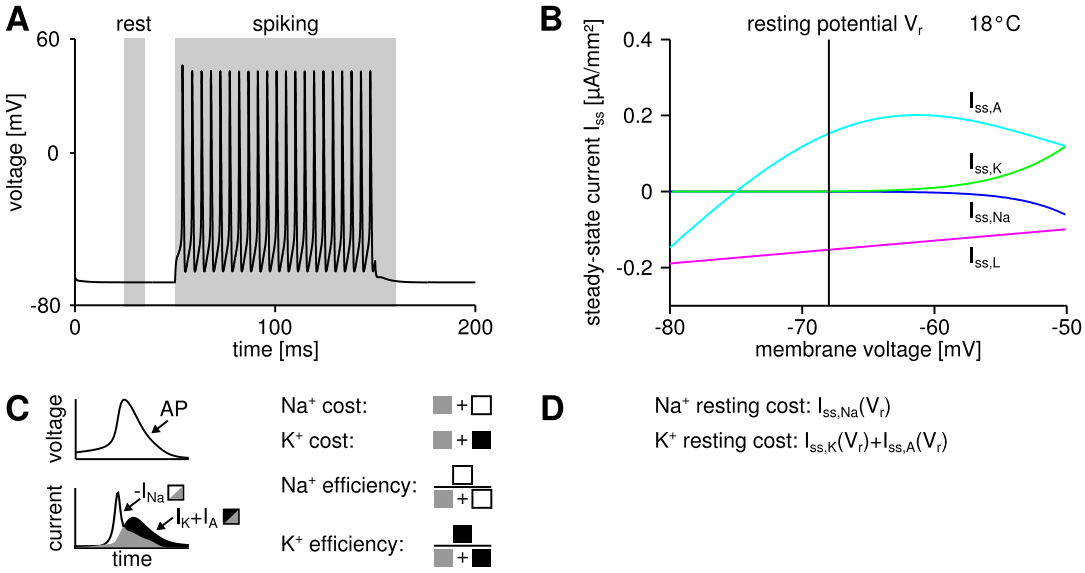

Figure 6.1 Measures of neuronal energy consumption and efficiency. **A:** Regimes of neuronal rest and spiking. **B:** Steady-state ionic currents for the four conductances of the Connor-Stevens model at 18°C. **C:** Single action potential with underlying sodium and potassium currents, and definitions of the spiking energy measures. **D:** Definitions of the resting energy measures.

stimulus onset t_{start} and 20 ms post stimulus offset t_{stop}, divided by the number of spikes elicited during this period, N_{s}:

$$\text{Na}^+\text{load/spike} = \int_{t_{\text{start}}}^{t_{\text{stop+20 ms}}} I_{\text{Na}} dt / N_{\text{s}}.$$

Considering that the Na-K-ATPase consumes one ATP molecule per extrusion of 3 Na^+ ions, this quantity is proportional to the number of ATP molecules per spike. The $Q_{10}(\text{Na}^+\text{load/spike})$ averaged across all input currents was used for further analysis (and referred to as Q_{10}(spiking cost), Figure 6.1*A*,*C*).

In addition, a measure of energy efficiency based on the separation of charges, that is, the fraction of the sodium current that was not counterbalanced by a simultaneous potassium current, was implemented (Crotty et al., 2006, cf. Figure 6.1*C*). As for estimation of the sodium-current-based cost, the stimulus period and the following 20 ms were evaluated. Note that the potassium current in the model comprised two components, $I_{\text{K,total}} = I_{\text{K}} + I_{\text{A}}$. Temperature effects on energy efficiency (estimated by the corresponding Q_{10} values) were highly similar to the inverse of those on spiking energy consumption.

Finally, both measures – the current-based cost and the charge-separation-based energy efficiency – were also implemented based on the potassium current instead of the sodium current. In other words, spiking cost was additionally quantified by the total potassium current, energy efficiency based on the fraction of the potassium current that was not counterbalanced by the sodium current.

6.1.2 Resting regime

According to the formalism proposed by Falk and Gerard (1954), the resting potential V_r of the Connor-Stevens model is given by

$$V_\mathrm{r} = \frac{E_\mathrm{A} \cdot g_\mathrm{A}(V_\mathrm{r}) + E_\mathrm{L} \cdot \bar{g}_\mathrm{L} + E_\mathrm{K} \cdot g_\mathrm{K}(V_\mathrm{r}) + E_\mathrm{Na} \cdot g_\mathrm{Na}(V_\mathrm{r})}{\bar{g}_\mathrm{L} + g_\mathrm{A}(V_\mathrm{r}) + g_\mathrm{K}(V_\mathrm{r}) + g_\mathrm{Na}(V_\mathrm{r})}. \tag{6.1}$$

The numerical solution of this expression for $V\mathrm{r}$ was used to evaluate the sodium current at rest,

$$I_\mathrm{Na,rest} = g_\mathrm{Na}(V_\mathrm{r}) \cdot (E_\mathrm{Na} - V_\mathrm{r}),$$

which defines the sodium-current based cost of the resting potential (assuming the current is proportional to the activity of the Na-K-ATPase at rest, cf. Figure 6.1*B*,*D*). Likewise, the potassium-current based cost is defined by

$$I_\mathrm{K\,,rest} = g_\mathrm{K}(V_\mathrm{r}) \cdot (E_\mathrm{K} - V_\mathrm{r}) + g_\mathrm{A}(V_\mathrm{r}) \cdot (E_\mathrm{A} - V_\mathrm{r}).$$

As the resting state is steady, the cost quantities do not depend on the gating variables' (in-)activation time constants and, consequently, the corresponding Q_{10} values do not have an impact on Q_{10}(resting cost).

6.2 Results

6.2.1 Temperature dependence of neuronal energy efficiency during rest and spiking

Metabolic cost is increasingly recognized as an important constraint for neural function (Attwell and Laughlin, 2001; Niven and Laughlin, 2008) and is likely to have shaped the design of neural systems – the more so if firing rates are large. In the grasshopper auditory periphery firing rates often exceed several hundred spikes per second, suggesting that metabolic cost may have played a role in the

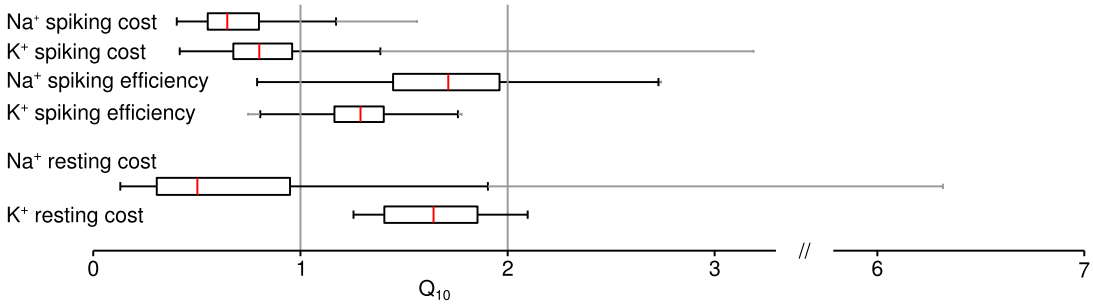

Figure 6.2 Temperature dependence of sodium and potassium based energy measures during rest and spiking. On average, neuronal energy consumption decreased and efficiency increased with increasing temperature during spiking activity, both for sodium and potassium based measures. At rest, the sodium and potassium based costs had opposite temperature dependencies. This can be attributed to a combination of hyperpolarization of the resting potential and increase in peak conductance at elevated temperatures (cf. Figure 6.4*A*), which on average increased the A-type steady-state current (the key player in potassium based resting cost) but decreased the sodium steady-state current (the key player in sodium based resting cost)

design of these cells. It is hence interesting to explore whether robustness to temperature changes compromises energy efficiency. To this end, we computed the energetic cost of spike generation and maintenance of the resting potential (Figure 6.1). Cost was quantified in terms of the total sodium current (per action potential or per time, respectively). To assess the changes of energy consumption with temperature, energy use was characterized by its Q_{10} value (here i.e., the ratio of energetic cost at 28 and 18°C) and averaged across input currents. For the majority of models, the energetic cost of an action potential decreased with heating (93% of models, Figure 6.2 and Figure 6.4*B*). On average, temperature-compensated spike generation models (25% of models with lowest RMSD) were slightly more costly than the most temperature-dependent models (25% of models with highest RMSD). Nevertheless, the minimum energy consumption was comparable in both groups. Resting cost was substantially lower than spiking cost, this trend increasing with higher firing rates. Sodium-current based resting cost tended to decrease with heating (77% of models, Figure 6.2 and Figure 6.4*A*). It was slightly lower for temperature-compensated models compared to strongly temperature-dependent models.

The sensitivity analysis (performed in analogy to the analysis of temperature dependence of firing rate in Chapter 5) revealed that the temperature dependence of the sodium conductance influenced energy consumption and efficiency of spike generation the most (Figure 6.3*A*).

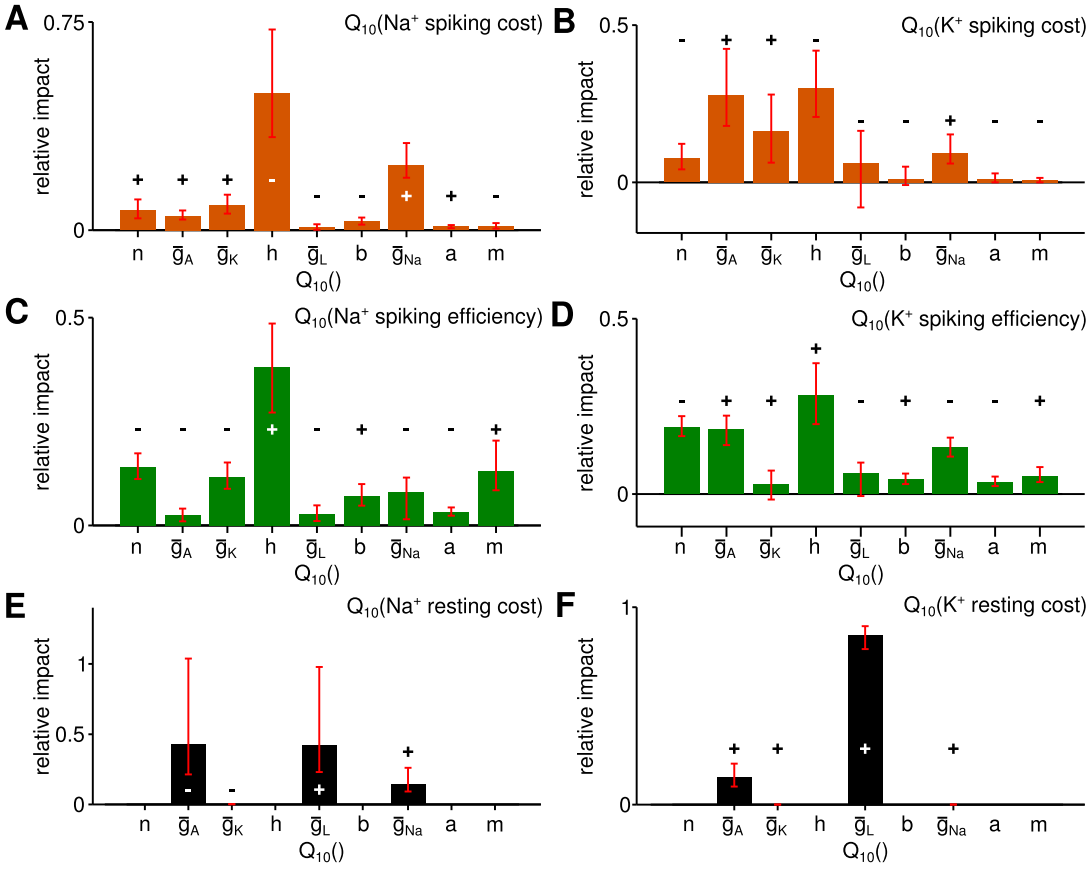

Figure 6.3 Sensitivity analysis to reveal parameter contributions to neuronal energy consumption and efficiency during rest and spiking. **A-D:** The temperature dependence of sodium inactivation was most influential on the temperature dependence of all *spiking* cost and efficiency measures. **E, F:** The temperature dependence of the leak and A-type potassium peak conductances had the strongest influence on sodium and potassium based *resting* cost. An increase in A-type potassium peak conductance with heating had opposite effects on sodium and potassium based resting cost. For the sodium cost, this can be ascribed to the associated hyperpolarization of the resting potential, which reduces the sodium steady-state current. For the potassium cost, the increase in the A-type steady-state current that is due to the increase in peak conductance outweighs the decrease in A-type steady-state current that is due to the hyperpolarization of the resting potential (cf. Figure 6.4*A*).

The impacts of conductance parameters on f-I curve temperature dependence and energy consumption were not significantly correlated in this case ($\rho = -0.23$, $p = 0.56$). In particular, the key parameters of largest influence on these features belonged to different channel groups: potassium channels in case of temperature compensation and sodium channels in case of energy efficiency of spike generation. We verified that the large influence of sodium channels was not biased by our sodium-current-based definition of metabolic cost. Three alternative measures – two quantifying energy efficiency based on the separability of sodium and potassium currents (Alle et al., 2009), the other defined by the total potassium current – all confirmed the temperature dependence of sodium channel inactivation $Q_{10}(h)$ as the most influential parameter for spiking cost (Figure 6.3*B-D*).

The sodium-current based resting cost was qualitatively influenced in a similar way as temperature dependence of firing rate (Figure 6.3*E*): for all four relevant Q_{10} parameters a reduction of resting cost co-occurred with a reduction in temperature dependence of firing rate (same sign of corresponding impacts, Figure 5.4*B*). For a potassium-current based resting cost the temperature dependence of leak channels had the dominant impact (Figure 6.3*F*). In contrast to the sodium-current based resting cost, the potassium-current-based cost was larger at higher temperatures. For the majority of models, inactivation of A-type potassium channels was lower at rest at the higher temperature (due to a more negative resting potential, cf. Figure 6.4*A*) and hence increased the A-type current. In summary, striving for temperature compensation does not have to compromise a neuron's energy efficiency. Both results (for spiking and resting cost) generalize beyond the specific choice of peak conductances in the Connor-Stevens model (Figure 6.5; robustness analysis according to Section 5.2.11).

6.3 Discussion

For auditory receptor neurons in the grasshopper, energy efficiency of spike generation is likely to be a relevant factor (cf. Niven and Farris, 2012). Firing rates in these cells approach 400 Hz and likely entail a high total cost of electrical signaling. Our results, however, show that temperature compensation need not impair energy efficiency of spike generation nor of maintenance of the resting potential. The rate of sodium channel inactivation (Figure 6.3*A*,*B*) proved to be most relevant in setting the energy consumption per spike generated, which is consistent with simulations and dynamic clamp experiments in various model systems (Alle et al., 2009; Hasenstaub et al., 2010; Sengupta et al., 2010). We

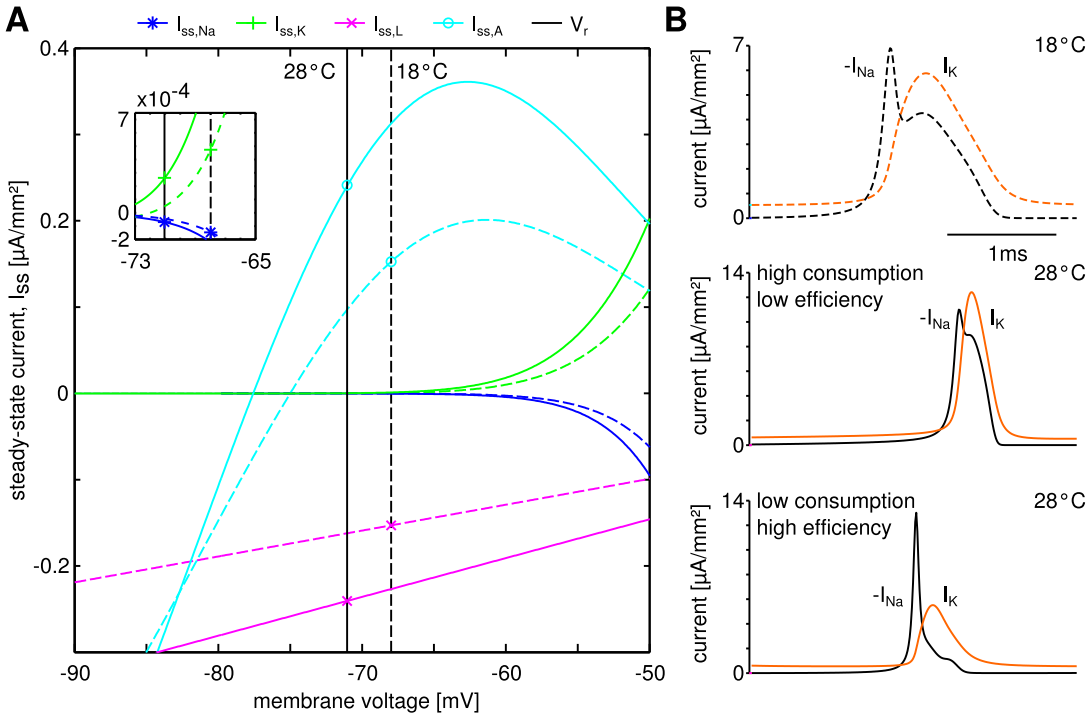

Figure 6.4 Temperature dependence of neuronal energy consumption and efficiency. **A:** Temperature dependence of the steady-state ionic currents at rest (using $Q_{10}(\alpha, \beta) = 3, Q_{10}(\bar{g}) = 1.5$). Black vertical lines indicate the resting potential. Solid and dashed lines correspond to 28 and 18°C, respectively. Note that here heating increases the magnitude of the A-type potassium and leak currents but decreases the magnitude of the delayed rectifier potassium and sodium currents (inset), which explains the qualitative difference between the sodium and potassium based Q_{10}(resting cost) (cf. Figure 6.2). **B:** Sodium and potassium current traces at different temperatures for the parameter configurations with highest and lowest energy consumption during spiking. Note the difference in overlap and amplitudes of potassium and sodium currents between the efficient and inefficient example.

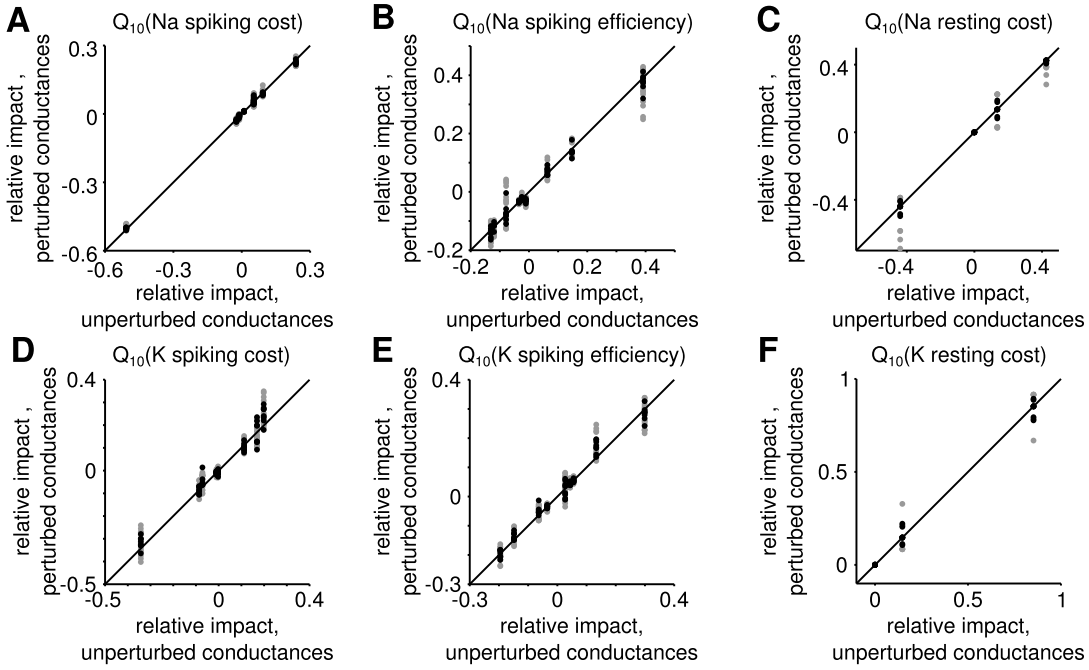

Figure 6.5 Sensitvity analysis results for neuronal energy consumption and efficiency were robust against perturbations of peak conductances at reference temperature. Following Figure 5.4, black and grey dots denote results for single-parameter- and combined perturbations, respectively. Perturbed vs. unperturbed sensitivities are shown for $Q_{10}(\mathrm{Na}^+$ spiking cost) (**A**), $Q_{10}(\mathrm{Na}^+$ spiking efficiency) (**B**), $Q_{10}(\mathrm{Na}^+$ resting cost) (**C**), $Q_{10}(\mathrm{K}^+$ spiking cost) (**D**), $Q_{10}(\mathrm{K}^+$ spiking efficiency) (**E**), and $Q_{10}(\mathrm{K}^+$ resting cost) (**F**).

demonstrated that energy efficiency improved with heating for a wide range of temperature dependencies of ion channels, as was previously described for a model with fixed Q_{10} values (Yu et al., 2012). A fast sodium inactivation limits the duration of the spike; this was consistent with the experimental data, as spike width decreased with heating (Figure 5.1*B*,*D*). Importantly, the key parameter regulating the energy efficiency of spiking played only a minor role in regulating temperature compensation of firing rate (Figure 5.4*B*, Figure 6.3*A*-*D*).

Apart from confirming the role of sodium channel inactivation, the analysis substantiated that the delayed- rectifier potassium channel kinetics (which were most influential to the robustness of firing rate) did not substantially contribute to metabolic costs based on potassium currents. Overall, our analysis focused on a major source of metabolic cost: the flow of Na^+ and K^+ ions which on larger time scales can be compensated by the Na-K-ATPase.

For completeness it should be noted, however, that in living cells metabolic costs can also arise from the flow of other ions not included in this thesis, like Ca^{2+}. Summarizing the considerations on metabolic cost, we find most noteworthy that from an evolutionary perspective, the relevant features – robustness of firing rate to temperature changes and reduction of metabolic cost – could both be achieved in parallel.

Part II

Neural models of behavior

7 Is cell-intrinsic temperature compensation general to the grasshopper's auditory system?

[1] In the preceding Part I of this thesis we saw that poikilotherms can maintain neuronal function across temperatures, solely using cell-intrinsic mechanisms. For the model organism considered here, the grasshopper, we found evidence for cell-intrinsic temperature compensation at the level of auditory receptor neurons. Notably, temperature compensation was not perfect, that is, there was a small effect of temperature on spike rates. If multiple neurons with compensation mechanisms similar to that proposed for the receptor neurons were connected in a network, this small effect could be amplified with every synapse, resulting in a stronger temperature dependence.

Moreover, neurons downstream in the network serve highly specific tasks, compared to the encoding of sound intensity in spike rate that is found at receptor-neuron level (Clemens et al., 2011). Such specific tuning is thought to arise from an intricate mix of excitatory and inhibitory inputs (Marquart, 1985; Stumpner and Ronacher, 1991; Clemens et al., 2012). It is unclear to what extent changes in temperature affect the balance of inhibitory and excitatory inputs, and whether a small temperature dependence of presynaptic neurons can disrupt specific tuning in postsynaptic neurons, with potentially detrimental effects on song recognition. In the following, we will hence quantify the effect of temperature on the stimulus preference of ascending neurons, two synapses downstream of the receptor neurons. Ascending neurons play a prominent role in song recognition, as they relay relevant sound information to the brain (cf. Section 2.2). Thus, in the following we shift the focus from the level of single neurons to the systems and behavioral levels.

[1] This chapter is based on joint work with Sarah Wirtssohn and Bernhard Ronacher (Humboldt-Universität zu Berlin). I am particularly grateful to Sarah Wirtssohn who performed the electrophysiological recordings. I was involved in study design, developed analytical tools, performed data analysis, and interpreted the results.

7.1 Introduction

Variable ambient temperatures pose two problems for acoustic communication between grasshoppers: first, changes in the temperature of the sender induce a change in speed of courtship song, due to temperature dependence of muscle activity, and second, neural processing of courtship song in the receiver can be affected by changes in temperature, because the biophysical and chemical processes that underlie neuronal signaling depend on temperature (cf. Sections 2.1 and 2.2).

Experimental observations suggest that song recognition in female grasshoppers is robust across temperatures (von Helversen, 1972, cf. Figure 2.2*E*). This implies the existence of a mechanism to compensate for neuronal temperature dependence somewhere along the auditory processing chain. Whether this mechanism is cell-intrinsic, as observed for auditory receptor neurons (see Chapter 5), or implemented at the level of neuronal networks (as proposed in Robertson and Money, 2012), has not been addressed yet.

Therefore, we here experimentally study the effect of temperature on early auditory processing in the grasshopper. More specifically, we obtained extracellular recordings from ascending neurons, the behaviorally relevant third auditory processing stage, at different temperatures, during presentation of acoustic noise. From the extracellular spike trains, we characterized the properties of linear temporal filtering and nonlinear computations of the network up to the recorded neurons, using the spike-triggered analysis framework (Schwartz et al., 2006, see Chapter 4 for an introduction). The estimated neural temporal filters (STAs) were simple feature detectors, as indicated by their mainly uni- or bimodal shape, over the observed temperature range. In response to an increase in temperature, filters became narrower and tended to become more negative, which opposes the hypothesis that intrinsic temperature compensation is effectively used throughout the auditory processing chain, and which contrasts the robustness of song recognition across temperatures that is observed at the behavioral level. Yet, there was no consistent effect of temperature on the nonlinear computations performed by the network.

The apparent mismatch between the temperature dependence of sound processing in ascending neurons and the temperature robustness of song recognition at the behavioral level will be addressed and resolved in Chapter 8, using the results presented in this chapter.

7.2 Methods

For a description of the experimental methods, see Chapter 3.

7.2.1 Summary statistics

Unless noted otherwise, median ± Median Absolute Deviation (MAD) are reported as robust summary statistics for population results.

7.2.2 Spike sorting

Single units were identified in extracellular voltage traces using the spike sorting approach described in Franke et al. (2010), omitting the ultimate filter-based template matching. The main steps are summarized in the following. First, voltage traces were high-pass filtered (cut-off frequency 100 Hz), spikes were detected using a Multiresolution Teager Energy Operator (MTEO) (Choi et al., 2006), then cut, aligned, whitened, and projected onto the six first principal components to form a low-dimensional representation for sorting. To sort spikes into putative units, a Gaussian mixture model was fit to the low-dimensional data, using expectation maximization. Then, the optimal mixture model was determined, by minimization of the Bayesian Information Criterion (Schwarz, 1978) on mixtures between 1 and 15 clusters.

7.2.3 Probabilistic tracking of extracellular neuronal units across temperatures

Extracellular recordings consisted of two different types of segments: on the one hand, segments of nearly constant temperature, during which the stimuli for estimation and evaluation of the L-N model (Section 7.2.4) were presented. On the other hand, segments during which the temperature was slowly changed, which interleaved segments of different constant temperatures. The width of spike waveforms is known to decrease with heating, which impedes spike sorting and can bear the risk of losing units if the temperature is changed. We attempted to track unit identity across temperatures, using the following approach. Briefly, recording segments during which the temperature was slowly changed were divided into overlapping chunks during which the temperature within each chunk did not change by more than 2°C. Spike sorting was performed individually for each chunk. Here, the first and last chunk of a temperature tracking segment were combined with the preceding and following segment of constant temperature, respectively. To track units, sorting

results from the overlapping part of two consecutive chunks were compared: confusion matrices were formed, indicating for each unit in one sorting the absolute and relative amount of spikes that were sorted into the units of the other sorting. Then, a unit in the first sorting was considered as matching to another unit of the second sorting if at least 50% of its spikes were assigned to that unit of the second sorting. This step was performed in order of descending cluster size. Subsequently, units in the second sorting were re-labeled according to the respective matched units in the first sorting. If a unit of the second sorting shared an equal proportion of spikes with two units of the first sorting, the match was assigned to the larger unit of the first sorting (i.e., the unit containing more spikes).

7.2.4 Estimation of neural filters and nonlinear properties

Properties of linear temporal filtering and nonlinear computations performed by the network up to the recorded neurons were estimated by fitting a L-N model (see Section 4.2) to the extracellular spike trains of each identified single unit, separately for individual temperatures. Linear temporal filters (STA filters) were calculated following the procedures outlined in Clemens et al. (2012). The corresponding nonlinearities were computed according to the Ratio-of-Gaussians (RoG) approach described in Section 4.2.

To assess STA significance, 'mock' STAs were generated by shuffling the spike train for a given neuron. Each STA sample was tested for significance, using the following procedure: First, the z-score $z_i = (x_i - \mu_i)/\sigma_i$ was computed for each STA sample x_i, using the mean μ_i and standard deviation σ_i of that sample in the mock STA distribution. Then, those STA samples were considered significant whose z-scores exceeded ±3.7087. This value constitutes the z-score equivalent of a Bonferroni-corrected p-value of 0.01. The fraction of significant positive or negative samples for a given STA was used to compute significance variables for observables shown in Figure 7.3.

7.2.5 Mix-of-Gaussians (MoG) filter model

To capture the main modes of the STA filters, a normalized mix of two Gauss functions, f,

$$G(t|\mu_1, \mu_2, \sigma_1, \sigma_2, m) = m \cdot N(t|\mu_1, \sigma_1) - (1 - m) \cdot N(t|\mu_2, \sigma_2)$$
$$f(t|\mu_1, \mu_2, \sigma_1, \sigma_2, m) = \frac{G(t|\mu_1, \mu_2, \sigma_1, \sigma_2, m)}{\mathrm{norm}(G)}.$$

was fitted to each filter. Here, $\mu_{1,2}, \sigma_{1,2}$ denote the means and standard deviations of the two Gauss functions $N(t|\mu,\sigma) = \frac{1}{\sqrt{2\pi}\sigma} \cdot \exp\left(\frac{-(t-\mu)^2}{2\sigma^2}\right)$. m denotes the relative weight of the positive Gauss function, and t is time. norm(G) is the Euclidean (L^2) norm of the raw filter, G. In this thesis, m is used as a measure of filter *modality*, where $m = 0$ and $m = 1$ indicate purely negative or positive filters, while $m = 0.5$ indicates a perfectly bimodal filter. Further, filter *bias* is defined as $b = |2m - 1|$.

7.2.6 Validation of the linear-nonlinear model

The predictive performance ρ of the L-N model was evaluated following the approach of Petersen et al. (2008), as used in Clemens et al. (2012). In brief, ρ denotes the Pearson correlation between the spike rate predicted by the L-N model and the empirical spike rate, normalized by the correlation of the spike rate in response to two non-overlapping sets of identical stimuli. The normalization corrects for the bias in the raw correlation that is due to the noise in the spike rate response.

7.2.7 Quantification of temperature dependence

For all observables X bounded by zero, temperature dependence was assessed using a Q_{10} model (Equation 5.2). The reference temperature T_0 was chosen as the 0.5°C temperature bin between 15 and 35°C for which most data points were available. Q_{10} and $X(T_0)$ were estimated using least squares nonlinear regression. For fitting, each observable X was weighted by a significance variable, as defined in Table 7.1. The chosen significance weight variables penalized filters with only few significant samples or a shape that did not match a mix of two Gaussians. While the Full Width at Half-Maximum (FWHMax) or Full Width at Half-Minimum (FWHMin) required either significant positive *or* negative STA samples, the STA width (i.e., the time between positive and negative lobe) required significant positive *and* negative samples. Likewise, filter modality and the two nonlinearity parameters required significant positive *or* negative STA samples. In addition, the nonlinearity parameters required a good exponential fit.

For observables that could change sign (e.g., the x-offset of the nonlinearity, x_0, cf. Figure 7.3*E*), temperature dependence was quantified using Pearson's linear correlation coefficient between the observable and temperature.

An observable was considered temperature dependent if the 5-95% confidence interval of the Q_{10} fit did not include the value 1 (i.e., temperature

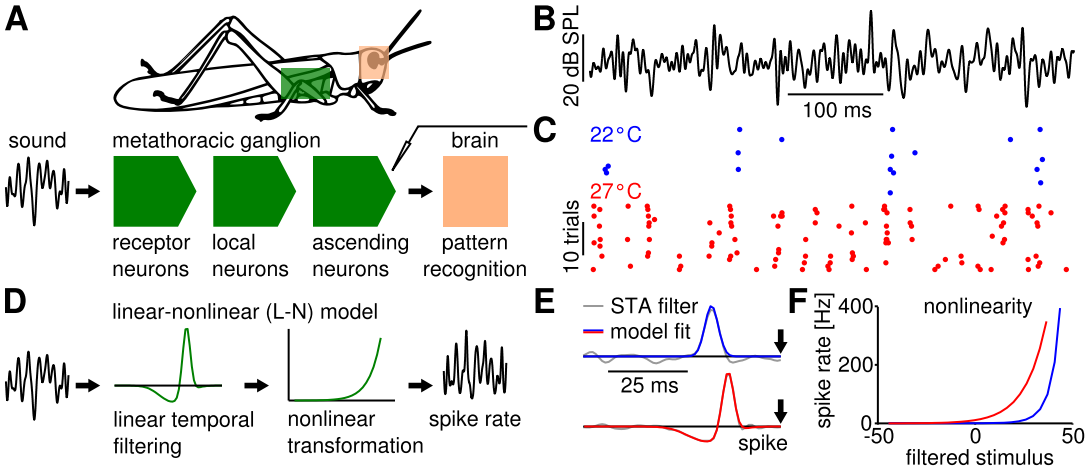

Figure 7.1 Estimation of ascending neuron stimulus preference from extracellular recordings. **A:** Experimental setup. Extracellular recordings were obtained from ascending neurons of the migratory locust during presentation of Randomly Amplitude-Modulated (RAM) acoustic noise. Ascending neurons constitute the third processing stage for auditory information and a bottleneck for signals going to the brain. Extraction of the stimulus (**B**) preceding each recorded spike (**C**) allows for estimation of the components of a L-N model (**D**). The L-N model consists of a linear temporal filter (the STA) that acts on the sound stimulus, and a static nonlinearity that transforms the filtered stimulus into spike rate. Neural filters (**E**) and nonlinearities (**F**) were estimated at different temperatures. A MoG model (blue and red lines in *E*) was fit to each filter (grey lines). Locust in *A* modified from Hildebrandt (2010).

invariance), or if the correlation of the observable and temperature was significant at the 0.05 level.

7.3 Results

Due to the prominent role of ascending neurons as a bottleneck in sound processing (cf. Section 2.2), we asked how the representation of sound at this level was affected by changes in temperature. To that end, extracellular recordings were obtained from ascending neurons at different temperatures during presentation of random sound-amplitude modulations (Figure 7.1*B,C*; see Methods for details). Spike sorting was used to identify single neuronal units at individual temperatures and, where possible, to track single units across temperatures (cf. Section 7.2.3). From the resulting spike trains of each neuronal unit at individual temperatures, neuronal filters (STAs) and nonlinearities (NLs) describing how a filtered stimulus is transformed into spike rate were estimated using the spike-triggered analysis formalism (Sections 4.2 and 7.2.6). A given STA and the corresponding NL constitute the two components of a L-N

model that can be used to predict the instantaneous spike rate of the recorded neuron to a novel stimulus (Simoncelli et al., 2004; Figure 7.1*D-F*). The average predictive performance of the L-N model[2] for all cells[3] amounted to 0.68 ± 0.18, which agreed with previous results for various local and ascending neurons in the same grasshopper species (Clemens et al., 2012). Lastly, temperature dependence was assessed for characteristic features of the neuronal filters, as described in the following. Note that in Chapter 8 the L-N model will be incorporated in a mathematical model of grasshopper behavior.

7.3.1 Auditory temporal filters are uni- or bimodal across temperatures

For various grasshopper species, the song envelope follows a simple syllable-pause structure, such that relevant information about sender identity must be contained in simple features such as syllable or pause duration, or syllable (pause) onset or offset (cf. Section 2.1). Intuitively, neuronal feature detectors should hence respond to simple amplitude-modulation patterns. Indeed, we found that most STA filters were uni- or bimodal, indicating a preference for increases, decreases, or changes in sound amplitude (relative to the mean). More specifically, STA filters were well described by a normalized Mix-of-Gaussians (MoG) model (Figure 7.2*E*; see Methods for details). The lobes of the Gaussians were separated, indicating that the filters were uni- or bimodal rather than of a 'Mexican hat' shape (Figure 7.2*A,B*). All filter properties for which temperature dependence was determined were extracted from MoG model fits. We refer to these fits as *filter* or *STA filter* in the following.

7.3.2 Temporal resolution of auditory processing increases with heating

The width of a temporal filter is indicative of the filter's temporal resolution, and correspondingly a maximal filter response can only be achieved for stimulus fluctuations of the time scale of the filter width or larger.

For each STA filter, the FWHMax and FWHMin, as well as the distance in time between negative and positive lobes (STA width) were determined.[4] Both

[2] That is, the normalized Pearson correlation between empirical and predicted spike rate; see Section 7.2.6 for details.

[3] That is, all $N = 101$ cells that produced spikes during presentation of the stimuli for model estimation *and* evaluation.

[4] Nb.: STA width was only defined for filters that had both a negative and a positive lobe; therefore, it could not be computed for perfectly unimodal filters.

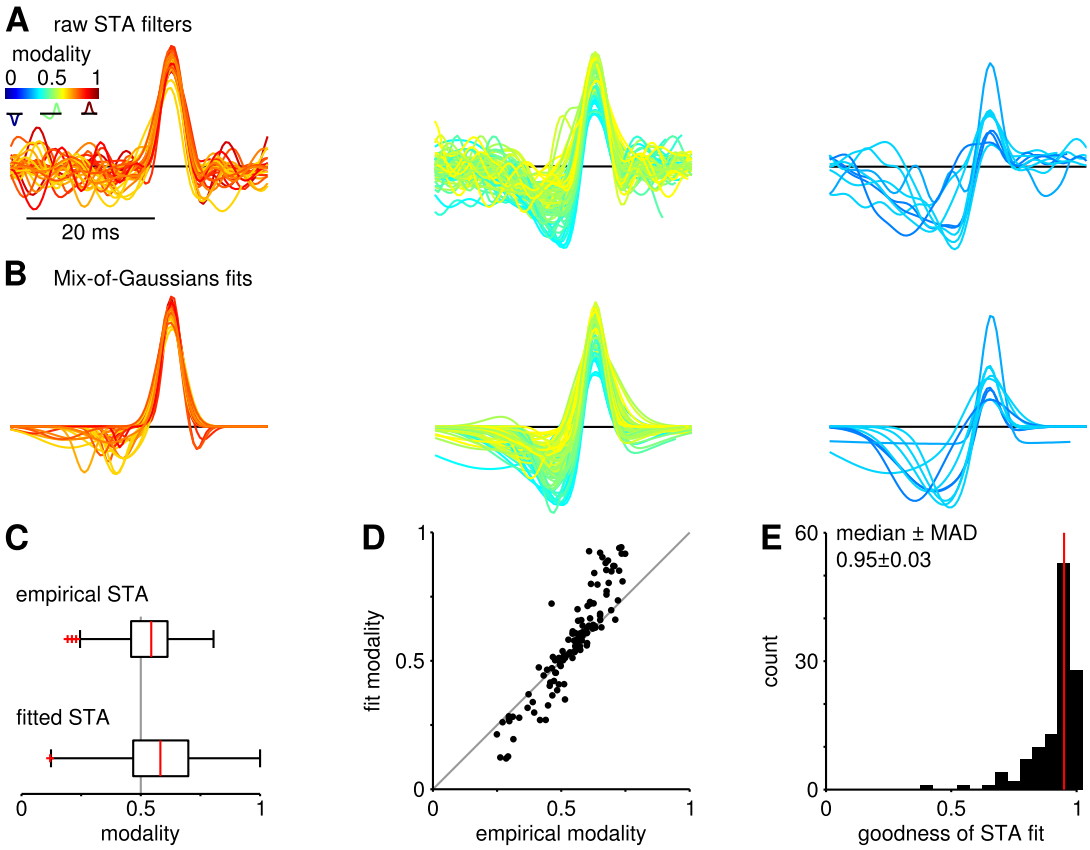

Figure 7.2 Temporal filters of ascending neurons at all recorded temperatures were uni- or bimodal. **A:** Raw filters, grouped by modality (i.e., the relative weight of the positive lobe) into positive, bimodal, and negative. Aligned to peak. **B:** MoG model fits to the filters in *A*. **C:** Modality distributions of empirical vs. fitted filters. Since the MoG model captures only the two main filter modes but not the noise, the modality range of fitted filters is larger. **D:** Modalities of raw and fitted filters were strongly correlated ($R = 0.92$, $P < 2\text{E-}49$). **E:** Goodness of MoG model fit was generally very high (0.95 ± 0.03, median ± MAD, $N = 120$).

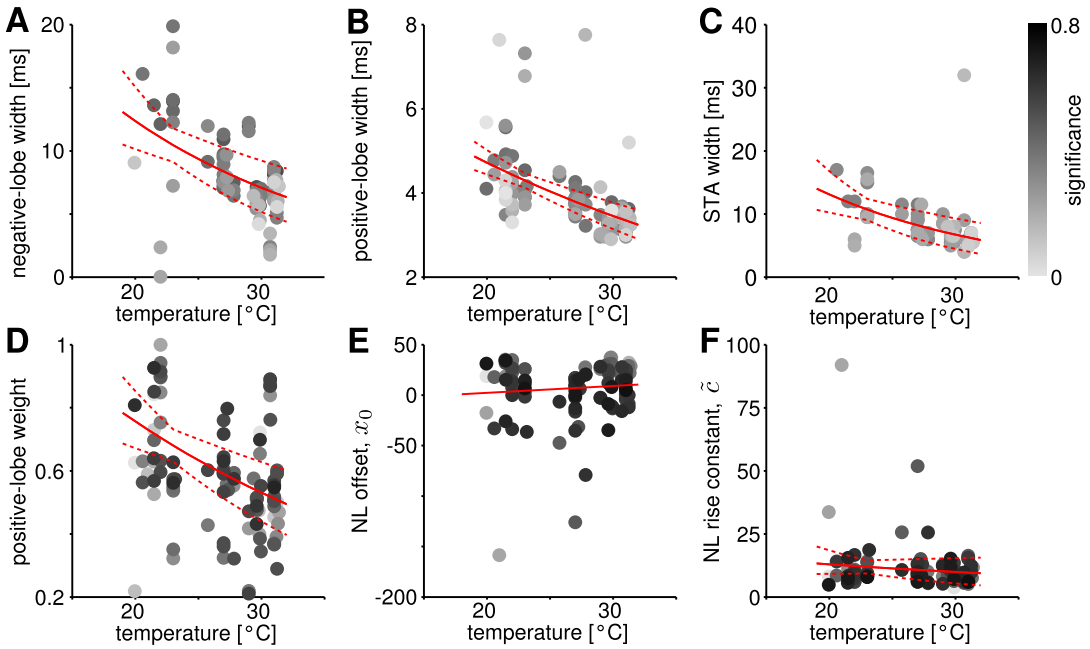

Figure 7.3 Temperature dependence of ascending neurons. Effect of temperature on the width of the negative and positive filter lobe (**A** and **B**, respectively), the peak-to-peak width (**C**), the relative weight of the positive lobe (**D**), and the offset and rise constant of the static nonlinearity (**E** and **F**). Red lines show Q_{10} model fits with 95% Confidence Intervals (CIs), except in *E*, where linear regression line is shown (see Table 7.1 for values). While filters on average became narrower and more negative with heating, nonlinearities were not consistently affected by changes in temperature.

single-lobe widths and the lobe-to-lobe distance decreased with heating at population level (Figure 7.3*A-C*; cf. Table 7.1 for Q_{10} values). Individual Q_{10} values for extracellular units that were tracked across temperatures were not distinguishable from the median population Q_{10} (p(median single-neuron Q_{10} = median population Q_{10}) > 0.05, signed rank test).

Concluding, the temporal resolution of ascending neurons increased with heating, which agrees with previous findings for receptor neurons and local interneurons in the same grasshopper species (Franz and Ronacher, 2002) and was expected given the increase in speed of ion channel opening and closing rates with an increase in temperature (Hille, 2001).

7.3.3 Temperature affects filter balance

For the uni- or bimodal STA filters the relative weight of the positive lobe, m (here termed *modality* of the filter), characterizes the response properties of the filter: While a filter with balanced positive and negative lobes ($m = 0.5$)

Table 7.1 Temperature dependence of ascending neurons and significance variables used as weights for Q_{10} model fits in Figure 7.3 and Figure 7.5.

Parameter	Symbol	Q_{10}	95% CI	Significance variable
Negative-lobe width	FWHMin	0.570	[0.44, 0.70]	$(\rho \cdot R^2 \cdot s^-)^{1/3}$
Positive-lobe width	FWHMax	0.730	[0.68, 0.79]	$(\rho \cdot R^2 \cdot s^+)^{1/3}$
Peak-to-peak width	w	0.510	[0.36, 0.66]	$(\rho \cdot R^2 \cdot s^- \cdot s^+)^{1/4}$
Relative positive-lobe width	w_r^+	0.950	[0.68, 1.20]	$(\rho \cdot R^2 \cdot s^- \cdot s^+)^{1/4}$
Filter modality	m	0.700	[0.60, 0.80]	$(\rho \cdot R^2 \cdot s_{\text{max}})^{1/3}$
Nonlinearity rise constant	$\tilde{c}$	0.770	[0.45, 1.10]	$(\rho \cdot R^2_{\text{NL}} \cdot R^2 \cdot s_{\text{max}})^{1/4}$
Nonlinearity offset	x_0	0.087[1]	0.39[2]	$(\rho \cdot R^2_{\text{NL}} \cdot R^2 \cdot s_{\text{max}})^{1/4}$

Correlation coefficient [1] and p-value [2].
ρ: predictive performance of the L-N model.
R^2, R^2_{NL}: goodness of fit, MoG filter model and exponential nonlinearity model, respectively.
$s^{\mp}$: fraction of significant negative/positive STA samples.
s_{max}: maximum value of $\{s^+, s^-\}$.

responds maximally to changes in the input, a biased filter responds maximally to constant stimulus segments of large positive or negative value relative to the mean stimulus ($m = 1$ or 0, respectively). Hence, balanced and biased filters can be called *differentiator*-like or *integrator*-like, respectively.

On average, filters became more negative with heating. Correspondingly, the relative weight of the positive lobe exhibited a decrease with heating at the population level (Figure 7.3*D*; Table 7.1). At single-unit level, this trend was consistent, although not statistically significant. Note that fitting the MoG model increased the modality range (Figure 7.2*C,D*), because the fits captured only the dominant filter lobes, not the small ones which are likely due to noise.

7.3.4 Temperature has no consistent effect on nonlinear processing of sound

The nonlinear stage of the L-N model of ascending neuron responses describes how the STA-filtered stimulus (i.e., the input to the nonlinearity) is transformed into spike rate.[5] For the majority of extracellular units presented here, the nonlinearities were monotonically increasing for most of the input interval (relative proportion of the monotonically increasing interval: $0.96 \pm 1.1\text{E-}16$; cf. Figure 7.4*A*). To quantify temperature dependence of the nonlinearity, we fit an

[5] For example, the nonlinearity specifies whether a stimulus that matches the shape of the filter (corresponding to a large input) elicits high or low spike rate.

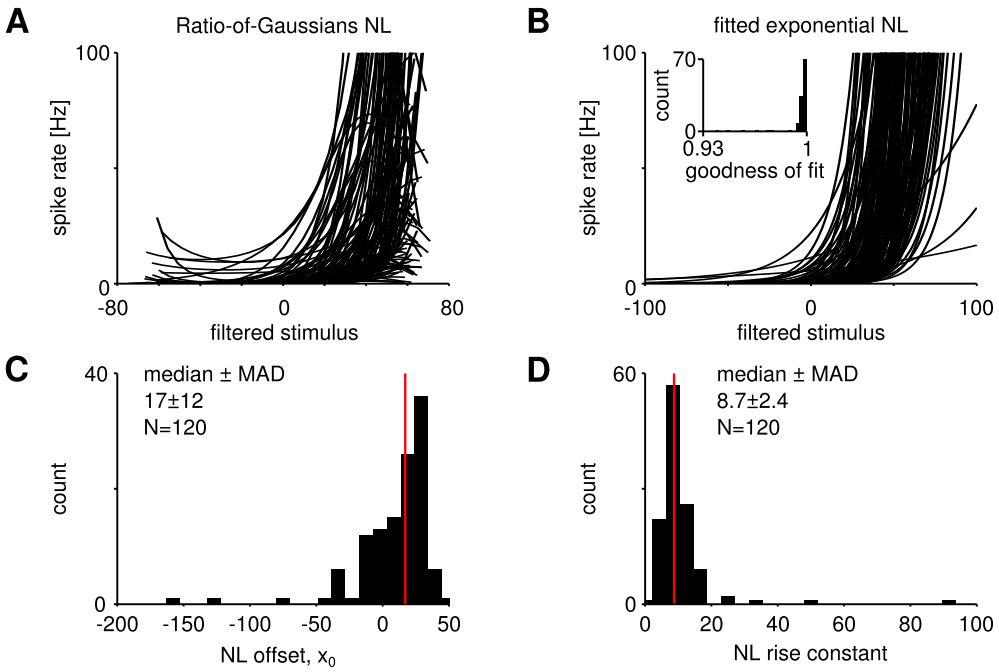

Figure 7.4 Static nonlinearities of ascending neurons at all recorded temperatures. **A:** Nonlinearities calculated according to the RoG formalism (see Methods for details). **B:** Exponential model fits to the nonlinearities in *A*. Inset shows the distribution of the goodness of fit, which was high for all nonlinearities.[a] **C,D:** Distribution of the offset parameter x_0 and the rise constant parameter $\tilde{c}$ of the exponential fit, pooled across all temperatures. Red lines mark the population median.

[a] Note that this was because the exponential fits were made on the input interval over which the RoG nonlinearity was monotonically increasing. The coefficient of determination for the *entire* input interval was 0.87 ± 0.13.

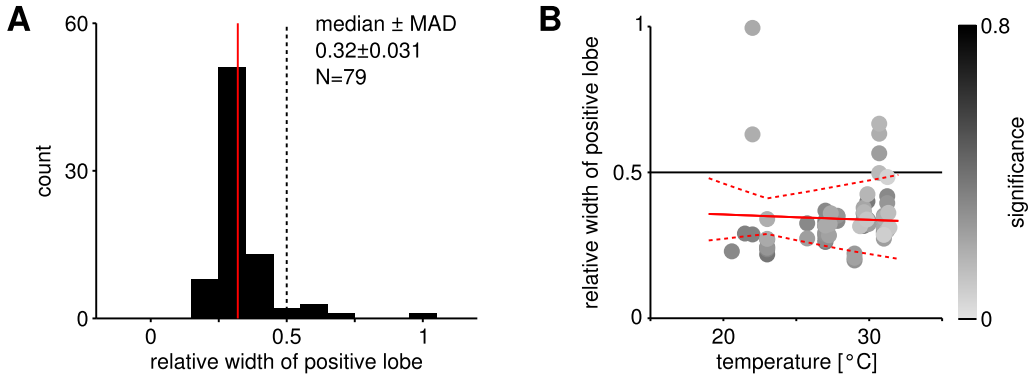

Figure 7.5 Relative filter-lobe width remained imbalanced across temperatures. **A:** On average, the positive filter lobe was narrower than the negative filter lobe (red line marks median; a relative width of 0.5 characterizes equally wide positive and negative lobes).[a] **B:** The relative width of the positive filter lobe was unaffected by changes in temperature.

[a] Nb.: the low N was due to the requirement of both a significant negative and positive lobe for calculation of the relative filter-lobe width.

exponential function to the increasing part of the nonlinearity, $r = \exp(\frac{x-x_0}{\tilde{c}})$ (Figure 7.4*B*) and determined the effect of temperature on each of the two fit parameters x_0 and $\tilde{c}$. Here, r denotes spike rate, and x denotes the filtered stimulus. x_0 is the input that elicits a spike rate of 1 Hz, $\tilde{c}$ is the rise constant of the nonlinearity (controlling its gain). Neither x_0 nor $\tilde{c}$ were consistently affected by temperature, both at population and single-unit level (Figure 7.3*E,F*; Table 7.1). Therefore, in Chapter 8 both parameters will be assumed constant across temperatures (if necessary, the measured median values are used; Figure 7.4*C,D*).

Concluding, there was no consistent effect of temperature on nonlinear processing in ascending neurons.

7.3.5 Imbalance of filter-lobe widths is maintained across temperatures

For the majority of the neural filters, the positive lobe was narrower than the negative lobe (Figures 7.2 and 7.5*A*), indicative of different temporal resolutions for distinct song features. This imbalance of lobe widths was maintained across temperatures (Figure 7.5*B* and Table 7.1). Therefore, the *relative* width of the positive and negative lobes will be assumed constant in Chapter 8.

7.4 Discussion

Here we tested whether the low degree of temperature dependence found in auditory receptor neurons of the grasshopper (Chapter 5) is a general characteristic of sound processing in the metathoracic ganglion. This would be in line with the temperature robustness of song recognition observed in previous experiments (von Helversen, 1972). In particular, we assessed the temperature dependence of sound processing at the level of ascending neurons. To that end, we first fitted L-N models to ascending neuron responses to sound, which were recorded at different temperatures. While the estimated linear stage of the L-N model[6] was modulated by temperature, the nonlinear stage[7] was not consistently affected by changes in temperature. More specifically, linear filters on average became narrower and more negative with heating, indicating a temperature dependence of sound processing in the grasshopper that contrasts the behaviorally observed robustness of song recognition across temperatures (von Helversen, 1972).[8]

7.4.1 Plausibility of the observed temperature effects

Temperature effect on filter width Physiological processes, such as the opening and closing of ion channels, speed up with heating (Hille, 2001). Therefore it is not surprising that the experimentally measured filters became narrower at higher temperatures. This agrees with a previous study in slices of chick nucleus laminaris, in which neural filters also became narrower with heating (Slee et al., 2010). Further, our results suggest that faster filters can resolve faster amplitude modulations. This is in line with previous findings of increased temporal resolution with heating in auditory receptor neurons, as well as local and ascending neurons of the grasshopper (Franz and Ronacher, 2002; Eberhard et al., 2015).

Possible mechanisms underlying the effect of temperature on filter modality Previous studies have characterized neural filters of local and ascending

[6] corresponding to the linear temporal filtering properties of the auditory network up to the recorded ascending neurons

[7] corresponding to the transformation of the filtered sound input to the spike rate of ascending neurons

[8] Note that for the present experiments migratory locusts were used, while the referenced robustness of song recognition was observed in *Chorthippus biguttulus*. Yet, an interpretation of experimental results in the locust with respect to auditory processing in *Ch. biguttulus* is valid, because the early stages of auditory processing are considered to be conserved across species (cf. Section 2.2).

neurons of the grasshopper only at single temperatures (Creutzig et al., 2009; Clemens et al., 2011, 2012). While filters of different local and ascending neurons recorded at 22°C were mostly positive (Clemens et al., 2012), ascending neuron AN12 had a negatively biased filter at 30°C (Creutzig et al., 2009).[9] While both studies are in agreement with our findings at individual temperatures, our results raise the question for a possible mechanism underlying the observed reduction in filter modality with heating.

In principle, either cell-intrinsic or network mechanisms can account for an increase in filter negativity with heating: Depending on the network structure, an increase in filter negativity can be interpreted as a net increase in inhibitory input or decrease in excitatory input that is necessary to elicit a spike. If less excitatory input is necessary to drive a neuron at higher temperatures, that means that the neuron's threshold decreases with heating. Such an effect of temperature on the neuronal threshold is biologically plausible, as evidence from single-neuron modeling suggests (see Chapter 5). Likewise, an increase in inhibitory input with heating is a biologically plausible mechanism to support spiking: it has been shown that brief inhibition preceding excitation can promote spiking (Dodla et al., 2006). The exact amount and timing of inhibition that best drive the postsynaptic neuron will depend on the neuron's excitability, which in turn can be temperature dependent (see Chapter 5).

Effectiveness of Inhibitory Post-Synaptic Potentials (IPSPs) decreases with heating, likely due to the faster potential dynamics with heating which in turn impede summation of IPSPs (Curras et al., 1991; Alger and Nicoll, 1982). If a more negative STA lobe corresponded to stronger inhibitory input, increased STA negativity could indicate that stronger activation of inhibitory inputs was required at higher temperatures, because of the decrease in inhibitory efficiency.

7.4.2 Cell-intrinsic temperature compensation is not a general feature of the grasshopper's auditory system

The results presented in this chapter suggest that the degree of temperature compensation found at the level of auditory receptor neurons is not present

[9] Note that in Creutzig et al. (2009), filters were computed using non-Gaussian stimuli, for which consistency of the STA framework is not guaranteed Chichilnisky, 2001; Paninski, 2003. The specific choice of stimulus statistics could also obfuscate a negative filter bias: the stimuli consisted of artificial grasshopper song, for which the probability of a loud sound is higher than that of a soft sound (because segments of high sound amplitude, that is, syllables, were chosen to have longer duration than segments of low sound amplitude, that is, pauses). Therefore it would be expected that a potential negative bias of the shown STA is underestimated.

at the level of ascending neurons. This does not necessarily imply that cell-intrinsic temperature compensation is not present in higher-order neurons: receptor neurons did not exhibit *perfect* temperature invariance, therefore the increased level of temperature dependence in ascending neurons could just be due to an amplification of the small intrinsic temperature dependence through a propagation of error within the network. To ultimately test the intrinsic temperature dependence of ascending neurons, intracellular recordings with current stimulation would be required.

Yet, the increased level of temperature dependence in ascending neurons contrasts the robustness of song recognition that is observed in grasshoppers at the behavioral level (von Helversen, 1972). To resolve this apparent mismatch between temperature dependence at the neuronal level and temperature robustness at the behavioral level, we next turned to computational modeling. More specifically, we ask, first, to what extent the observed temperature dependence of neural filters alters song recognition in a computational model, and second, whether filters exist for which the observed temperature dependence promotes temperature robustness of song recognition.

8 Time-warp invariant song recognition with temperature-dependent neural filters

8.1 Introduction

The experimental evidence described in Chapter 7 suggests that changes in temperature significantly affect temporal filtering of sound in ascending neurons of the grasshopper. These neurons are likely to facilitate robustness of song recognition against the temperature dependence of song (so called *time warp*, Creutzig et al., 2009), although direct links between their filtering properties and song recognition remain largely unknown. Intuitively, a temperature dependence of temporal filtering in these neurons should translate to a temperature dependence of song recognition. Behavioral experiments show, however, that time-warp invariant song recognition is surprisingly robust across temperatures (von Helversen, 1972). To better understand how song recognition can be maintained across temperatures if the filtering properties of the neurons involved are temperature dependent, we introduced a mathematical model of grasshopper song preference that was based on simplified neural filters and incorporated the experimentally observed temperature dependence. More specifically, our aim was, first, to use the model to reproduce time-warp invariant recognition of simplified artificial grasshopper songs as reported previously (von Helversen, 1972; von Helversen and von Helversen, 1983), and second, to test whether song recognition could be maintained across temperatures with temperature-dependent neural filters.

In this chapter, first the main features of the model are described (for illustrations of all model stages, see Figure 8.1C). Subsequently, the dependence of song-feature recognition on individual parameters of the model is discussed, and concluding, the effect on song-feature recognition of introducing the experimentally measured temperature dependence to the model is assessed, and it is shown that temperature compensation of time-warp invariant song recognition can be achieved with temperature-dependent neural filters.

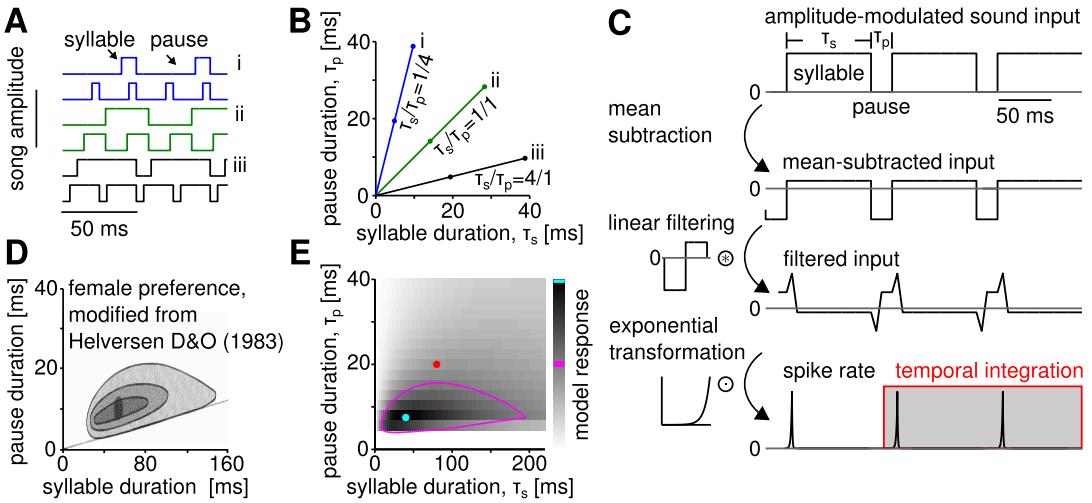

Figure 8.1 A filter-based model of song-feature recognition. Artificial grasshopper song, consisting of alternating segments of high and low sound amplitude (*syllables* and *pauses*), served as model input (**A**). The ratio of syllable and pause duration is used by grasshoppers as an auditory cue for species identity that is independent of the time-warping effect of temperature on syllable and pause duration. In *syllable-pause space* (**B**), songs with a constant syllable-pause ratio lie on lines through the origin (cf. *A*). Behavioral experiments have shown that females exhibit time-warp invariant song preference (**D**, modified from von Helversen and von Helversen, 1983), which we sought to reproduce in the following model: **C:** The model first subtracted the mean from the input song (second row). Then, a uni- or bimodal filter acted on the mean-subtracted input (third row), followed by an exponential transformation of the filtered input into spike rate (fourth row). As a final processing step, the spike rate was integrated over a fixed time window (fourth row, red window), which produced a single number that characterized the model response to song with a given syllable-pause combination. Model responses to all syllable-pause combinations on a uniform grid formed a *response map* (**E**), comparable to female preference maps (*D*). The red circle in *E* corresponds to the song shown in *C*. The cyan circle marks the syllable-pause combination of maximal model response. The 50% contour line is shown in magenta color. Filters with a negative bias exhibited syllable-pause ratio preferences in the range of experimentally observed values (cf. *D* and *E*, negatively biased linear filter shown in *C*).

8.2 A filter-based model of song-feature recognition

The envelope of the male song of the grasshopper species *Chorthippus biguttulus* can be described as a sequence of alternating segments of high and low sound amplitude, termed syllables and pauses (cf. Figure 2.1*A*). Auditory neurons in the metathoracic ganglion of the female extract information from an incoming song, and pass on this information to neurons in the brain, which in turn evaluate the information and, after a few seconds, form the decision whether to respond to the incoming song (von Helversen and von Helversen, 1994, cf. Chapter 2). Here we considered a song-recognition model that was based on a cascade of simplified versions of these processing stages: The input to the model consisted of artificial grasshopper song, consisting of syllables and pauses with amplitudes s and p and durations τ_s and τ_p, respectively. At the first processing stage, the mean sound amplitude

$$\mu = \frac{s \cdot \tau_s + p \cdot \tau_p}{\tau_s + \tau_p}$$

was subtracted from the input. This was motivated by evidence for a representation of sound at the level of local interneurons (the second layer of metathoracic neurons) that is independent of mean sound level (Hildebrandt et al., 2015). At the second processing stage, the mean-subtracted input was filtered by a temporal filter $f(t)$ and subsequently transformed to an instantaneous spike rate $r(t)$, using an exponential nonlinearity. These two steps constituted a L-N model, as commonly used to describe spike rates of neurons in sensory systems, including the auditory system of the grasshopper (cf. Section 4.2). In particular, here the L-N model corresponded to the representation of sound at the level of ascending neurons. In the preceding Chapter 7, linear filters and nonlinearities of ascending neurons were estimated at different temperatures. We incorporated the main experimental findings in the model: filters were uni- or bimodal, nonlinearities were largely monotonically increasing and therefore well described by an exponential. At the final processing stage, the spike rate output of the L-N cascade was integrated over a fixed time window of length W, mimicking a hypothetical readout neuron in the brain.

The mathematical steps of the model are briefly summarized in the following. For detailed calculations, see Appendix B.1. The time course of one syllable-pause pair $S(t)$ can be described as

$$S(t) = p \cdot H(\tau_p - t) + s \cdot H[t - (\tau_s + \tau_p)] \cdot H(t - \tau_p),$$

with the Heaviside step function,

$$H(x) = \begin{cases} 0, & x < 0, \\ 1, & x \geq 0. \end{cases}$$

Conventionally, here song starts with a pause. With the previous definition of the average song amplitude μ over one syllable-pause pair, the mean-subtracted song is given by

$$S - \mu = \frac{1}{\tau_s + \tau_p} \cdot \Big(p \cdot H(\tau_p - t) \cdot \tau_p + s \cdot H[t - (\tau_s + \tau_p)] \cdot H(t - \tau_p) \cdot \tau_s \Big).$$

The response of a temporal filter $f(t)$ to the mean-subtracted song is then given by the convolution

$$x(t) = f(t) * (S(t) - \mu),$$

with

$$f(t) = ma \cdot H(w - t) - (1 - m)a \cdot H(2w - t) \cdot H(t - w).$$

Here, a and w constitute the filter amplitude and width, m constitutes the *modality* of the filter (as for the experimental filters, $m = 1$ or $m = 0$ indicated positive or negative unimodal filters, while $m = 0.5$ indicated a bimodal filter).

The exponential transformation of the filtered input into spike rate $r(t)$ was

$$r(t) = \exp\left(\frac{x - x_0}{\tilde{c}} \right),$$

with rise constant $\tilde{c}$ and offset x_0. Then, the integral over the spike rate response to one syllable-pause combination of song is

$$N_1 = \int_0^{\tau_s + \tau_p} r(t) dt,$$

and correspondingly the integral over all syllable-pause pairs within a window of length W,

$$N = \underbrace{\frac{W}{\tau_s + \tau_p}}_{n_{sp}} \cdot N_1.$$

If n_{sp} is not an integer value, this is an approximation of the filter response to the remaining part of the final syllable-pause pair as the relative amount of the response to a full syllable-pause pair. This approximation is valid for $W \gg \tau_s + \tau_p$, as found in *Chorthippus biguttulus* which integrates song over several seconds (von Helversen and von Helversen, 1994). N was evaluated analytically, separately for each case arising from the combination of Heaviside step functions in the expressions for S and f (see Appendix B.1).

Importantly, due to the exponential nature of the nonlinearity, the mean subtraction step of the model factorizes into the *normalization matrix* $M(\tau_s, \tau_p)$:

$$\begin{aligned} r(t) &= \exp\left(\frac{\int_0^{2w} d\tau f(\tau) \cdot (S(t-\tau) - \mu) - x_0}{\tilde{c}}\right) \\ &= \exp\left(\frac{\int_0^{2w} d\tau f(\tau) \cdot S(t-\tau)}{\tilde{c}}\right) \cdot \exp\left(\frac{-x_0}{\tilde{c}}\right) \cdot \underbrace{\exp\left(\frac{wa\mu(1-2m)}{\tilde{c}}\right)}_{M} \end{aligned}$$

Hence, the relation between the response N_{raw} of a song-recognition model that lacks the mean-subtraction step and the full model is given by

$$N = M \cdot N_{\text{raw}}$$

After inserting the definition of μ, the normalization matrix becomes

$$\begin{aligned} M &= \exp\left(\frac{(\frac{s\tau_s + p\tau_p}{\tau_s + \tau_p})aw(1-2m)}{\tilde{c}}\right) \\ &= \exp\left(\frac{(\frac{s\tau_s/\tau_p + p}{\tau_s/\tau_p + 1})aw(1-2m)}{\tilde{c}}\right). \end{aligned}$$

Here it is evident that for perfectly bimodal filters ($m = \frac{1}{2}$), the normalization matrix equals unity for all syllable-pause combinations. Hence, for bimodal filters, the song-recognition model response N simplifies to N_{raw}, that is, the response of the model without mean subtraction.

8.2.1 Model assumptions

For consistency between the model and the experimental results of Chapter 7, the filter amplitude a was chosen such that the Euclidean norm of the filter equaled unity:

$$\begin{aligned}
\text{norm}(f) &= \sqrt{\int |f|^2 dt} \\
&= \sqrt{\int |m \cdot a \cdot H(w-t) - (1-m) \cdot a \cdot H(2w-t) \cdot H(t-w)|^2 dt} \\
&= \sqrt{w \cdot m^2 a^2 + w \cdot a^2 (1-m)^2} \\
&= a \cdot \sqrt{w(m^2 + (1-m)^2)} \stackrel{!}{=} 1 \\
\Leftrightarrow a &= \frac{1}{\sqrt{w(m^2 + (1-m)^2)}}, \quad w > 0.
\end{aligned}$$

Hence, the filter amplitude was a function of filter width w and filter modality m.

We defined the *contrast* of song as the difference of syllable and pause amplitudes, $c := s - p$. Throughout this thesis we assumed for simplicity $p = 0$ and hence $s = c$.

From the preceding calculations and the definitions of song and filter, it is evident that the main parameters that determine the value of the model response for a given combination of syllable and pause durations are the filter modality, m, the filter width, w, and the ratio of the song contrast to the rise constant of the nonlinearity, $c/\tilde{c}$, which we here refer to as the *relative song contrast* or *relative sound level*.

8.2.2 Parameter sweep for model sensitivity analysis

To estimate sensitivities of the song-recognition model to perturbations in the parameters filter width w, filter modality m, and the relative song contrast, $c/\tilde{c}$, model response maps were computed for the parameter ranges and syllable-pause combinations on a uniform polar grid using the values specified in Table 8.1. The uniform polar grid was used to avoid biases in the calculation of song-feature preferences that were based on polar coordinates. The relation of

Table 8.1 Parameters of the song-recognition model.

Parameter	Symbol	Range	Step	Unit
Filter width	w	5-25	5	ms
Filter modality	m	0-1	0.025	—
Relative song contrast	$c/\tilde{c}$	2-10	2	—
Time scale	R	0-4000	2.5	ms
Species identity	θ	0-$\pi/2$	$\pi/500$	rad

Cartesian coordinates (syllable and pause duration τ_s, τ_p) to polar coordinates (time scale R and species identity θ) is

$$\tau_s = R \cdot \cos\theta,\ \tau_p = R \cdot \sin\theta.$$

Importantly, the parameter ranges were chosen to include the experimentally observed values for filter width and modality (cf. Figure 7.3), and the behaviorally relevant range of relative song contrasts (as motivated in Section 8.3.3).

8.2.3 Measures of song preference

All measures of song preference described in the following are derived from the *response map* of the previously described song-recognition model for a given filter and nonlinearity, that is, the map of all model responses to songs on a grid of syllable-pause pairs.

Syllable and pause preference The syllable-pause combination $(\tau_{\mathrm{s,max}}, \tau_{\mathrm{p,max}})$ at which the model response was maximal defined the *preferred* syllable and pause duration for a given filter and nonlinearity (cyan circle in Figure 8.2*A*).

Preference time scale We used the Euclidean distance from the preferred syllable-pause combination to the origin, $R_{\max} = \sqrt{\tau^2_{\mathrm{s,max}} + \tau^2_{\mathrm{p,max}}}$, as an overall measure of the *time scale* of syllable-pause preference (length of the cyan arrow in Figure 8.2*A*).

Species preference Under the assumption that songs of different grasshopper species are dominated by specific syllable-pause ratios, the ratio of the preferred syllable and pause duration, $\left(\frac{\tau_s}{\tau_p}\right)_{\max}$, can indicate the preference of

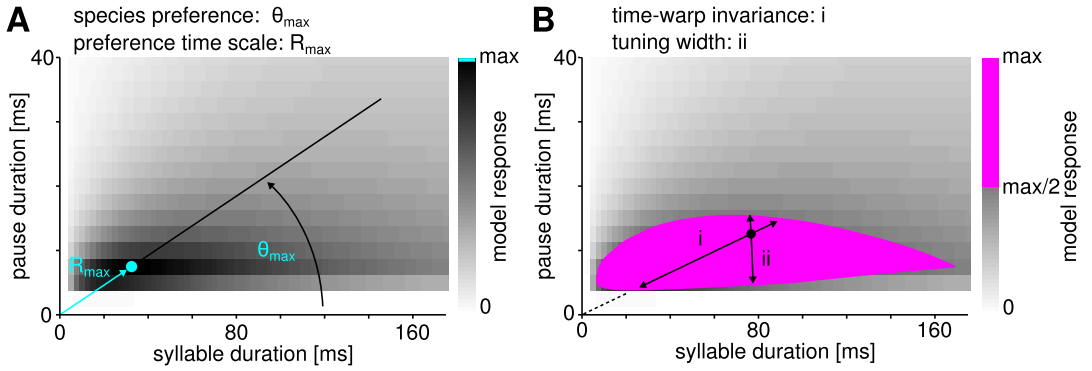

Figure 8.2 Measures of song preference. **A:** Model response map with point of maximal response (cyan color). *Species preference* and *preference time scale* were the angular and radial polar coordinate, respectively, of the syllable-pause combination of maximal response. **B:** Model response map with filled 50% contour (magenta color). *Tuning width* and *time-warp invariance* were the standard deviations of the angular and polar coordinates, respectively, of all points within the contour.

the model for a grasshopper species producing songs with that ratio. Since the ratio is singular for $\tau_p \to 0$, we used the angular polar coordinate of the maximal response (angle between the x-axis and the solid black line in Figure 8.2*A*), $\theta_{\max} = \operatorname{acot}\left(\frac{\tau_s}{\tau_p}\right)_{\max}$ as a more convenient measure of *species preference*.[1] However, further measures are necessary to quantify how many different syllable-pause pairs with the preferred ratio are responded to, and how broad the tuning for syllable-pause ratio is, that is, how many other syllable-pause ratios close to the preferred one are responded to.

Time-warp invariance Grasshopper song is temperature dependent, due to the innate temperature dependence of the song-producing muscles. This temperature dependence induces a speed-up of song with heating. Hence, changes in temperature result in a *time-warping* of song. Interestingly, the syllable-pause ratio of grasshopper song is invariant to time-warping of song, and therefore suitable for robustness of song recognition against temperature changes of the sender of song. For the song-recognition model, *time-warp invariance* was defined as the standard deviation of the *radial* polar coordinate of all syllable-pause pairs within the 50% contour of the response map, termed $\sigma(R_{50})$ (this is proportional to the length of the arrow with index *i* in Figure 8.2*B*). A model that responds selectively to one syllable-pause combination will exhibit

[1] Note that the syllable-pause ratio and hence also the *species preference* are related to the *duty cycle* of song, d, via $d = \frac{\tau_s}{\tau_s+\tau_p} = \frac{1}{1+\frac{\tau_p}{\tau_s}}$.

a small variability in the radial direction. In contrast, a model that responds to many syllable-pause combinations with the preferred syllable-pause ratio will exhibit a large variability in the radial direction.

Tuning width of species preference Similar to the measure of time-warp invariance, the *tuning width* of species preference was defined as the standard deviation of the *angular* polar coordinate of all syllable-pause pairs within the 50% contour of the response map, termed $\sigma(\theta_{50})$ (this is proportional to the length of the arrow with index *ii* in Figure 8.2*B*). A model that responds selectively to songs with one specific syllable-pause ratio will exhibit a small variability in the angular direction and is hence selective for one grasshopper species. In contrast, a model that responds to many different syllable-pause ratios will exhibit a large variability in the angular direction and hence accepts songs of many different grasshopper species.

Preference bias The *preference bias* was defined as the absolute deviation of the species preference from $\pi/4$. Hence, the preference bias quantifies how unbalanced, that is, how different from unity, the preferred syllable-pause ratio is.

8.3 Results

8.3.1 Reproduction of grasshopper song preference

For filters with a positive or negative modality bias, time-warp invariant responses to different inputs with a fixed ratio of syllable and pause duration could be reproduced (Figure 8.1*D,E*). Intuitively, the underlying mechanism was the following: the biased filter responded maximally to inputs that exhibited amplitude modulations similar to the shape of the filter. For filters with a negative bias, such inputs corresponded to songs with longer syllables than pauses, because the mean-subtraction stage of the song-recognition model effectively reduced syllable amplitude and increased pause amplitude. This rendered the mean-subtracted input more similar to the filter than the raw input (compare the raw and mean-subtracted inputs to the filter shape in Figure 8.1C). The simplified shape of the filters used in the model facilitated the analytical calculation of the filter response. Species preferences in a numerical model with MoG filters comparable to those identified in the experiments, however, were similar to those in the song-recognition model with simplified

filters of similar width and modality (cf. Appendix B.2.1 and Figure B.2), which justifies the simplifying assumption of box-shaped filters.

Concluding, we introduced a simple song-recognition model that incorporated a L-N model stage which mimicked the spike rate of ascending neurons. This model was capable of reproducing time-warp invariant song recognition, as found in behaving grasshoppers.

8.3.2 The mechanism underlying time-warp invariant song recognition in the model

For a more detailed understanding of how time-warp invariant song recognition arises in the model, we again consider the normalization matrix M,

$$M = \exp\left(\frac{wac}{\tilde{c}} \cdot (1-2m) \cdot \frac{\tau_s/\tau_p}{\tau_s/\tau_p + 1}\right), \quad s = c, p = 0. \tag{8.1}$$

Note that for a bimodal filter ($m = 0.5$), $M = 1$, and therefore the responses of the model with and without mean-subtraction step are equal (cf. Figure 8.3*A-Ci*). In Equation 8.1, we replaced the syllable and pause amplitudes to take the values used in all simulations of this chapter, but the following arguments hold for the more general case $s > p$. M depends on the ratio of the syllable and pause durations, and the sign of $(1-2m)$ determines whether M is maximal for $\tau_s/\tau_p \to 0$ ($m = 1$) or for $\tau_s/\tau_p \to \infty$ ($m = 0$). This is important to explain the emergence of a selectivity for finite syllable-to-pause ratios (and hence time-warp invariant song recognition), as described in the following: for a negative unimodal filter, the response to raw (i.e., not normalized) song is maximal if $\tau_s \to 0$ and hence $\tau_s/\tau_p \to 0$ (cf. Figure 8.3*Aiii* and Appendix B.1). Hence, the negative unimodal filter is an integrator for pauses (red curve in Figure 8.3*Diii*). For normalized song, however, the integrator property is counter-acted by the normalization matrix, which is maximal for $\tau_s/\tau_p \to \infty$ (cf. Figure 8.3*Biii* and black line in *Diii*). The result is a selectivity for a finite syllable-pause ratio $0 < \tau_s/\tau_p < \infty$ (Figure 8.3*Ciii* and blue line in *Diii*), that is, the emergence of time-warp invariant song recognition.

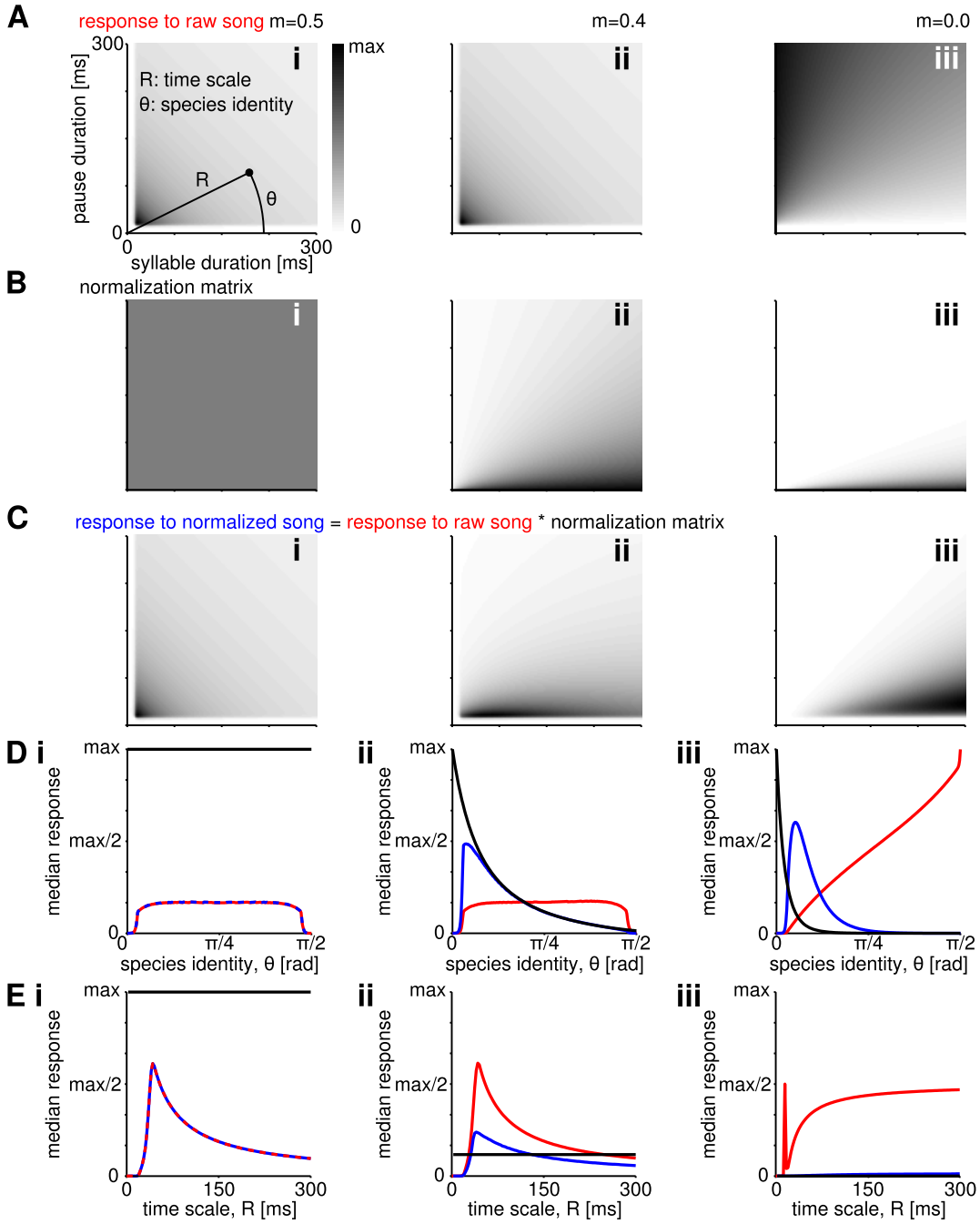
A
response to raw song m=0.5
m=0.4
m=0.0
i
ii
iii
max
0
300
pause duration [ms]
R: time scale
θ: species identity
R
θ
0
300
syllable duration [ms]
B
normalization matrix
C
response to normalized song = response to raw song * normalization matrix
D i
ii
iii
median response
max
max/2
0
π/4
π/2
species identity, θ [rad]
E i
150
time scale, R [ms]

Figure 8.3 (*previous page*) The mechanism underlying time-warp invariant song recognition. **A:** Responses of a song-recognition model lacking the mean-subtraction step, for three filters of different modality ($m = 0.5, 0.4, 0.0$ in *i,ii,iii*, respectively). **C:** The responses of the full model including the mean-subtraction step mathematically corresponds to a multiplication of the responses to the raw song (*A*) with a normalization matrix (**B**) that is a function of syllable and pause duration and filter modality. **D:** Species preference, that is, tuning for species identity (θ), arose in the full model for *biased* filters (cf. blue curves in *ii,iii* with *i*). **E:** Tuning for time scale (R) arose in the full model for *bimodal* filters (cf. blue curve in *i* with *ii,iii*). Note that while for bimodal filters the full model showed only tuning for time scale, and for unimodal filters only tuning for species identity, filters that were in-between exhibited both tuning for time scale and species identity (blue curves in *D,E ii*).

8.3.3 Effects of filter width and filter modality on song preference

Because temperature affected the width and modality of filters of ascending neurons (Chapter 7), we systematically studied the effect of these two parameters on song-feature recognition in a behavioral model. To that end, we independently varied syllable and pause length of the input song to create model response maps for filters of different width and modality. From each response map, features were extracted that characterized the selectivity of a filter for song. In particular, the model's *species preference* was assessed, its *preference time scale* as well as the *tuning width* and the *time-warp invariance* of its preference (see Section 8.2.3 for definitions of all measures and Figure 8.2 for illustrations). Importantly, we assumed that the ratio of syllable and pause duration is a crucial parameter for species recognition, as has been proposed for the grasshopper (von Helversen, 1972). In other words, this ratio determines the *species preference*, while the range of other ratios that are responded to, the *tuning width*, determines the selectivity of the grasshopper. The more songs with the preferred syllable-pause ratio but different syllable and pause lengths are responded to, the better the *time-warp invariance*.

Since individual response maps were quantitatively affected by the *relative song contrast*, that is, the ratio of the song contrast c to the rise constant of the nonlinearity, $\tilde{c}$, we further varied $\frac{c}{\tilde{c}}$ within a realistic range, as motivated in the following. In the wild, grasshopper song attenuates with increasing distance from the sender (around 6 dB per distance doubling), and additionally due to scattering of sound in the vegetation (around 6-18 dB per m; Lang, 2000). Within the communication range of grasshoppers (5-100 cm; Lang, 2000), sound levels of 18-90 dB SPL are realistic (Loher, 1957; Lang, 2000). Further, in the present experiments the rise constant of the filter nonlinearity was estimated

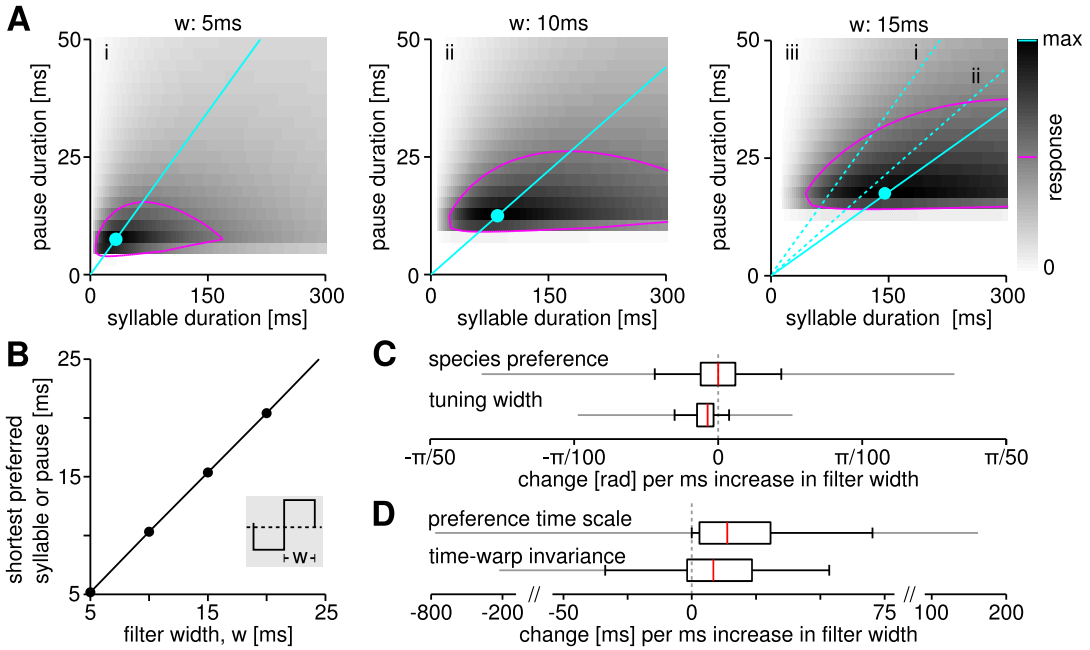

Figure 8.4 The effect of filter width on song preference. For the abstracted filters used in the song-recognition model, the parameter w determined the width of the positive and negative lobe, as well as the distance between the centers of the positive and negative lobe (**B**, inset). An increase in filter width weakly affected species preference and tuning width (**C**) but could induce large changes of the preference time scale and time-warp invariance (**D**). Further, filter width determined the shortest possible preferred syllable and pause length (**B**). Dashed lines in **A***iii* show the species preference of the filter in the plots to the left, with different width. Solid grey lines in *C,D* indicate ranges of the respective distribution outside the 1st and 99th percentiles which contained outliers. *C,D* show how much each observable changes with an increase in filter width of 1 ms, which corresponded to a change in temperature of around 1°C (cf. Figure 7.3*C*). The variability in *C,D* is due to changes in filter modality and relative song contrast.

as $\tilde{c} = 8.7 \pm 2.4$ (Figure 7.4*D*). This motivated our choice of $\frac{c}{\tilde{c}} \in \{2, 4, \ldots, 10\}$ for the parameter sweep that produced the following results. Importantly, with this choice, the song-recognition model exhibited song-feature preferences as observed in behaving grasshoppers (von Helversen, 1972; von Helversen and von Helversen, 1983).

Influence of filter width Changes in filter width weakly affected species preference and tuning width (Figure 8.4*C*). In contrast, increasing filter width led to large changes of the time scale and the time-warp invariance of species preference (Figure 8.4*D*). Also, filter width determined the minimal possible preferred syllable and pause length (Figure 8.4*B*), which was expected, since

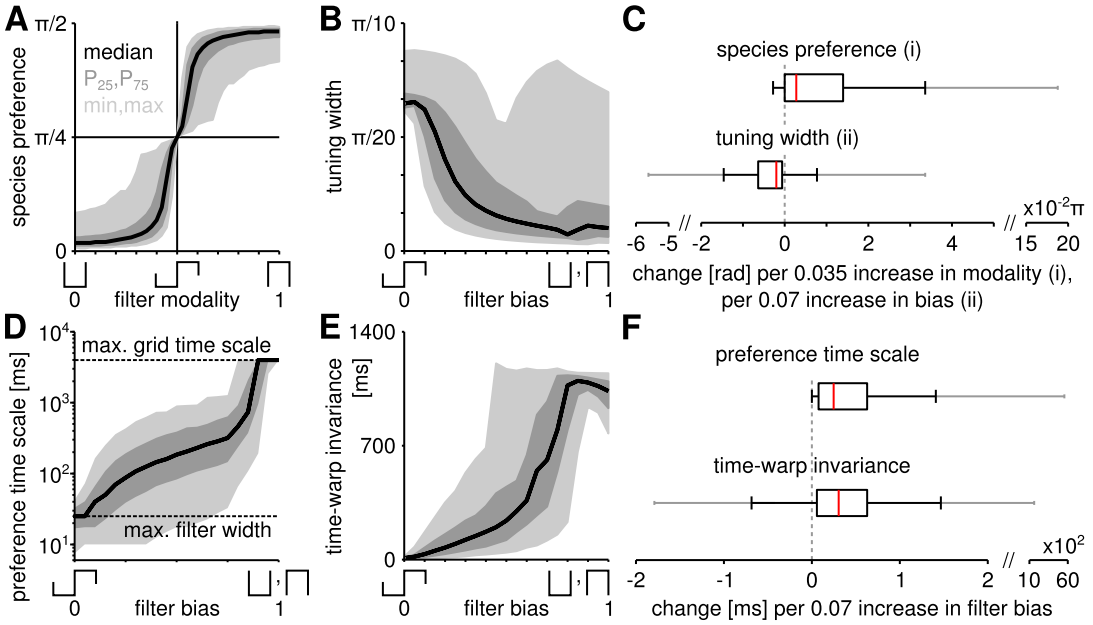

Figure 8.5 The effect of filter modality and bias on song preference. Filter modality strongly affected *species preference* (**A**): Only filters with a dominant negative lobe (i.e., modality $m \leq 0.5$) could prefer species with syllable-pause ratios larger than 1 (i.e., *species preference* $\leq \pi/4$), and vice versa. An increase in *filter bias* ($b = |2m - 1|$) facilitated preference for syllables and pauses much longer than the filter width, and hence increased the *preference time scale* (**D**; maximal filter width was 25 ms). Further, an increase in filter bias improved species preference tuning, since *tuning width* decreased (**B**), and *time-warp invariance* increased (**E**). Box plots in **C,F** show derivatives of the observables in *A,B,D,E* with respect to filter modality (*Ci*) or filter bias (*Cii*,*F*). Shown are the changes in the observable with an increase in modality of 0.035 or an increase in bias of 0.07 (corresponding to a change in modality of ±0.035). These values correspond to a temperature change of around 1°C (cf. Figure 7.3*D*). In *C,F*, the variability is due to changes in filter width and relative song contrast; solid grey lines indicate ranges of the respective distribution outside the 1st and 99th percentiles which contained outliers.

a decrease in filter width implies an increase in temporal resolution. Example response maps to illustrate these effects are shown in Figure 8.4*A* (maps were created using a negatively biased filter (modality 0.35) of widths 5, 10, and 15 ms, which corresponds to a temperature range of 16.3°C, assuming $Q_{10}(w) = 0.51$.

Concluding, changes in temperature could impair song recognition, mainly due to the corresponding effects of filter width on the time scale and time-warp invariance of species preference.

Influences of filter modality and bias Species preference monotonically increased with filter modality (Figure 8.5*C*). Importantly, only filters with a

dominant negative lobe could exhibit a preference for species with syllable-pause ratios greater than one (correspondingly, species preference$< \pi/4$), and vice versa (Figure 8.5*A*). Also, for biased filters a further increase in bias would in most cases only mildly alter species preference (cf. saturation in Figure 8.5*A* for modalities close to the extremes). Apart from species preference, all observables shown in Figure 8.5 were even functions of modality and hence only depended on filter bias, $b = |2m - 1|$. We therefore report the dependence of these observables on filter bias instead of modality.

The time-warp invariance of species preference increased (Figure 8.5*E,F*), and tuning width decreased, for an increase in filter bias for the majority of parameter combinations (Figure 8.5*B,C*).

Further, an increase in filter bias increased the time scale of the species preference and hence enabled tuning for syllable and pause durations much larger than the filter width (Figure 8.5*D,F*).

Concluding, although filter modality constituted a crucial parameter for species preference, the reduction in filter modality at higher temperatures observed in the experimental data had differential effects on song recognition. That is, time-warp invariance increased and species tuning became narrower with heating only for those filters for which the decrease in filter modality corresponded to an increase in filter bias. Importantly, this increase in time-warp invariance as well as the increase in preference time scale could oppose the respective effects with heating that were due to a decrease in filter width (cf. Figure 8.4*D*).

8.3.4 Effect of relative song contrast on song preference

While filter width and modality constituted parameters that were solely related to the receiver of communication signals, the relative song contrast $c/\tilde{c}$ was by definition related to both the sender and the receiver of sound: The song contrast c depends on the distance between sender and receiver and the power of song production, whereas the rise constant $\tilde{c}$ of the nonlinearity is a feature of the sound processing network in the receiver. This will be important for the interpretation of the following results.

Increasing the relative song contrast on average led to narrower and more time-warp invariant species tuning and increased the preference time scale (Figure 8.6*A-C,E*). Further, an existing preference bias[2] would increase with increasing relative song contrast. The previous results showed that a biased

[2] that is, the absolute deviation of the species preference from $\pi/4$, which corresponds to the absolute deviation of the preferred syllable-pause ratio from unity; see Section 8.2.3 for details

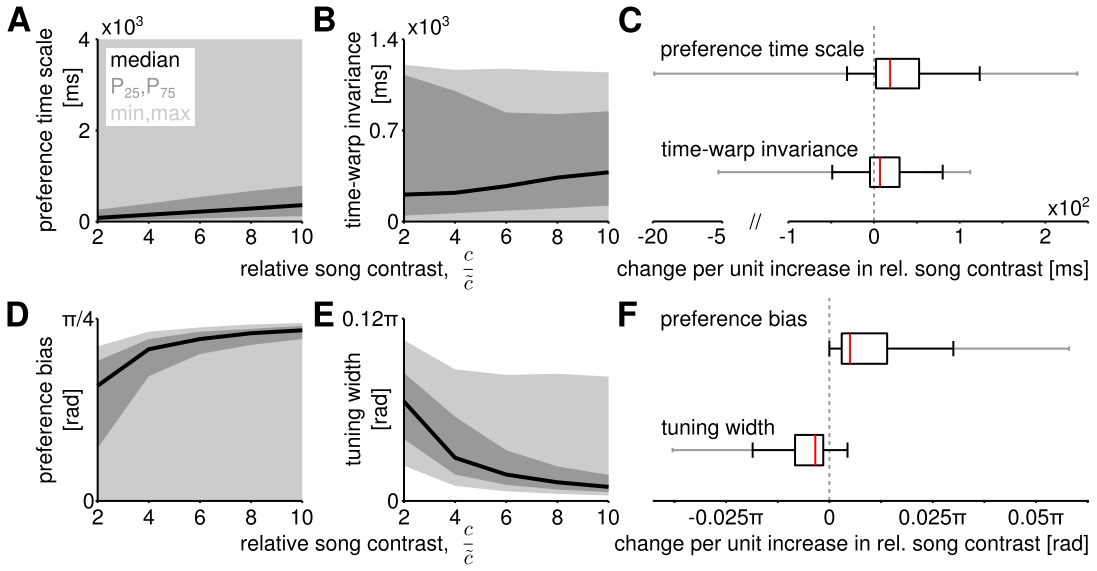

Figure 8.6 The effect of relative song contrast on song preference. Preference time scale (**A**), time-warp invariance (**B**), preference bias (**D**), and tuning width (**E**) as functions of the stimulus sound intensity relative to the gain of the nonlinearity (*relative song contrast*). The preference bias is the absolute deviation of the species preference from $\pi/4$ and characterizes how unbalanced (i.e., different from unity) the preferred syllable-pause ratio is. **C:** Sensitivity of preference time scale and time-warp invariance for changes in relative song contrast. **F:** Sensitivity of preference preference bias and tuning width for changes in relative song contrast. The variability in *C,F* is due to changes in filter width and filter modality. On average, an increase in relative song contrast increased the time-warp invariance of tuning, enabled preference of longer syllables or pauses (*C*) and increased existing biases in syllable-pause ratio or species preference (*F*). Further, an increase in relative song contrast sharpened species tuning (*F*).

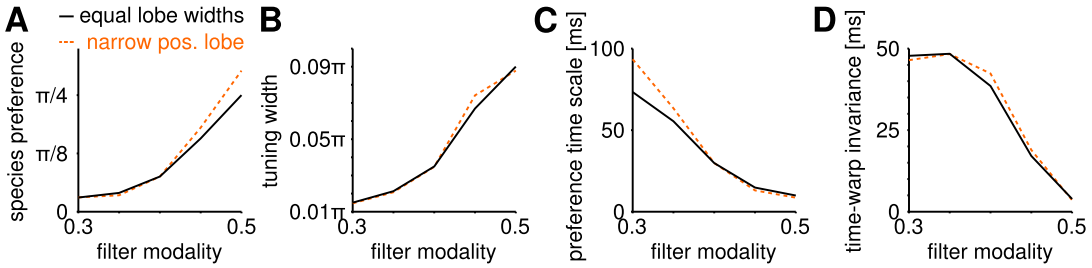

Figure 8.7 The effect of relative lobe width on song recognition. Experimentally measured filters on average exhibited narrower positive lobes compared to negative lobes (cf. Figure 7.5), while in the song-recognition model, equal widths were assumed for both filter lobes. **A-D:** Changing the relative widths of the positive and negative filter lobes while keeping filter modality constant had little effect on song recognition. Black lines correspond to equal widths of the positive and negative lobe (i.e., a relative width of the positive lobe of 0.5), orange dashed lines correspond to a narrower positive lobe (relative width of 0.3, as in the experiments). Species preference differed slightly more for bimodal filters compared to biased filters (*A*), while the difference in preference time scale was larger for biased filters (*C*).

filter is required to establish a preference bias (Figure 8.5*A*). Therefore, the enhancing effect of relative song contrast on preference bias only applied for biased filters.

Concluding, males producing courtship song of high sound level contrast can improve time-warp invariant song recognition and sharpen species tuning in females that utilize biased filters in song recognition.

8.3.5 Effect of relative lobe width on song preference

For most experimental filters, positive lobes were narrow compared to negative lobes (cf. Figure 7.5). For simplicity, in the song-recognition model we have so far considered filters with equal widths of the positive and negative lobe. Therefore we next used numerical simulations to test how song-feature preference was affected by a corresponding change in relative filter-lobe width.[3] We found that changing the relative lobe width overall had little influence on song preference Figure 8.7. Yet, species preference was slightly more affected for bimodal filters compared to biased filters (Figure 8.7*A*), while the difference in preference time scale was larger for biased filters (Figure 8.7*C*).

[3] Syllable and pause duration were varied between 1 and 201 ms, filter width and relative song contrast were kept constant at 5 ms and 4, respectively. The relative width of the positive lobe could take two values: 0.3 (as in the experiments), or 0.5 (as in the model).

Concluding, the effect of the relative filter lobe width on song recognition is small and not qualitative, which justifies the simplifying assumption of equal positive lobe widths in the song-recognition model.

8.3.6 Time-warp invariant song recognition across temperatures

The preceding paragraphs suggest that species preference in the song-recognition model is largely determined by filter modality. Further, for biased filters, small changes in filter width and modality only mildly affected species preference, which raised the question whether such filters were particularly suitable for successful species recognition across temperatures. Therefore, we next tested over which temperature range a negatively biased filter could maintain a preference for songs of the grasshopper *Chorthippus biguttulus*, under the assumption of the experimentally observed temperature dependencies for filter width and modality. The choice of a negative bias at a reference temperature of 29.5°C was determined by previous experimental results.[4] Figure 8.8*A* shows a filter that was 16 ms wide and had a negative bias ($m = 0.35$) at 29.5°C. The filter was subject to temperature changes between -11 and +11°C, assuming the experimentally observed temperature dependencies for filter width and modality ($Q_{10}(w) = 0.51, Q_{10}(m) = 0.70$, cf. Chapter 7). Except for the lowest temperature, four measures of song preference exhibited little variation across temperatures (Figure 8.8*C*,*D*). Importantly, species preference of the model matched the preference of behaving grasshopper females across temperatures (black circles in Figure 8.8*C* correspond to behavioral results from von Helversen, 1972). Likewise, pause preference matched experimental data (Figure 8.8*E*).

The observed robustness of species preference across temperatures was due to a cancellation of the opposing effects on species preference of a decrease in filter width and a decrease in filter modality for negative filters (Figure 8.9*A*; the black trajectory marks species preference as shown in panel Figure 8.8*C*). Notably, this cancellation of effects was also observed for the tuning width and time-warp invariance (Figure 8.9*B*,*C*). Note however that the cancellation would not be present for a filter with strong positive bias that is subject to the experimentally observed temperature dependencies.[5] Yet, for any filter

[4] More specifically, the syllable-pause ratio preferences derived from Figure 20 in von Helversen (1972) (also reproduced in Figure 2.1*E*) at 35°C were 5.3 and 6.0 (corresponding to species preferences of 0.06π and 0.05π), respectively, and at 24°C 3.2 and 3.75 (corresponding to species preferences of 0.1π and 0.08π), suggesting filter modalities around 0.3 to 0.4 for the reference temperature (cf. Figure 8.5*A*).

[5] For positively biased filters, the black trajectory in Figure 8.9*A-C* would be shifted to the right but remain its shape. Hence, in contrast to the shown trajectory of the more negative

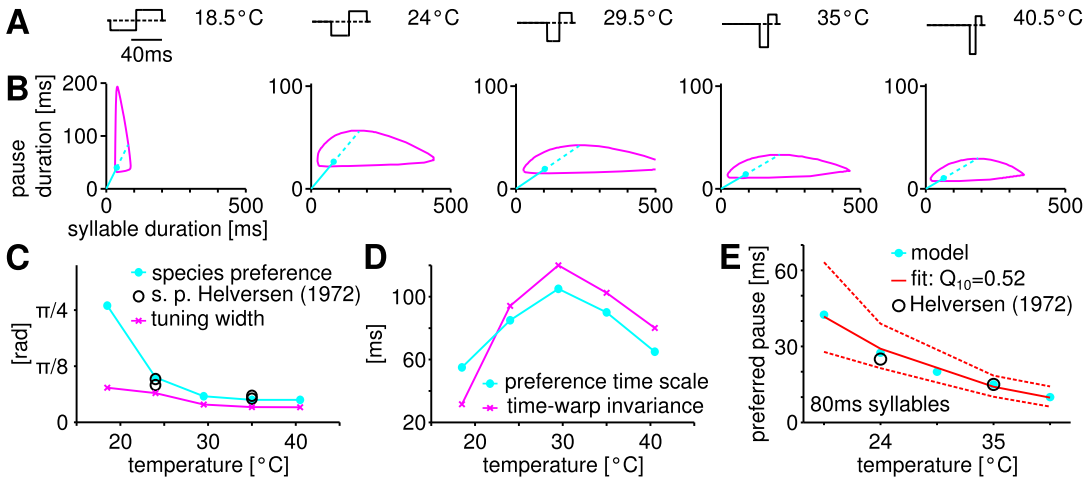

Figure 8.8 Time-warp invariant song recognition across temperatures. Species preference remained nearly constant over a range of 15°C, for a filter with negative bias and experimentally observed temperature dependencies of filter width and modality ($Q_{10}(w) = 0.51, Q_{10}(m) = 0.7$, width and modality at 29.5°C: $w = 16$ ms, and $m = 0.35$). Filter (**A**) and corresponding response maps (**B**) shown at temperatures between 28.5 and 40.5°C. Cyan marks the maximal response, magenta marks the 50% contour. Note the different y-axis scale in the response map at 18.5°C. **C:** Temperature dependence of species preference and tuning width (cyan and magenta colors, respectively). Black circles in *C,E* mark experimental values calculated from Figure 20 of von Helversen (1972). **D:** Temperature dependence of time-warp invariance and preference time scale (magenta and cyan color, respectively). **E:** Temperature dependence of pause preference for a fixed syllable duration, for comparison with data from von Helversen (1972). Red dashed lines indicate 95% CI of the Q_{10} fit.

with a negative bias, an increase in temperature will only mildly affect species preference (correspondingly, all trajectories would remain in the blue-colored half of Figure 8.9*A*).

Concluding, the experimentally measured temperature effects on neural filters are highly compatible with robust song recognition across temperatures, in particular for filters exhibiting a negative modality bias.

8.4 Discussion

Here we presented a simple, analytically tractable model of song recognition in the grasshopper. A L-N cascade constituted the core of the model, which facilitated incorporation of the experimental results of Chapter 7. Two additional

filter, the shifted trajectory would traverse regions of large changes in the three measures of song preference.

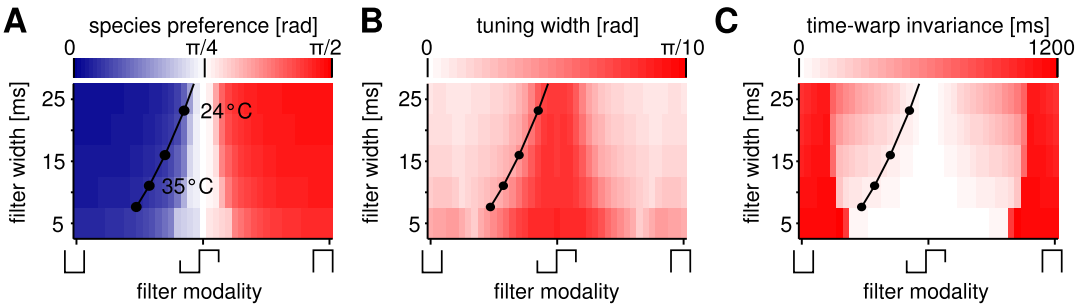

Figure 8.9 Temperature robustness via cancellation of temperature effects on filter width and modality. Temperature robustness of song recognition was due to a cancellation of the effects of filter width and filter modality on species preference (**A**), tuning width (**B**), and time-warp invariance (**C**). The black trajectories correspond to the filters in Figure 8.8*A*.

processing steps, that is, input mean subtraction and temporal integration of the L-N model output, completed the model. The model was able to reproduce time-warp invariant song recognition as well as its robustness across temperatures, as observed in females of the species *Chorthippus biguttulus*. Importantly, temperature robustness of song recognition in the model was achieved based on temperature-dependent temporal filters. This resolves the apparent mismatch between temperature dependence of neural processing and temperature robustness of song recognition, that was discussed in Chapter 7.

Further, we assessed the sensitivity of song recognition to changes in all relevant model parameters. While the L-N cascade, as well as the output integration, were used in previous models of song-feature preference in grasshoppers and crickets (cf. Section 4.2), there were essential differences to our model:

First, the model described here contained a crucial processing stage that was not present in previous models, that is, the mean-subtraction step. This processing stage was essential for the reproduction of the characteristic tuning for syllable-pause ratio found in *Chorthippus biguttulus* females, which facilitates robustness of song recognition against the temperature dependence of male song production. None of the previous models attempted to reproduce this specific type of tuning, nor the incorporation of temperature effects on the female.

Second, our model was analytically tractable, which on the one hand facilitated clear identification of model parameters that were crucial for the reproduction of behavioral results, and on the other hand facilitated efficient computation of high-resolution response maps. Calculations in the cited studies were entirely numerical.

Third, both the filter and the nonlinearity of our model had the simplest shapes, which largely simplified identification of the roles of individual parameters in song recognition, compared to using Gabor-like filters, or sigmoidal nonlinearities. Yet, once the roles of individual parameters were established, it was easy to identify the effects of using more realistic filters and nonlinearities (cf. Appendix B.2).

8.4.1 The role of biased filters in auditory processing

The behavioral song preference of *Chorthippus biguttulus* was reproduced in our song-recognition model only for negatively biased filters. This is in agreement with the negatively biased filters of ascending neuron AN12 reported for *Chorthippus biguttulus* (Creutzig et al., 2009). The authors attributed to AN12 a prominent role for timescale invariant song recognition but did not study the effect of temperature on the shape of its filter. Our results suggest that a single neuron such as AN12 can be used for successful recognition of grasshopper song across a broad range of temperatures, as long as it maintains a biased filter. Yet, the majority of filters in our dataset were bimodal or positively biased (cf. Figure 7.2). For bimodal filters, a temperature dependence of filter modality induced the strongest temperature dependence of species preference, which challenges their role in robust species recognition across temperatures. Hence, does the majority of ascending neurons not contribute to song recognition in *Chorthippus biguttulus*?

Selective sampling from ascending neurons This is possible if brain neurons involved in mating decisions assess input only from metathoracic neurons with negatively biased filters. Current knowledge suggests that the metathoracic network constitutes a general sound processing module shared by different grasshopper species, from which species-specific neurons in the brain selectively read out the relevant information (Neuhofer et al., 2008). While the results presented here suggest that ascending neuron AN12 provides crucial information for time-warp invariant song recognition to the brain of *Chorthippus biguttulus*, other ascending neurons could provide such information for other grasshopper species, including those that restrict courtship to a narrow temperature range, or those that inhabit an environment with little temperature variation. Also, it should be noted here that other ascending neurons might as well serve purposes in song recognition that are merely unrelated to time-warp invariant song recognition, that we focused on here.

Broad sampling from ascending neurons Alternatively, multiple neurons with filters of different negativity could provide input to the brain. Then, for *Chorthippus biguttulus* robustness of time-warp invariant pattern recognition would only be achieved above a critical temperature at which the majority of filters has become negatively biased. This critical temperature is likely above the known lower limit of song recognition of around 20°C (cf. Figure 7.3*D*), but further studies are necessary to test this hypothesis.

A role for positively biased filters in predator avoidance As another possibility, neurons with positively biased filters could be 'left-overs' from times when the auditory system was primarily used for predator avoidance rather than for partner selection (Stumpner and von Helversen, 2001). Potential early predators include bats that use echolocation to detect insects during flight or while resting on vegetation (Neuweiler, 1990). With few exceptions, the majority of echolocating bats exhibit low duty cycles (Jones, 1999; Fenton et al., 2012) well below 50%[6], with decreasing inter-pulse intervals as the bat approaches its target (Nolen and Hoy, 1986). The song-recognition model presented here exhibits tuning for such low duty cycles if filters with a positive modality bias are used (cf. Figure 8.5*A*), which supports the hypothesis that positive filters played a role in predator avoidance at earlier times. In particular, the decrease in inter-pulse intervals of bat calls, at fixed duty cycle, would correspond to a trajectory in syllable-pause space that is stretched in the radial direction, similar to time-warped grasshopper songs that biased filters are capable of detecting. Future experiments could test whether ascending neurons with filters of different bias receive inputs from receptor neurons with different spectral tuning. If ascending neurons with positively biased filters received inputs mainly from receptors sensitive to ultrasound, the bat-detector hypothesis would be supported.

8.4.2 Assumptions, limitations, and predictions of the model

Here we introduced a model in which time-warp invariant pattern recognition emerged from a cascade of mean subtraction, linear filtering, exponential transformation, and temporal integration. The choice of these particular steps is discussed in the following.

The mean-subtraction step The mean-subtraction step of the song-recognition model can be interpreted as an adaptation to mean sound level. Detailed

[6] This corresponds to a species preference $\geq \pi/4$.

adaptation dynamics were ignored, which is partly justified because adaptation to mean sound level in local neurons (i.e., the inputs to ascending neurons, which constitute the linear filtering stage in our model) of the grasshopper is fast compared to the timescale of song evaluation. The former acts on a timescale of 10 to 100 ms (Hildebrandt et al., 2015), the latter on a timescale on the order of 1 to 10 s (Clemens et al., 2014; Hartbauer and Römer, 2014). However, future studies should address the quantitative difference between our model and one with realistic adaptation dynamics. A suitable candidate model was proposed in Benda and Herz (2003), and later applied to describe intensity invariance in first-order auditory interneurons of the cricket (Benda and Hennig, 2008). In particular, the cited model achieves intensity invariance through spike-frequency adaptation with realistic dynamics.

The nonlinearity The nonlinearity used in our model was a simple exponential function, which monotonically increased for increases in its input. Experimentally observed nonlinearities often exhibited a decay in spike rate for large input values. While this difference in the nonlinear stage of the song-recognition model did not affect song-feature preference for songs of low contrast, song preference did change for songs of high contrast (Figure B.3*B,C*).This was due to an increase in the amplitude of the filtered stimulus with an increase in song contrast, beyond the exponential regime of the RoG nonlinearity. Regardless of the type of nonlinearity, a way to maintain stable song recognition across stimulus contrasts would be an adaptation of the exponential regime[7] of the nonlinearity to the song contrast. Adaptation to stimulus contrast or variance has been found in retinal circuits of a broad range of species (Smirnakis et al., 1997; Chander and Chichilnisky, 2001; Kim and Rieke, 2001), as well as in the auditory cortex and inferior colliculus of the ferret and the auditory forebrain of the zebrafinch (Rabinowitz et al., 2011; Dahmen et al., 2010; Nagel and Doupe, 2006; for a review, see Wark et al., 2007), and some evidence for sound level invariance of temporal processing in local and ascending neurons of the grasshopper has been reported (Weschke and Ronacher, 2007; Hildebrandt et al., 2015). Yet, contrast adaptation has not been found in first-order auditory interneurons of the cricket (Benda and Hennig, 2008). Thus, further experiments are necessary to test whether contrast adaptation is, first, present in the early auditory system of the grasshopper, and second, maintained across temperatures. If so, this could be highly beneficial for robustness of time-warp invariant song recognition (also see Section 8.4.4).

[7] For sigmoidal nonlinearities, this would correspond to the dynamic range.

Level of abstraction The neural filters in our model and experimental data most likely result from an interplay of excitatory and inhibitory inputs (Marquart, 1985; Stumpner and Ronacher, 1991). Since the full connectivity of the metathoracic network in the grasshopper is unknown, our model's level of abstraction is justified. Connectivity patterns that lead to negatively biased filters could be predicted using supervised learning or the Nonlinear Input Model framework (McFarland et al., 2013). Further, recent experimental evidence suggests that the pulse interval preference of the cricket can be achieved partly due to post-inhibitory rebound excitation through a non-spiking interneuron (Schöneich et al., 2015). Determination of the temporal filters at individual stages of the proposed *feature detector* circuit could reveal possible realizations of distinct degrees of filter bias (cf. Fig. 5C in Schöneich et al., 2015).

8.4.3 Relation to previous models of time-warp invariant song recognition

Time-Warp Invariant Pattern Recognition (TWIPR) has been extensively studied in neuronal network models. Two previous models were developed in the context of time-warp invariant recognition of human speech (Hopfield and Brody, 2000, 2001; Gütig and Sompolinsky, 2009). Both models were based on synaptic learning in order to recognize a specific pattern and hence do not lend themselves for a direct comparison to our model.

Yet, two other previous models were similar to our model in that they were geared towards a description of grasshopper behavior, that is, time-warp invariant recognition of the characteristic on-off pattern of song with a comparatively small set of neurons (Gollisch, 2008; Creutzig et al., 2010). As in our model, adaptation constituted a crucial component for the successful reproduction of behavior in these models. Both models assumed more complex networks to reproduce grasshopper behavior: While the Gollisch model (Gollisch, 2008) was a network of four neurons in three layers, it assumed specific onset and offset signals as input to the network. In the grasshopper, onset or offset selectivity is first achieved by local neurons, the second auditory processing stage (Clemens et al., 2012). Therefore, if the Gollisch model were mapped to the auditory system of the grasshopper, a total of five layers of neurons would be necessary for TWIPR. The Creutzig model (Creutzig et al., 2010) required the output neuron to integrate the activity of three ascending neurons in order to reproduce grasshopper behavior. In contrast, our results suggested that integration over only one of these neurons, AN12, could suffice, because this neuron exhibits a negatively biased filter. A possible reason why

the Creutzig model required two additional processing steps is that adaptation dynamics were too fast to produce an effective subtraction of the average sound intensity over a full syllable-pause combination.

We chose a phenomenological model of grasshopper behavior that was consistent with electrophysiological data. The model was simple enough to allow for investigation of the influence of filter parameters on song preference. In particular, the L-N processing stage of the model represented the filtering performed by all stages of the metathoracic network of the grasshopper. The previous models of TWIPR were more detailed at the cellular level, that is, included dynamics of membrane voltage, synaptic conductances, cell-intrinsic bursting or adaptation. While such model realism is desirable, it would have hindered identification of crucial parameters for, and ultimately the mechanism underlying, TWIPR in our model. All dynamics in the aforementioned models (and hence the respective time constants) are likely to be affected by temperature (Hille, 2001), raising the question whether and how the mechanisms underlying TWIPR in these models can remain functional across temperatures. Since no previous model addressed the problem of temperature-dependent model components, further research is necessary to test the limits of these models under the influence of temperature.

8.4.4 Just the right amount of robustness

The selective pressure on the receiver to develop time-warp invariant song recognition, which is due to the temperature dependence of male song, is counterbalanced by the pressure to avoid confusion of conspecific songs with those of sympatric species (von Helversen and von Helversen, 1994). For perfectly unimodal filters, the song-recognition model exhibited maximal time-warp invariance but lost selectivity for time scale (cf. Figure 8.3*D*,*E*). In the case of multiple sympatric species that produce songs of similar syllable-pause ratio but largely separated time scales (cf. Figure B.4*A*), unimodal filters are therefore not optimal, because they increase the chance of song confusion. Rather, biased bimodal filters are optimal, as they allow for recognition of time-warped songs in the relevant temperature range while maintaining a time scale preference.

Time-warp invariance in the model further depended on the relative song contrast, $\frac{c}{\tilde{c}}$, which implies that the maintenance of a constant *relative* song contrast[8] promotes robustness of time-warp invariant song recognition across different *absolute* song contrasts, c. This would be highly useful, because some

[8] for example, via adaptation of $\tilde{c}$ in response to different song contrasts

grasshoppers ramp up the sound amplitude in the course of song (Loher, 1957; von Helversen, 1972), and the contrast arriving at the female's ear depends on the distance of the male. However, song contrast can provide information about male fitness (Franzke and Reinhold, 2012), which would be lost if the receiver of sound (here: the female) exhibited adaptation to song contrast.

Further studies are required to test whether adaptation of the relative song contrast is exploited in order to increase robustness of song recognition, or whether this is neglected to facilitate recognition of additional fitness cues. Evidence that contrast adaptation is not exploited, which would agree with the latter hypothesis, has been found in crickets (Benda and Hennig, 2008).

9 Conclusion

Inevitably, the body temperature of poikilothermic animals follows the ambient temperature. Despite the temperature dependence of physico-chemical cellular processes, many important vital functions are maintained across the typical temperature ranges that these animals encounter. How is this achieved at the level of nervous systems? In the present thesis, I have proposed mechanisms at the level of single cells and small networks that allow poikilothermic animals to maintain nervous system function across temperatures.

More specifically, I have demonstrated that, in order to achieve temperature robustness of neuronal spike rate, poikilotherms may exploit compensatory mechanisms already at the level of individual primary sensory neurons (Chapter 5), such as auditory receptor neurons in the grasshopper, at no additional metabolic cost compared to strongly temperature-dependent neurons (Chapter 6). Further, I have shown that, despite temperature-robust sound-intensity encoding in receptor neurons, sound processing in higher-order sensory neurons of the grasshopper is significantly affected by changes in temperature (Chapter 7), which contrasts the known temperature robustness of song recognition at the behavioral level. I resolved this apparent mismatch between the observed temperature dependence of sound processing at the neural level and temperature robustness at the behavioral level, using a mathematical model of song recognition that captured the main aspects of neural sound processing, including its temperature dependence (Chapter 8).

The proposed neural mechanisms of temperature compensation are based on the mutual cancellation of the effects of temperature-dependent processes, as known from temperature compensation of circadian rhythms and central pattern generators (Hastings and Sweeney, 1957; Ruoff, 1992; Xu and Robertson, 1996; Barclay et al., 2002; Katz et al., 2004; Tang et al., 2010; Robertson and Money, 2012): At the single-cell level, the cancellation of temperature dependencies of ionic conductances facilitates maintenance of the encoding of sound intensity in the neuronal spike rate (Part I). At the network level, the cancellation of

temperature dependencies of neural filtering facilitate maintenance of species recognition (Part II).

In the following, I briefly recapitulate the main themes of this thesis, and provide suggestions for future research.

Cell-intrinsic vs. network-based temperature compensation This thesis introduced mechanisms to generate temperature-compensated output in single nerve cells or small networks of neurons, both based on temperature-dependent subprocesses. In the former case, different temperature-dependent ionic conductances within a *single neuron* were combined in a way that resulted in temperature-compensated spike rates. In the latter case, the effects of temperature on different filtering properties of the *network* interacted such that the ability of the model to recognize song was maintained across temperatures. Intriguingly, both types of temperature compensation, cell-intrinsic and network-based, were observed in *the same* model system – the auditory system of the grasshopper. This raises two questions: First, if a cell-intrinsic mechanism of temperature compensation developed in the grasshopper, why is it not abundant throughout the network? Second, why is a cell-intrinsic mechanism necessary at all, if temperature compensation can be achieved at the network level?

To answer the first question, it is important to note that receptor neurons did not exhibit perfect temperature *invariance*, but a *low* temperature dependence. Error propagation could amplify this small temperature dependence of single neurons in the network, resulting in a large temperature dependence at the level of behavior. Nevertheless, it is useful to limit temperature dependence of the input layer. Receptor neurons convert sound pressure to a spike signal, enabling postsynaptic neurons to infer from that spike rate information about the sound intensity of incoming stimuli. If receptor neuron spike rates exhibited a stronger dependence on temperature, postsynaptic neurons could not distinguish, for example, whether an increase in spike rate resulted from an increase in sound intensity or temperature. Further, the *population* code of receptor neurons is transformed to a sparse, *labeled line* code at the level of ascending neurons (Clemens et al., 2011). In other words, while the population rate of multiple receptor neurons is used to generate the representation of sound in postsynaptic local and ascending neurons, for read-out neurons in the brain it is more important to receive input from the *relevant* ascending neurons at all, rather than *how much*. From this point of view, it seems more important to implement temperature compensation at the receptor neuron rather than the ascending neuron level.

The generation of a *sparse* code in ascending neurons is also relevant for the second question, that is, why cell-intrinsic temperature compensation is useful if compensation is also present at the network level: Receptor neurons can produce spikes at high rates, up to several hundreds per second. If temperature dependence were stronger, heating would increase the number of generated spikes, which most likely would increase the overall energy consumption (cf. Chapter 6; Niven and Laughlin, 2008). Furthermore, receptor neurons outnumber ascending neurons, and spike rates of receptor neurons are typically higher than those of ascending neurons (Vogel et al., 2005). Also from that point of view, it is most sensible to establish temperature compensation in particular at the receptor neuron level.

Concluding, poikilotherms may employ temperature compensation at different levels, that is, the level of single neurons or networks, to achieve different goals – in this case, accuracy and energy efficiency of sound level encoding on the one hand, and robustness of song recognition on the other hand. Importantly, different mechanisms of temperature compensation are not mutually exclusive, but can be used in parallel within the same organism.

Neuronal computation under multiple constraints Nervous systems evolved to increase the chance of survival[1] for organisms living in an ever-*changing* environment (Allman, 2000). The design of nervous systems is constrained by *external* factors (available environmental or sensory cues, e.g., light, chemical or acoustic signals, temperature), and by *internal* factors, such as the energetic demands of neurogenesis, neuronal wiring, or action potential generation, or accuracy of computations (Laughlin et al., 1998; Laughlin and Sejnowski, 2003; Niven and Laughlin, 2008).

I have shown that the nervous systems of poikilothermic animals can cope with both external and internal constraints. More specifically, the results presented in Part I suggest that temperature as an external constraint is overcome by establishing a cell-intrinsic compensatory mechanism. Furthermore, the internal constraint of energetic costs associated with action potential generation and maintenance of the resting potential is overcome by largely basing the compensatory mechanism on ionic conductances that are of low relevance for energy consumption.

This thesis focused on point-neuron models, that is, models without spatial dimensions. Therefore, space-related constraints were not addressed here. The reliability of action potential propagation along the axon depends on the composition and distribution of ionic conductances in the axon and is

[1] that is, by locating food sources and avoiding hazard

metabolically expensive in cortical pyramidal neurons (Hallermann et al., 2012). Given the differential effects of temperature on individual conductances that were addressed in this thesis, reliable propagation across temperatures is not self-evident. Further studies are required to test how the compatibility of energy efficiency and temperature compensation of spike rate is constrained by reliable action potential propagation.

A unified model of filter-based pattern recognition Communication in many insects is based on signals consisting of simple on-off patterns. In the grasshopper, the neuronal circuitry devoted to the processing and recognition of such patterns in courtship song consists of comparatively few neurons and is conserved across species (Neuhofer et al., 2008). Yet, song preferences are phenotypically highly diverse even in closely related species, raising the question for the evolutionary transformations of the neural circuitry (Hennig et al., 2004).

In Chapter 8, I proposed a simple yet biologically motivated mathematical model with the original aim of reproducing time-warp invariant song recognition as observed in *Chorthippus biguttulus* females.

Apart from fulfilling its original aim, preliminary results (see Appendix B.3) suggest that the model further captures the song preferences of three sympatric grasshopper species. This is in line with the hypothesis that these species share neural circuitry devoted to sound processing, which evolution transformed to allow for species separation (Hennig et al., 2004; cf. Section 9.1). In a future study, the model could be fitted to published data on behavioral song preferences in different related species (e.g., von Helversen and von Helversen, 1994; Schul, 1998; Hennig et al., 2004; Rothbart and Hennig, 2012). Patterns or correlations in the fitted parameters could provide insights on the aforementioned evolutionary circuit transformations that lead to diverse song preferences.

Moreover, the model is general regarding the sensory modality and can hence be used to predict neural filters involved in time-warp invariant recognition of on-off patterns in other sensory systems. Species whose courtship relies on such patterns include spiders (vibratory signals; Schüch and Barth, 1990), fireflies (visual signals; Carlson et al., 1976; Lewis and Cratsley, 2008), frogs, and crickets (acoustic signals; Gerhardt and Doherty, 1988; Pires and Hoy, 1992; Kostarakos and Hedwig, 2012). As shown in this thesis for song recognition in the grasshopper, the model can be used to estimate how temperature effects on filter shape translate to recognition performance in other animals. For example, the wandering spider *Cupiennius salei* uses vibratory courtship signals,

which exhibit a syllable-pause structure as courtship song of the grasshopper. Like in the grasshopper, the syllable-pause ratio constitutes one of the most important parameters to influence the female response rate (Schüch and Barth, 1990). Intriguingly, this parameter is conserved across behaviorally relevant temperatures (Shimizu and Barth, 1996), and duty-cycle selective interneurons have been identified (Friedel and Barth, 1995).[2] However, information about the courtship signal-processing circuit of the spider is lacking[3], and filter properties of the duty-cycle tuned interneurons have not been studied yet. Hence, the model could be used to motivate and guide future experiments to unravel the neural circuitry underlying spider courtship.

Further, if the temporal dimension is replaced by space in the model, spatial filters with modality bias are able to detect spatial patterns across a broad range of spatial scales.[4] Hence, the model generalizes to spatial on-off patterns and therefore can be used for *space-warp* or *scale*-invariant pattern recognition, which has potential applications in computer vision, such as stable recognition of the duty cycle of a grating across different distances.

The model successfully bridges the gap between the level of computations in a network of neurons and the behavioral level. Yet, it does not make specific assumptions of how the network computations are realized in terms of a concrete circuit. Future computational studies could attempt to identify the few parameters of the model with circuit parameters, such as the balance of excitation and inhibition in the network or the delay between inhibition and excitation. Ultimately, this could lead to a library of network motifs that generate preferences for specific input patterns. These predicted circuits then provide a concrete target for electrophysiological experiments. As a starting point, neural filters could be determined for different neurons in established circuits (e.g., Schöneich et al., 2015; cf. Section 9.1, Item 2).

9.1 Outlook and open questions

The research described in this thesis raises the following questions, which can be addressed in future experiments or theoretical studies:

1. Is the proposed mechanism of cell-intrinsic temperature compensation, particularly with respect to the mechanosensory transduction, actually implemented in receptor neurons? Real neurons likely contain more types of conductances than used in the model of Chapter 5 (Wicher et al.,

[2] Nb.: the duty cycle d is related to the syllable-pause ratio τ_s/τ_p, with $d = 1/(1 + \tau_p/\tau_s)$.
[3] which is also due to the low suitability of spiders for electrophysiological experiments
[4] Note that this refers to patterns in one spatial dimension, such as gratings.

2001), providing additional dimensions for temperature compensation and its separation from other constraints.

2. What time course of inhibitory and excitatory inputs to ascending neurons is required to produce the observed neural filters of different modality? This will be of particular relevance for a biophysical implementation of the proposed song-recognition model. A highly promising lead is provided by Schöneich et al. (2015): a re-analysis of their existing spiking data could prove how a bimodal neural filter can be created using a mix of excitation and delayed inhibition. Alternatively, a purely computational implementation of the network, combined with a subsequent analysis of the filters at each processing stage, could provide insights on possible circuit realizations of different filters.[5]

3. Do the time scales of neural filters involved in song recognition in *Chorthippus brunneus*, *Chorthippus biguttulus*, and *Chorthippus mollis* differ? The song-recognition model predicts that time-scale separation of song preference, as observed in these three sympatric grasshopper species, is mainly achieved by establishing neural filters of distinct time scales (cf. Figure 2.1*D* and Chapter 8).

4. Along the lines of Item 2: If the filter time scales differ between species (cf. Item 3), are they created based on delay lines (i.e., differences in wiring length), or via exploitation of different axon diameters that alter propagation speed (Hutchinson et al., 1970)?[6]

5. Is mean subtraction from the input a required computational step in order to reproduce behavioral song preferences of *Chorthippus biguttulus*, as the modeling results presented here suggest? Spike-frequency adaptation of local neurons can account for such mean subtraction, as shown for crickets (Benda and Hennig, 2008). Therefore, a testable prediction of the song recognition model would be that time-warp invariance of song recognition is lost if spike-frequency adaptation is blocked in local

[5] Connectivity patterns that result in filters of different bias could be predicted using supervised learning or the Nonlinear Input Model framework (McFarland et al., 2013).

[6] A testable hypothesis would be that smaller species use narrower axons due to space constraints (Niven and Farris, 2012), which leads to broader neural filters and correspondingly increases the time scale of song preference. A drawback of narrow axons is the decreased information rate and timing precision (Perge et al., 2012), which could correspond to an increased range of accepted syllable-pause pairs, that is, broader tuning. Concluding, differences in axon diameter could account for the differences in time scale and tuning width of song preference in *Chorthippus mollis*, *Chorthippus biguttulus*, and *Chorthippus brunneus* (cf. Figure 2.1*D*), due to the different size of these species (Perdeck, 1958).

neurons, either pharmacologically (cf. Peron and Gabbiani, 2009) or using optogenetic inactivation of adaptation channels (cf. Pulver et al., 2009).[7]

6. Do ascending neurons in female grasshoppers exhibit adaptation to song contrast? Given an implementation of the proposed song-recognition model, this adaptation would increase robustness of song preference, but the ability would be lost to use loudness of song (i.e., high contrast) as a cue for male fitness (cf. Chapter 8). This could be tested with experiments identical to those in Chapter 7, except for the use of stimuli of different contrasts.

7. Is the proposed combination of feed-forward adaptation, filtering, and integration used by species other than the grasshopper (e.g., spiders, fireflies, crickets, or even mammals), for time-warp or scale invariant pattern recognition?

9.2 Final remarks

In the present thesis, I proposed mechanisms for poikilothermic animals to prevent the inevitable effects of temperature on processes at the microscopic level from affecting the functionality of the nervous system and ultimately behavior. The existence of such mechanisms had been presumed for a long time, which probably led Krehl and Soetbeer (1899) to the conclusion that poikilotherms[8] are *not* a *Spielball der Umgebung*, that is, a *plaything of their surroundings*. While they pointed out how poikilotherms could control their body temperature by means of convection or changing the color or surface of their skin, this thesis focused on mechanisms that allowed for – or even relied on – a temperature dependence of basic processes inside the body. This further challenges the *Spielball/plaything* notion, also for animals that lack explicit capabilities for thermoregulation.

[7] It is debatable though whether the suggested experiments are too invasive to allow for quantification of behavioral preferences.

[8] here: reptiles and amphibians

A Appendix to Part I

A.1 Definition of the Connor-Stevens model

The Connor-Stevens model reads

$$\begin{aligned} C_{\mathrm{m}}\frac{dV}{dt} &= I_{\mathrm{C}} - I_{\mathrm{L}} - I_{\mathrm{Na}} - I_{\mathrm{K}} - I_{\mathrm{A}} \\ &= I_{\mathrm{C}} - \bar{g}_{\mathrm{L}} \cdot (V - E_{\mathrm{L}}) - \bar{g}_{\mathrm{Na}} m^3 h \cdot (V - E_{\mathrm{Na}}) \\ &\quad - \bar{g}_{\mathrm{K}} n^4 \cdot (V - E_{\mathrm{K}}) - \bar{g}_{\mathrm{A}} a^3 b (V - E_{\mathrm{A}}). \end{aligned}$$

All gating variables $x \in \{n, m, h, a, b\}$ followed first-order kinetics. Specifically, for the opening and closing rates of the (in-) activation variables, α and β, we have:

$$\begin{aligned} \alpha_m &= \frac{0.38 \cdot (V + 29.7)}{1 - \exp(-0.1 \cdot (V + 29.7))}, \\ \beta_m &= 15.2 \cdot \exp(-0.0556 \cdot (V + 54.7)), \\ \alpha_h &= 0.266 \cdot \exp(-0.05 \cdot (V + 48)), \\ \beta_h &= \frac{3.8}{1 + \exp(-0.1 \cdot (V + 18))}, \\ \alpha_n &= \frac{0.02 \cdot (V + 45.7)}{1 - \exp(-0.1 \cdot (V + 45.7))}, \\ \beta_n &= 0.25 \cdot \exp(-0.0125 \cdot (V + 55.7)). \end{aligned}$$

For the steady-state (in-)activation functions $x_\infty, x \in \{a, b\}$, and the time constant of (in-)activation, τ_x, we have:

$$\tau_a = 0.3632 + \frac{1.158}{1 + \exp(0.0497 \cdot (V + 55.96))},$$
$$a_\infty = \left(\frac{0.0761 \cdot \exp(0.0314 \cdot (V + 94.22))}{1 + \exp(0.0346 \cdot (V + 1.17))}\right)^{1/3},$$
$$\tau_b = 1.24 + \frac{2.678}{1 + \exp(0.0624 \cdot (V + 50))},$$
$$b_\infty = \left(\frac{1}{1 + \exp(0.0688 \cdot (V + 53.3))}\right)^4.$$

A.2 Fisher information

This appendix analytically shows how information transmission in single neurons is affected by changes in temperature. The results were published in Roemschied et al. (2014).

For a spike generation process $f(I)$, the Fisher information $J(I)$ is a measure of how accurately a particular input current I can be decoded from the firing-rate response $f(I)$. It is formally defined as

$$J(I) = \int \left(\frac{\partial}{\partial I} \ln P(f|I)\right)^2 P(f|I) df,$$

with the conditional probability density of the spike rate given an input current, $P(f|I)$, characterizing the output noise (i.e., spike rate variability). We consider two empirical response models for the spike rate density: Poissonian and input-independent Gaussian, reading

$$P_{\mathrm{P}}(\tilde{f}|I) = \frac{(f(I) \cdot b)^{\tilde{f} \cdot b}}{(\tilde{f} b)!} \cdot \exp(-f(I) b) \text{ and}$$
$$P_{\mathrm{G}}(\tilde{f}|I) = \frac{1}{\sqrt{2\pi\sigma^2}} \cdot \exp\left(-\frac{(\tilde{f} - f(I))^2}{2 \cdot \sigma^2}\right),$$

respectively. For the Poisson case, b denotes the time bin during which a certain spike count N_{sp} is observed. It is assumed to be sufficiently large that N_{sp}/b is well approximated by the mean firing rate $f(I)$. σ^2 denotes the variance of the

Gaussian probability density. The corresponding Fisher information is given by

$$J_{\mathrm{P}}(I) = \frac{(f'(I))^2}{f(I)} \text{ and}$$
$$J_{\mathrm{G}}(I) = \frac{(f'(I))^2}{\sigma^2},$$

respectively.

To compare Fisher information for the spike generation model introduced in Chapter 5 across different temperatures, it was averaged across a fixed interval of output firing rates $[f_{\min}, f_{\max}]$. Accordingly, the input current interval $[I_{\min}, I_{\max}]$ was computed for each model and temperature. Average Fisher information reads

$$\langle J \rangle = (I_{\max} - I_{\min})^{-1} \int_{I_{\min}}^{I_{\max}} dI\, J(I).$$

For low noise, the average Fisher information is a lower bound to the neuron's capacity to transmit information (Kostal et al., 2013),

$$C_{\mathrm{low}} = \ln\left(\frac{\int dI\, J(I)}{\sqrt{2\pi e}}\right).$$

Exploiting the square-root shape of firing-rate curves for $I \geq I_0$, $f(I) = A \cdot \sqrt{I - I_0}$, and $f'(I) = A/2 \cdot (I - I_0)^{-1/2}$, it follows that

$$\frac{1}{\Delta I} \equiv \frac{1}{I_{\max} - I_{\min}} = \frac{A^2}{f_{\max}^2 - f_{\min}^2}. \tag{A.1}$$

For the Poisson probability density, Fisher information is given by

$$\begin{aligned}\langle J_{\mathrm{P}} \rangle &= \frac{1}{\Delta I} \int_{I_{\min}}^{I_{\max}} dI\, A/4 \cdot (I - I_0)^{-3/2} \\ &= \frac{1}{\Delta I} \cdot (-A/2) \left[(I - I_0)^{-1/2}\right]_{I_{\min}}^{I_{\max}} \\ &= \frac{1}{\Delta I} \cdot (-A^2/2) \left[(A\sqrt{I - I_0})^{-1}\right]_{I_{\min}}^{I_{\max}}.\end{aligned}$$

With Equation A.1, it can be expressed as

$$\begin{aligned}\langle J_\mathrm{P}\rangle &= \frac{1}{\Delta I}\cdot(-A^2/2)(1/f_\mathrm{max}-1/f_\mathrm{min})\\ &= \frac{A^2}{f_\mathrm{max}^2-f_\mathrm{min}^2}\cdot(-A^2/2)(1/f_\mathrm{max}-1/f_\mathrm{min})\\ &= A^4\cdot\frac{1}{2f_\mathrm{max}f_\mathrm{min}(f_\mathrm{max}+f_\mathrm{min})}.\end{aligned}$$

For a Gaussian probability density, we get

$$\begin{aligned}\langle J_\mathrm{G}\rangle &= \frac{1}{\Delta I}\int_{I_\mathrm{min}}^{I_\mathrm{max}} dI\, A^2/(2\sigma^2)\cdot\frac{1}{I-I_0}\\ &= \frac{A^2/(2\sigma^2)}{\Delta I}\cdot[\ln(I-I_0)]_{I_\mathrm{min}}^{I_\mathrm{max}}\\ &= \frac{A^2/(2\sigma^2)}{\Delta I}\cdot\ln\left(\frac{I_\mathrm{max}-I_0}{I_\mathrm{min}-I_0}\right)\end{aligned}$$

instead. Fisher information in this case reads

$$\langle J_\mathrm{G}\rangle = \frac{A^4}{\sigma^2(f_\mathrm{max}^2-f_\mathrm{min}^2)}\cdot\ln\left(\frac{f_\mathrm{max}}{f_\mathrm{min}}\right).$$

Because only the gain of the firing-rate curve, A, depends on temperature in $\langle J_\mathrm{P}\rangle$ and $\langle J_\mathrm{G}\rangle$, the temperature dependence of Fisher information is given by

$$Q_{10}(\langle J_\mathrm{P}\rangle) = Q_{10}(\langle J_\mathrm{G}\rangle) = [Q_{10}(A)]^4.$$

For the average value across a fixed output interval $[f_\mathrm{min}, f_\mathrm{max}]$, Fisher information is invariant to shifts of the threshold. A heating-induced increase in the accuracy of a decoder hence requires an increase in gain of the firing-rate curve, i.e., $Q_{10}(A) > 1$. This is true for all spike-generation models considered in Chapter 5.

A.3 Optimal vs. inverse optimal dimensional stacking

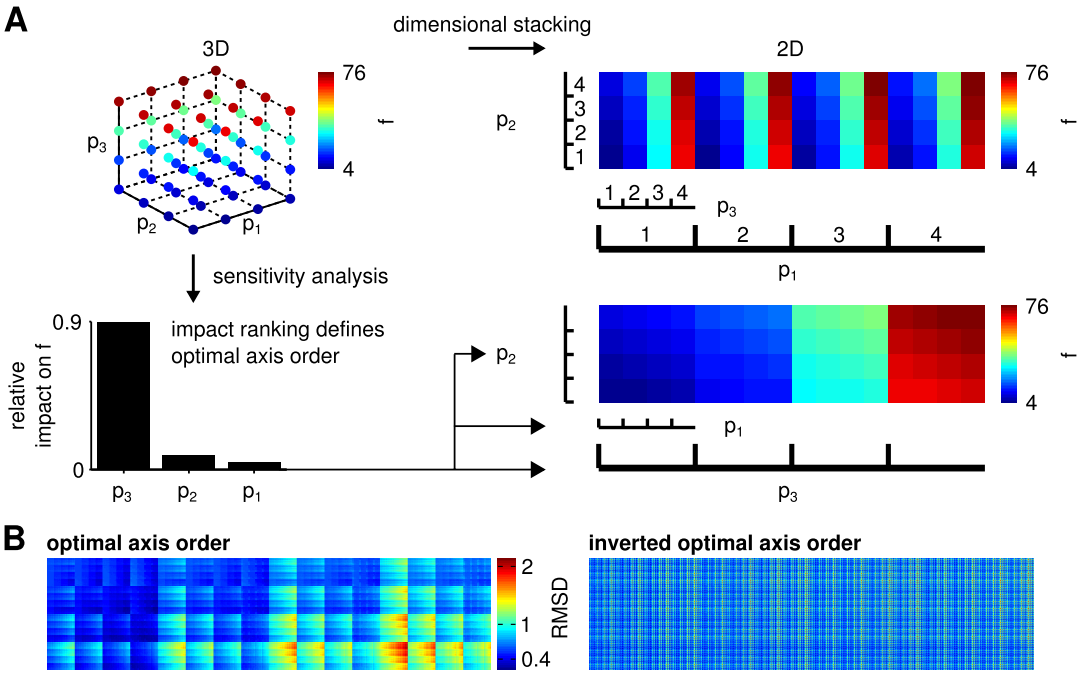

Figure A.1 Optimal vs. inverse optimal dimensional stacking **A:** Dimensional stacking maps a function of N parameters (here: three) onto a two-dimensional image, by representing different parameters on different *scales* of the x- and y-axis. Therefore, $N!$ different axis arrangements and hence different possible images exist, which differ in their visual informativeness[a]. Therefore, optimization of the axis order is required, in particular for high-dimensional functions. **B:** This becomes strikingly clear when comparing the optimal and inverted optimal axis orders of Figure 5.4*C*, where sensitivity analysis was used for axis optimization (see Chapter 5 for details).

[a] because changes at large scales of the image are easier to perceive than at small scales

A.4 Temperature compensation in the Traub-Miles model

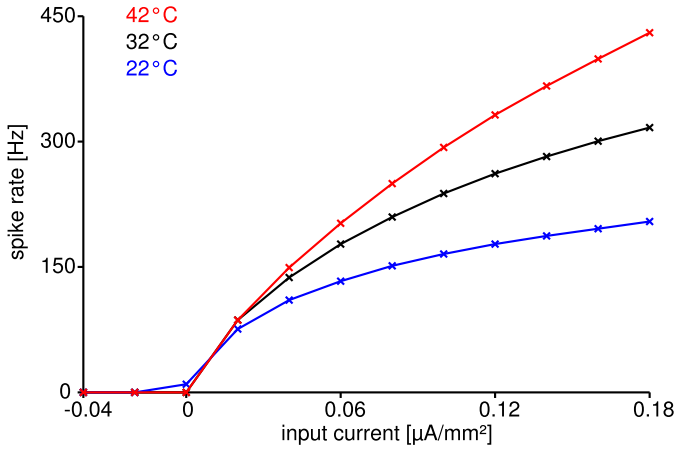

Figure A.2 Temperature compensation in the Traub-Miles model. Temperature compensation of spike generation was also possible in a structurally different Traub-Miles model despite a realistic temperature dependence of its three conductances (g_L,g_K,g_{Na}). Shown are the model at reference temperature (32°C for this model, black curve), and the model heated up by 10°C (red curve) or cooled down by 10°C (blue curve), with temperature-dependence parameters that minimize the RMSD of the corresponding f-I curves within the physiologically realistic range (identical to that explored for the Connor-Stevens model; for peak conductances, $Q_{10}(\bar{g}) \in [1.2, 2]$, and for transition rates of the (in-) activation variables, $Q_{10}(\alpha, \beta) \in [2, 4]$). Optimal parameters minimizing the RMSD were identified by a genetic algorithm (see Section 5.2.9 for details). Relative changes in firing rate were on the order of those observed experimentally (RMSD=0.34 comparing the curves at 32 and 42°C, and RMSD=0.55 comparing the curves at 22 and 32°C).

B Appendix to Part II

B.1 Analytical calculation of the song-recognition model response to song

The song-recognition model defined in Chapter 8 was evaluated analytically, as shown in the following. Recall the definitions of song, $S(t)$, and the temporal filter, $f(t)$:

$$S(t) = p \cdot H(\tau_p - t) + s \cdot H[t - (\tau_s + \tau_p)] \cdot H(t - \tau_p),$$
$$f(t) = ma \cdot H(w - t) - (1 - m)a \cdot H(2w - t) \cdot H(t - w).$$

Due to the Heaviside step function H in the definitions of both filter and song, a case analysis was required. For brevity, here only one example case is shown, namely $2w \leq \tau_s, \tau_p$, with filter-lobe width w, and syllable and pause lengths τ_s, τ_p. Calculations for all other cases are straight-forward.

In Chapter 8 it was shown that the full response of the song-recognition model, N, including mean subtraction from the input song, factorizes into a term that corresponds to the response of the same model without mean subtraction (N_{raw}), and a normalization matrix (M), $N = N_{\text{raw}} \cdot M$. Here,

$$N_{\text{raw}} = \frac{W}{\tau_s + \tau_p} \cdot \underbrace{\int_0^{\tau_s+\tau_p} dt \exp\left(\frac{1}{\tilde{c}} \int_0^{2w} d\tau f(\tau) S(t - \tau)\right)}_{*} \cdot \exp\left(\frac{-x_0}{\tilde{c}}\right).$$

To simplify the evaluation of the convolution, the integration over time (term $(*)$) is first divided into parts I to VI according to Figure B.1. This choice ensures that either at least one of the single filter lobes is convolved with a constant segment of song (e.g., VI), or one of the filter lobes transitions from syllable to pause (or pause to syllable) during the convolution, over a time course of length w (e.g., the positive filter lobe in I). Consider for example term III, in which both filter lobes are convolved only with the pause. The convolution of

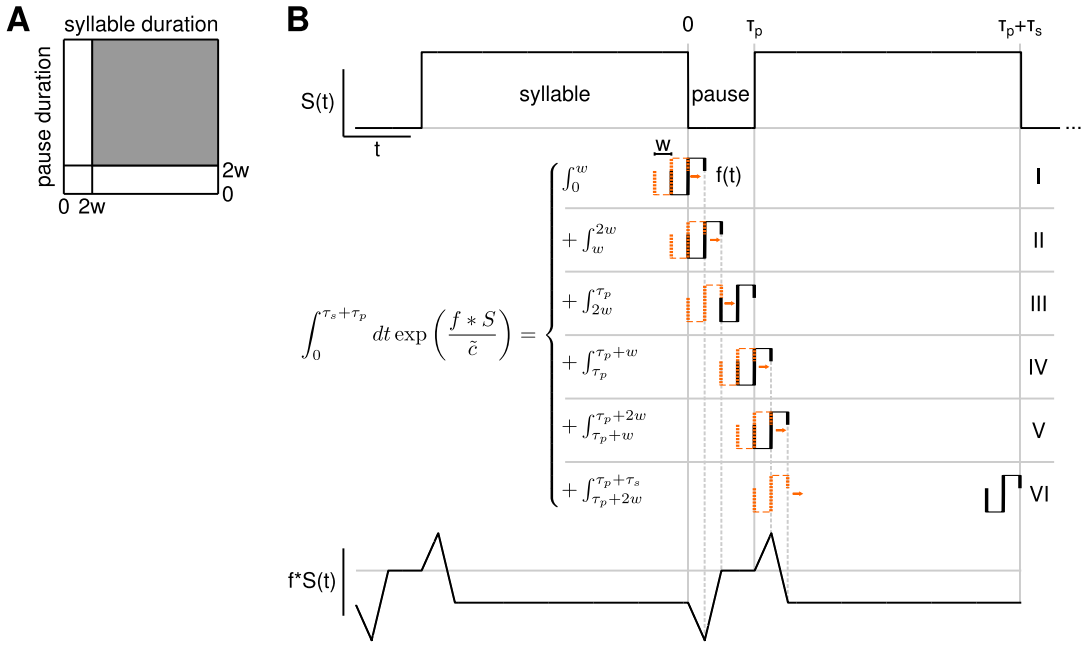

Figure B.1 Analytical integration of filter response to song. **A:** Calculations shown in this appendix are valid for syllable and pause durations larger than twice the single-lobe width of the filter, $2w \leq \tau_s, \tau_p$. **B:** The convolution of song S and filter f for times 0 to $\tau_s + \tau_p$ can be divided into six parts (I to VI). This choice ensures that either at least one of the single filter lobes is convolved with a constant segment of song (e.g., VI), or one of the filter lobes transitions from syllable to pause (or pause to syllable) during the convolution, over a time course of length w (e.g., the positive filter lobe in I). Within each of the chosen intervals, the convolution $f * S$ is constant or linear.

the positive and negative lobe at each point in time *within* the pause evaluates to $mwap$ and $-(1-m)wap$, respectively. Hence, the convolution for the entire filter evaluates to $(2m-1)wap$. Now consider term I, in which the positive filter lobe initially overlaps with the syllable and then transitions to a full overlap with the pause, within a time interval of length w. The response of the positive filter lobe between times 0 and t can be parametrized as $mwas + t \cdot (ma(p-s))$. The response of the negative filter lobe is constant for this segment and equals $-(1-m)was$.
Using the substitution $s = c,\ p = 0$ as in the main text, term I correspondingly evaluates to

$$\begin{aligned}
\mathrm{I} &= \int_0^w dt \exp\left(\frac{m}{\tilde{c}}(wac - act) + \frac{1-m}{\tilde{c}}(-wac)\right) \\
&= \int_0^w dt \exp\left(\frac{(2m-1)wac}{\tilde{c}} - \frac{mac}{\tilde{c}}t\right) \\
&= \exp\left(\frac{(2m-1)wac}{\tilde{c}}\right) \cdot \left(\frac{-\tilde{c}}{mac}\right) \cdot \left[\exp\left(\frac{-mwac}{\tilde{c}}\right) - 1\right] \\
&\underset{m\to 0}{\to} w \cdot \exp\left(\frac{-wac}{\tilde{c}}\right).
\end{aligned}$$

The last step resulted from a first-order Taylor expansion of $\left[\exp\left(\frac{-mwac}{\tilde{c}}\right) - 1\right]$ around $m = 0$. Evaluation of the remaining terms is analogous,

$$\begin{aligned}
\mathrm{II} &= \exp\left(\frac{(m-1)wac}{\tilde{c}}\right) \cdot \left(\frac{\tilde{c}}{(1-m)ac}\right) \cdot \left[\exp\left(\frac{(1-m)wac}{\tilde{c}}\right) - 1\right] \underset{m\to 1}{\to} w, \\
\mathrm{III} &= \tau_p - 2w, \\
\mathrm{IV} &= \left(\frac{\tilde{c}}{mac}\right) \cdot \left[\exp\left(\frac{mwac}{\tilde{c}}\right) - 1\right] \underset{m\to 0}{\to} w, \\
\mathrm{V} &= \exp\left(\frac{mwac}{\tilde{c}}\right) \cdot \left(\frac{\tilde{c}}{(m-1)ac}\right) \cdot \left[\exp\left(\frac{(m-1)wac}{\tilde{c}}\right) - 1\right] \\
&\underset{m\to 1}{\to} w \cdot \exp\left(\frac{wac}{\tilde{c}}\right), \\
\mathrm{VI} &= (\tau_s - 2w) \cdot \exp\left((2m-1)\frac{wac}{\tilde{c}}\right).
\end{aligned}$$

Before combining the terms, we first define a few abbreviations:

$$\begin{aligned}
\exp_{\pm} &= \exp\left(\pm\frac{wac}{\tilde{c}}\right),\\
\exp_{12} &= \exp\left(\frac{wac}{\tilde{c}}\cdot(1-2m)\right) = \exp_{-}^{2m-1},\\
\exp_{21} &= \exp\left(\frac{wac}{\tilde{c}}\cdot(2m-1)\right) = \exp_{+}^{2m-1} = \exp_{12}^{-1}.
\end{aligned}$$

Hence, for large $\frac{wac}{\tilde{c}}$, $\exp_{+} \gg 1$ and $\exp_{-} \to 0$. Assuming $w, a, \frac{c}{\tilde{c}} > 0$,

$$\exp_{12} = \begin{cases} 1 & , m = \frac{1}{2} \\ \exp_{-} < 1 & , m = 1 \\ \exp_{+} > 1 & , m = 0 \end{cases}$$

$$\exp_{21} = \begin{cases} 1 & , m = \frac{1}{2} \\ \exp_{+} > 1 & , m = 1 \\ \exp_{-} < 1 & , m = 0 \end{cases}$$

Then,

$$N_{\text{raw}} = \frac{W}{\tau_s + \tau_p}\cdot\left(\tau_s\cdot\exp_{21} + \tau_p + K\right)\cdot\exp\left(\frac{-x_0}{\tilde{c}}\right).$$

Here, for $0 < m < 1$,

$$\begin{aligned}
K = &-2w\cdot(\exp_{21}+1)\\
&+\exp_{21}\cdot\left(-\frac{\tilde{c}}{mac}\right)\cdot\left[\exp\left(-\frac{mwac}{\tilde{c}}\right)-1\right]\\
&+\exp\left(\frac{(m-1)wac}{\tilde{c}}\right)\cdot\left(\frac{\tilde{c}}{(1-m)ac}\right)\cdot\left[\exp\left((1-m)\frac{wac}{\tilde{c}}\right)-1\right]\\
&+\exp\left(\frac{mwac}{\tilde{c}}\right)\cdot\left(\frac{\tilde{c}}{(m-1)ac}\right)\cdot\left[\exp\left((m-1)\frac{wac}{\tilde{c}}\right)-1\right]\\
&+\left(\frac{\tilde{c}}{mac}\right)\cdot\left[\exp\left(\frac{mwac}{\tilde{c}}\right)-1\right].
\end{aligned}$$

For $m \to 0$,

$$K \to -w\cdot(\exp_{-}+1) + \frac{2\tilde{c}}{ac}\cdot\left(1-\exp_{-}\right).$$

For $m \to 1$,

$$K \to -w \cdot (1 + \exp_+) + \frac{2\tilde{c}}{ac} \cdot \Big(\exp_+ - 1\Big).$$

Hence, K is independent of syllable and pause duration for all values of m.

For $m = 1$,

$$\begin{aligned}
&\exp_{21} = \exp_+ > 1 \\
\Rightarrow\ &\exp_+ = 1 + R, \quad R > 0 \\
\Rightarrow\ &N_{\text{raw}} = \frac{W}{\tau_s + \tau_p} \cdot \Big(\tau_s \cdot (1 + R) + \tau_p + K\Big) \cdot \exp\Big(\frac{-x_0}{\tilde{c}}\Big) \\
&\qquad = \frac{W}{\tau_s + \tau_p} \cdot \Big(\tau_s + \tau_p + R \cdot \tau_s + K\Big) \cdot \exp\Big(\frac{-x_0}{\tilde{c}}\Big) \\
&\qquad = W \cdot \exp\Big(\frac{-x_0}{\tilde{c}}\Big) \cdot \left(1 + R \cdot \frac{\tau_s}{\tau_s + \tau_p}\right) \\
&\qquad = W \cdot \exp\Big(\frac{-x_0}{\tilde{c}}\Big) \cdot \left(1 + R \cdot \frac{1}{1 + \tau_p/\tau_s}\right)
\end{aligned}$$

Hence, for $m = 1$, N_{raw} is maximal for $\tau_s/\tau_p \to \infty$. Likewise, for $m = 0$, N_{raw} is maximal for $\tau_s/\tau_p \to 0$. In other words, in the song-recognition model without mean-subtraction step, a positive (negative) unimodal filter acts as an *integrator* for syllable (pause) duration (cf. Figure 8.3*Aiii*).

For $m = \frac{1}{2}$, we get:

$$K = -4w + 4\frac{\tilde{c}}{ac} \cdot \left[\exp\Big(\frac{wac}{2\tilde{c}}\Big) - \exp\Big(-\frac{wac}{2\tilde{c}}\Big)\right].$$

Further,

$$\begin{aligned}
N_{\text{raw}} &= \frac{W}{\tau_s + \tau_p} \cdot \Big(\tau_s + \tau_p + K\Big) \cdot \exp\Big(\frac{-x_0}{\tilde{c}}\Big) \\
&= W \cdot \left(1 + \frac{1}{\tau_s + \tau_p} \cdot K\right) \cdot \exp\Big(\frac{-x_0}{\tilde{c}}\Big).
\end{aligned}$$

Here it is evident that for perfectly bimodal filters and the considered syllable-pause regime, $2w \leq \tau_s, \tau_p$, the response to song of the model without mean subtraction, N_{raw} is inversely related to the *song period*, $\tau_s + \tau_p$, indicating a *differentiator-like* selectivity[1]. Importantly, since for bimodal filters the normal-

[1] The response of a bimodal filter is maximal for minimal song period, i.e., for the maximal number of *transitions* from syllable to pause.

Table B.1 Parameters of the MoG filter bank.

Parameter	Symbol	Range	Step	Unit
Positive-lobe position	μ_1	-30	—	ms
Peak-to-peak distance	$\mu_1 - \mu_2$	1-20	1	ms
Positive-lobe weight	M	0-1	0.025	—
Positive-lobe width	σ_1	1-6	1	ms
Negative-lobe width	σ_2	1-6	1	ms

ization matrix M equals unity, the same holds for the response of the full model, $N = N_{\text{raw}} \cdot M \rightarrow N_{\text{raw}}$.

B.2 Validation of song-recognition model approximations

Although the song-recognition model introduced in Chapter 8 was developed such that the experimental results of Chapter 7 could be easily incorporated, a few simplifying assumptions were made that are justified in the following. More specifically, a Linear-Nonlinear (L-N) model constituted an essential element of the model, in which the linear and nonlinear stage was based on a box-shaped linear filter and an exponential nonlinearity, respectively. Here we used numerical simulations to test to what extent these approximations altered three measures of song feature preference that were computed from model response maps: *species preference*, *tuning width*, and *time-warp invariance* (see Chapter 8 for definitions).

Filter matching To match a given box filter of modality m and width w to a MoG filter, first a bank of MoG filters $f(t|\mu_1, \mu_2, \sigma_1, \sigma_2, M)$ was created (see Chapter 7 for definitions), using the parameters specified in Table B.1. For each of the resulting MoG filters, the modality m_{MoG}, the peak-to-peak distance $\Delta\mu$, the FWHMin, f_-, and FWHMax, f_+, were determined. Then, the MoG filter that minimized the objective function $(m - m_{\text{MoG}})^2 + (w - \Delta\mu)^2 + (w - f_-)^2 + (w - f_+)^2$ was defined as the matching filter.

Nonlinearities Three types of nonlinearities $r = D(x)$ were used: an exponential, $r = \exp\left(\frac{x - x_0}{\tilde{c}}\right)$, with parameters obtained from fits to experimental data[2],

[2] cf. Figure 7.4

Table B.2 Parameter sweep.

Parameter	Symbol	Range	Step	Unit
Filter modality	m	0-1	0.125	—
Filter width	w	5-10	5	ms
Relative song contrast[1]	$\frac{c}{\tilde{c}}$	6	—	—
Song contrast[2]	c	10-50	10	dB SPL

[1] This was used to compare box and MoG filters.
[2] This was used to compare different nonlinearity types.

$x_0 = 7.4$ and $\tilde{c} = 10.1$, a matching RoG nonlinearity, $r = p_1 \cdot \frac{N(x|p_2,p_3)}{N(x|p_4,p_5)}$, with $p_1 = 24.0$, $p_2 = 11.1$, $p_3 = 0.0$, $p_4 = 13.8$, and a matching sigmoidal nonlinearity, $r = \frac{p_1}{1+\exp\left(\frac{-(x-p_2)}{p_3}\right)}$, with $p_1 = 90.4$, $p_2 = 48.2$, and $p_3 = 8.5$ (see Figure B.2*C*). The matching was performed by means of a nonlinear fit over all inputs smaller than that corresponding to the peak of the RoG nonlinearity.

Parameter sweep Response maps were created for all combinations of the parameters specified in Table B.2, using zero-padded filters of 128 ms total length.

B.2.1 Song feature preferences of box and MoG filters are highly correlated

To determine the effect of approximating MoG filters with box-shaped filters, first equivalent MoG filters were identified that matched box filters of a given modality and peak-to-peak width. Then, response maps were computed for each filter (see preceding paragraph 'Parameter sweep'), from which the song feature preferences were determined (Figure B.2*A*). For each song intensity contrast, the correlation of song preferences of the MoG filters and the box filters was determined (Figure B.2*B*). Across all contrasts, the song feature preferences were highly correlated, which justifies the simplifying assumption of box-shaped filters (Figure B.2*C*).

B.2.2 Correlation of song preferences for different nonlinearities depends on song contrast

The song-recognition model in Chapter 8 was based on an exponential nonlinearity that transformed the filtered sound input to spike rate. Most of

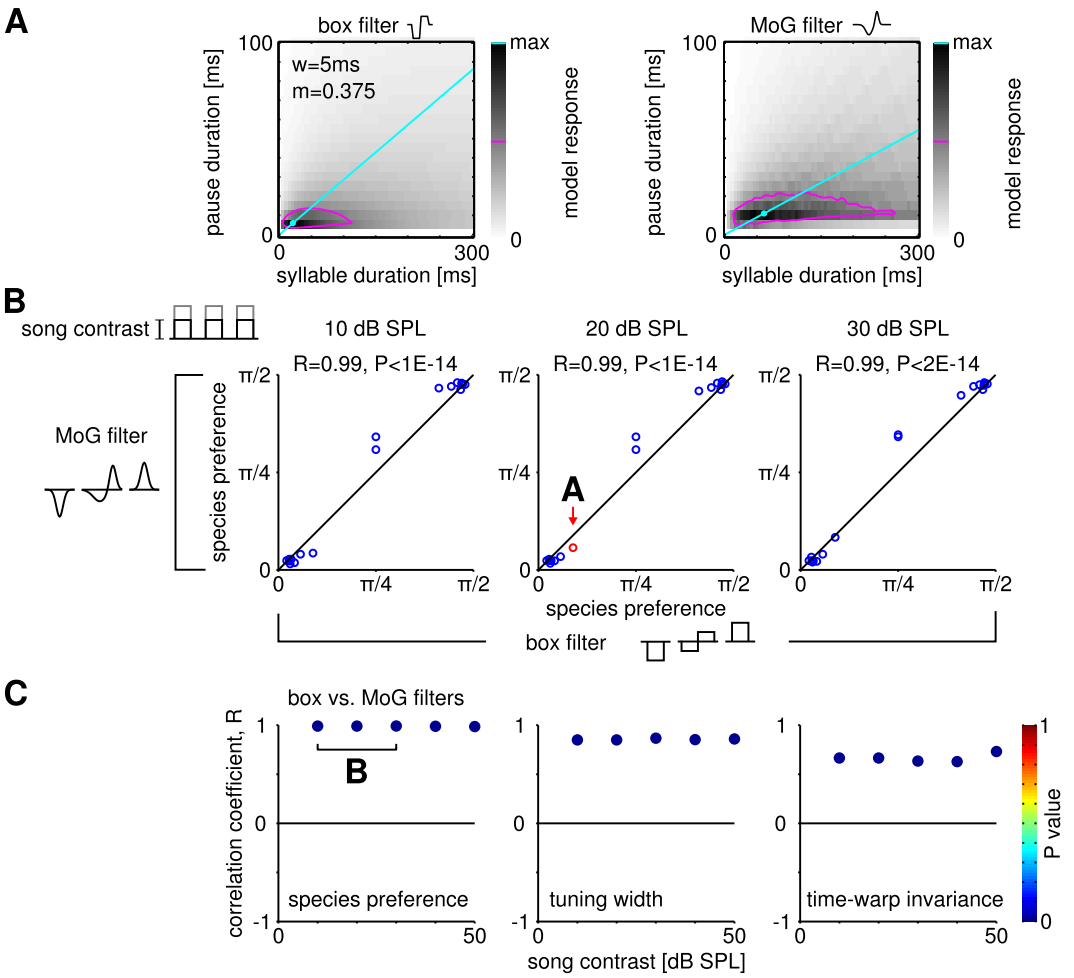

Figure B.2 Song feature preferences of box and MoG filters are highly correlated. **A:** Model responses to artificial song of various contrasts were created using box-shaped filters on the one hand, and MoG filters on the other hand. Here, the same exponential nonlinearity was used to compute the song feature preferences for both filter types. Filter width and modality were varied but matched for the two filter types to create summary statistics. From each pair of maps, song feature preference was assessed, as described in Figure 8.2. For each song contrast, the correlation between song preference measures for the two filter types was computed. **B:** Correlation of the species preference for the two filter types, for three different song contrasts; the red point corresponds to the example shown in panel *A*. **C:** All measures of song feature preference were highly correlated between the two filter types.

the experimentally measured nonlinearities in Chapter 7 were monotonically increasing over most of the considered input interval. However, for large inputs, an exponential nonlinearity is unrealistic. To assess the effect of approximating more biologically plausible types of nonlinearities with an exponential nonlinearity, song feature preferences of different filters were computed analogously to the approach described in the previous paragraph, this time using a fixed RoG or sigmoidal nonlinearity on the one hand, and the corresponding fitted exponential on the other hand (Figure B.3*A*).

While tuning width and time-warp invariance were highly correlated between the two nonlinearity types for all song contrasts, the correlation of the species preference between the two nonlinearity types decreased and ultimately became decorrelated or anticorrelated for song contrasts above 40 dB SPL (Figure B.3*B*,*C*)[3]. This was expected: while for sufficiently high song contrast a large input to the exponential nonlinearity produces a large output, the same input to the RoG or sigmoidal nonlinearity produces a small output. Therefore, at sufficiently high song contrast, the optimal input to the RoG nonlinearity is an *imperfect* match of filter and stimulus[4], while the optimal input to the exponential nonlinearity is a *perfect* match of filter and stimulus.

The majority of measured RoG nonlinearities was monotonically increasing for almost the entire input interval, which also explains the high quality of the exponential fits (cf. Figure 7.4). This justifies the simplifying assumption of an exponential nonlinearity for sound intensities and nonlinearity rise constants close to those used and measured in the experiments. Since the experiments were performed using a single mean and standard deviation of the sound intensity, further experiments are required to test whether the auditory system adapts the rise constant of the nonlinearity to changes in the mean sound intensity. This would provide a means of robust song recognition across sound levels, as discussed in Chapter 8.

[3] Recall that the standard deviation of the Gaussian sound intensity distribution used in the experiments was 6 dB SPL. Hence, more than 99.7% of the sound intensities were within ±18 dB SPL around the mean. Therefore, the sound intensity contrast that the auditory system was exposed to was well below 40 dB SPL for most of the stimulus duration.

[4] Recall that the input to the nonlinearity is the filtered stimulus. Hence, a large input to the nonlinearity is achieved for stimuli that match the filter shape.

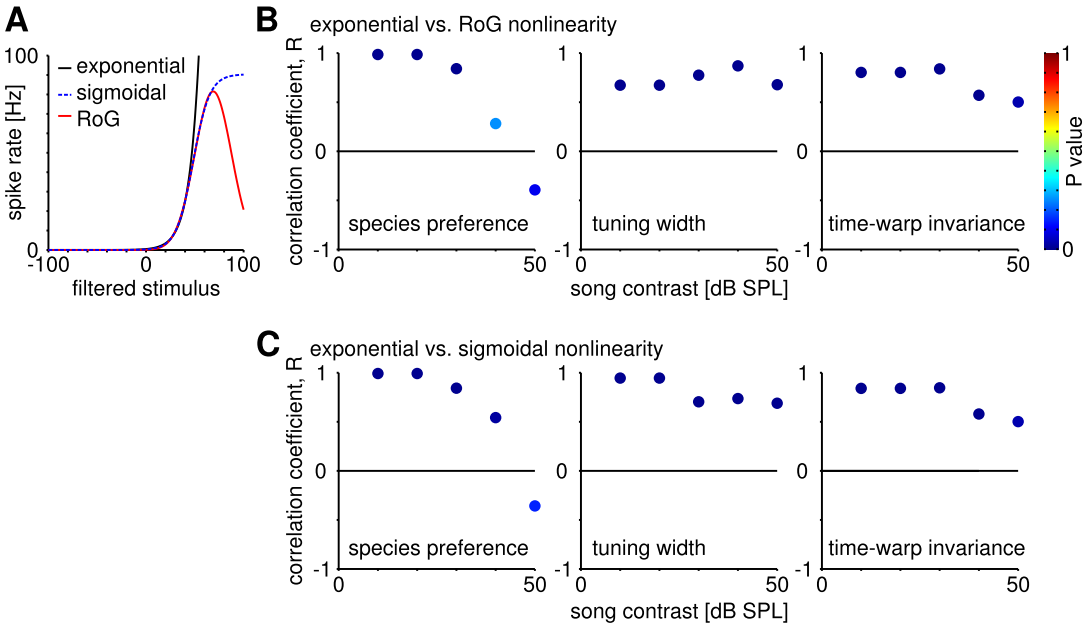

Figure B.3 Realistic nonlinearities can be approximated by a matching exponential nonlinearity. **A:** Model response maps for artificial song of various contrasts were created using an exponential nonlinearity with rise constant $\tilde{c} = 10$ and offset $x_0 = 7$ on the one hand and a matched RoG or sigmoidal nonlinearity on the other hand. Here, the same MoG filters were used to compute the song preference for the three nonlinearity types. Filter width and modality were varied to create summary statistics, as in Figure B.2. **B, C:** Measures of song preference obtained with the exponential nonlinearity were most correlated with those obtained using one of the two alternative nonlinearity types for song contrasts close to, or below, the sound amplitudes present in the stimuli used for filter estimation.

B.3 The model captures song preferences of sympatric grasshopper species

For the three sympatric grasshopper species *Chorthippus brunneus*, *Ch. biguttulus*, and *Ch. mollis*, evidence has been found for separated time scales of song preference (von Helversen and von Helversen, 1994, cf. Figure 2.1*D*). Due to the close relation of these species, they are likely to share neural hardware to some extent. Therefore we asked whether a separation of preference time scales is possible in the song-recognition model. Apart from the cited figure no data were available for quantitative fits of the model parameters to the behavioral maps. Hence, we merely resorted to a fast fit by eye, for a proof of concept.

Indeed, a full separation of preference time scales was feasible in the song-recognition model, purely based on differences in filter width, modality, and the relative song contrast (Figure B.4). Here, filter width was crucial for time scale separation, while filter modality and relative song contrast were mainly used to match behavioral data (cf. Figure 2.1*D*).

Concluding, if related grasshopper species share a neuronal implementation of the proposed song-recognition model, the development of distinct filter widths is sufficient to separate the time scales of song preference.

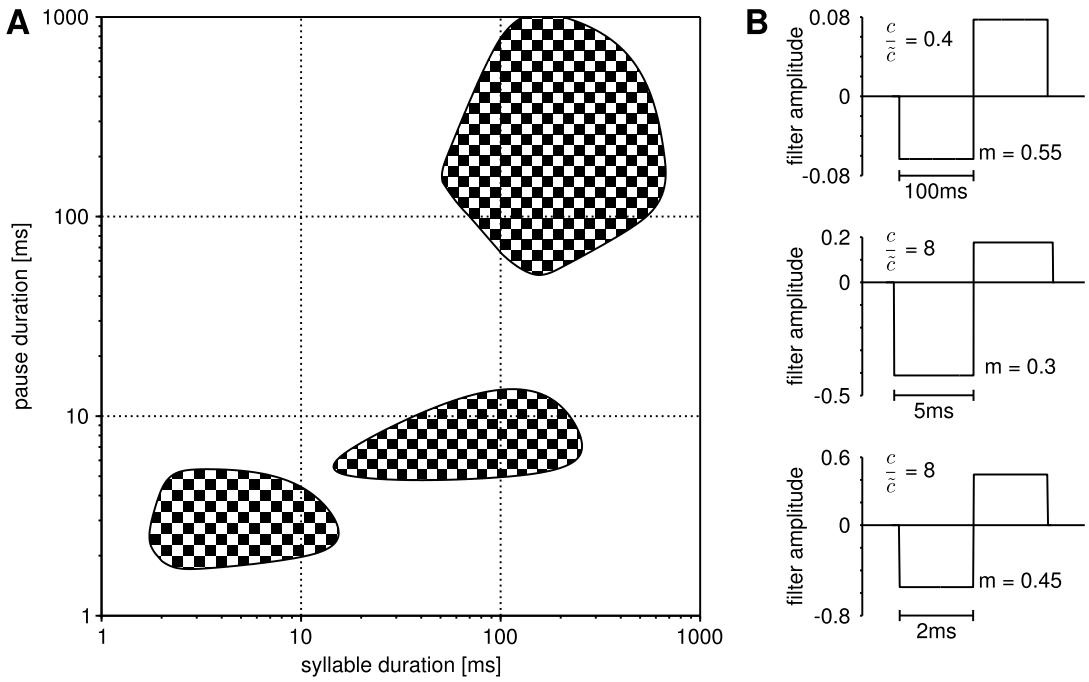

Figure B.4 Separate time scales of song preference in the song-recognition model. **A:** The song-recognition model reproduces song preferences of separated time scales as observed in the three sympatric grasshopper species *Chorthippus brunneus*, *Ch. biguttulus*, and *Ch. mollis* (cf. 2.1*D*). **B:** Distinct song preferences in *A* arose mainly due to differences in filter width (note the different time scales), while filter modality and relative song contrast ($\frac{c}{\hat{c}}$) were used for fine tuning of the shape of the response maps.

Acknowledgments

First and foremost I want to thank **Susanne Schreiber** for her generosity and support throughout the years, for giving me freedom to develop and trust, for asking constructive questions and reminding me of the big picture. I highly value the positive working environment you created, and am proud to be one of your first PhD students. Not unimportantly, I was quite happy to have a supervisor who shared that sweet tooth.

I probably would still confuse crickets with grasshoppers (let alone males with females) if **Bernd Ronacher** had not been my experimental supervisor. I greatly benefited from your scientific and supervisory experience, and in particular your open mind for computational and theoretical ideas. Many thanks for being a very laid-back collaborator and an impressive source of out-of-print or pre-digital papers.

Large parts of my research would not have been possible without the experimental work meticulously performed by **Monika Eberhard** and **Sarah Wirtssohn**. Thanks, not only for enjoyable and fruitful collaborations, but also for taking the time to explain your work to me. **Jan-Hendrik Schleimer**, you are incredible, both in terms of helpfulness and a very dry sense of humor. Thanks for information theory, filters, and hanging out in Cambridge.

I felt very lucky with all the wonderful colleagues at the **Institute for Theoretical Biology**, the **Bernstein Center for Computational Neuroscience**, in particular in the **Computational Neurophysiology** and **Behavioral Physiology** groups. I've had wonderful office mates, who were not only a great resource for answers to scientific questions, but fun to see every day: **Urs Bergmann**, **Susana Contreras**, **Owen Mackwood** (triangle choke!), **Pia Rose**, **Henning Sprekeler**, **DJ Sterling**, **Simon Weber**, **Katharina Wilmes**, **Wei Wu**, and **Ekaterina Zhuchkova**.

I am grateful for being a member of the graduate program **GRK 1589/1**, which is also due to all the great people involved, from my fellow **GRK students** (in particular **Sinem Balta**, **Jorge Jaramillo**, **Gundula Meckenhäuser** and her running group, and **Alex Susemihl**), to the PIs and admins. Special thanks to **Benjamin Lindner** and **Henning Sprekeler** for serving on my GRK committee, to **Felix**

Franke and **Robert Pröpper** for sharing their spike-sorting code, and to **Jan Clemens**, **Jonas Finck**, **Florian Rau** (my main man for design, and rheinischer Singsang), **Michael Reichert** and **Nicole Stange** for so many helpful grasshopper-related remarks and discussions.
Many thanks for the friendliest and most helpful administrative support, provided by **Vanessa Casagrande**, **Robert Martin**, **Margret Franke**, **Julia Schaeffer**, **Camilla Groiss**, **Elvira Lauterbach**, **Karin Winklhöfer**, and on the IT side by **Andreas Hantschmann**, **Tiziano Zito**, and **Rike-Benjamin Schuppner**.
I very much enjoyed developing projects for, and supervising students during, **Richard Kempter**'s Acquisition and Analysis of Neural Data course. Also, I thank **Benedikt Salmen** for the opportunity to develop Matlab tutorials for students of the Medical Neuroscience MSc program of the Charité.
Many inspiring scientific discussions shaped my way of thinking – thanks to **Jan Benda**, **Ronald Calabrese**, **Fabrizio Gabbiani**, **Matthias Hennig**, **Jannis Hildebrandt**, **James Hudspeth**, **Simon Laughlin**, **the Marder lab**, **Astrid Prinz**, **Silke Sachse**, **Inés Samengo**, and **Barbara Webb**.
I would like to express my gratitude to **Mala Murthy** for her hospitality, which allowed me to spend an extremely motivating time in her lab at the Princeton Neuroscience Institute. I am grateful to **Jan Clemens** and **Alexandria Hammons** for introducing me to experimental work with fruit flies.
Also, I felt very lucky to become a part of the **CAJAL course on Behaviour and Neural Systems** – those three weeks in Lisbon were outstandingly motivating for me. Special thanks to **Adam Kampff, Tania Li Chen, Benjamin de Bivort, Mason Klein**, and **Shuo Chen** – and all those superstitious flies.
I am grateful for having a wonderful family who supported me – thanks, in particular to **Mom**, **Christian and Estella**, with **Matteo, Isabella, and Cecilia**, **Margot and Uli**[1], **Christa and Uwe**. Also, I truly appreciate having amazing friends who were there when I needed them – **Stephan**, **Jon**, **Luisa**, **Lorenz**, **Michael**, **Arnulf**, **Michi**, **Gunnar**, **Otto**, and **Sebastian**. Extra thanks to **Arnulf**, **Eric**, **Flo**, **Jon**, **Jonas**, **Lorenz**, **Katha**, and **Uli** for proofreading parts of this thesis.
Words cannot express how thankful I am for going through all of this with **Anne** – thank you for every day together, for talking, problem solving, and being patient.
Last but not least, I gratefully acknowledge financial support from the following sources: **Deutsche Forschungsgemeinschaft** (SFB618, GRK1589/1), **German Federal Ministry of Education and Research** (01GQ1001A, 01GQ0901), **Organization for Computational Neuroscience**, the **Champalimaud Foundation**, **Federation of European Neuroscience Societies**, and the **HU-Princeton Strategic Partnership**.

[1] Mit Eurer Postkarte kam das *Ei*!

Bibliography

Abrams TW, Pearson KG (1982) Effects of temperature on identified central neurons that control jumping in the grasshopper. Journal of Neuroscience 2:1538–1553.

Alger BE, Nicoll RA (1982) Feed-forward dendritic inhibition in rat hippocampal pyramidal cells studied *in vitro*. Journal of Physiology 328:105–123.

Alle H, Roth A, Geiger JRP (2009) Energy-efficient action potentials in hippocampal mossy fibers. Science 325:1405–1408.

Allman JM (2000) Evolving brains. Scientific American Library New York.

Attwell D, Laughlin SB (2001) An energy budget for signaling in the grey matter of the brain. Journal of Cerebral Blood Flow and Metabolism 21:1133–1145.

Baccus SA, Meister M (2002) Fast and Slow Contrast Adaptation in Retinal Circuitry. Neuron 36:909–919.

Bada JL (2013) New insights into prebiotic chemistry from Stanley Miller's spark discharge experiments. Chemical Society Reviews 42:2186–2196.

Ball P (2015) H2O: A biography of water. Hachette UK.

Barclay J, Atwood H, Robertson M (2002) Impairment of central pattern generation in *Drosophila* cysteine string protein mutants. Journal of Comparative Physiology A 188:71–78.

Barr TCJ, Holsinger JR (1985) Speciation in cave faunas. Annual Review of Ecology and Systematics 16:313–337.

Benda J (2002) Single neuron dynamics. Ph.D. thesis, Humboldt-Universität zu Berlin, Mathematisch-Naturwissenschaftliche Fakultät I.

Benda J, Bethge M, Hennig M, Pawelzik K, Herz AVM (2001) Spike-frequency adaptation: Phenomenological model and experimental tests. Neurocomputing 38-40:105–110.

Benda J, Hennig RM (2008) Spike-frequency adaptation generates intensity invariance in a primary auditory interneuron. Journal of Computational Neuroscience 24:113–136.

Benda J, Herz AVM (2003) A universal model for spike-frequency adaptation. Neural Computation 15:2523–2564.

Bestmann H, Dippold K (1989) Temperature dependence of electrophysiological responses of lepidopteran antennae. Zeitschrift für Naturforschung C 44:333–344.

Bidau CJ (2014) Patterns in orthoptera biodiversity. I. Adaptations in ecological and evolutionary contexts. Journal of Insect Biodiversity 2:1–39.

Boulant JA, Dean JB (1986) Temperature receptors in the central nervous system. Annual Review of Physiology 48:639–654.

Boyan G, Ball E (1993) The grasshopper, *Drosophila* and neuronal homology (advantages of the insect nervous system for the neuroscientist). Progress in Neurobiology 41:657–682.

Bullock TH (1955) Compensation for Temperature in the Metabolism and Activity of Poikilotherms. Biological Reviews 30:311–342.

Burkhardt D (1959) Effect of temperature on isolated stretch-receptor organ of the crayfish. Science 129:392–393.

Burrows M (1989) Effects of temperature on a central synapse between identified motor neurons in the locust. Journal of Comparative Physiology A 165:687–695.

Carlson AD, Copeland J, Raderman R, Bulloch AGM (1976) Role of interflash intervals in a firefly courtship (*Photinus macdermotti*). Animal Behaviour 24:786–792.

Chander D, Chichilnisky EJ (2001) Adaptation to Temporal Contrast in Primate and Salamander Retina. Journal of Neuroscience 21:9904–9916.

Chichilnisky EJ (2001) A simple white noise analysis of neuronal light responses. Network: Computation in Neural Systems 12:199–213.

Choi JH, Jung HK, Kim T (2006) A new action potential detector using the mteo and its effects on spike sorting systems at low signal-to-noise ratios. IEEE Transactions on Biomedical Engineering 53:738–746.

Clemens J, Hennig RM (2013) Computational principles underlying the recognition of acoustic signals in insects. Journal of Computational Neuroscience 35:75–85.

Clemens J, Krämer S, Ronacher B (2014) Asymmetrical integration of sensory information during mating decisions in grasshoppers. Proceedings of the National Academy of Sciences 111:16562–16567.

Clemens J, Kutzki O, Ronacher B, Schreiber S, Wohlgemuth S (2011) Efficient transformation of an auditory population code in a small sensory system. Proceedings of the National Academy of Sciences 108:13812–13817.

Clemens J, Wohlgemuth S, Ronacher B (2012) Nonlinear computations underlying temporal and population sparseness in the auditory system of the grasshopper. Journal of Neuroscience 32:10053–10062.

Connor JA, Walter D, McKown R (1977) Neural repetitive firing: modifications of the Hodgkin-Huxley axon suggested by experimental results from crustacean axons. Biophysical Journal 18:81–102.

Coro F, Perez M (1990) Temperature affects auditory receptor response in an arctiid moth. Naturwissenschaften 77:445–447.

Creutzig F, Benda J, Wohlgemuth S, Stumpner A, Ronacher B, Herz AVM (2010) Timescale-invariant pattern recognition by feedforward inhibition and parallel signal processing. Neural Computation 22:1493–1510.

Creutzig F, Wohlgemuth S, Stumpner A, Benda J, Ronacher B, Herz AVM (2009) Timescale-invariant representation of acoustic communication signals by a bursting neuron. Journal of Neuroscience 29:2575–2580.

Crotty P, Sangrey T, Levy WB (2006) Metabolic energy cost of action potential velocity. Journal of Neurophysiology 96:1237–1246.

Culver DC, Pipan T (2009) The biology of caves and other subterranean habitats. Oxford University Press, USA.

Curras MC, Boulant JA (1989) Effects of ouabain on neuronal thermosensitivity in hypothalamic tissue slices. American Journal of Physiology 257:R21–28.

Curras MC, Kelso SR, Boulant JA (1991) Intracellular analysis of inherent and synaptic activity in hypothalamic thermosensitive neurones in the rat. Journal of Physiology 440:257–271.

Dahmen JC, Keating P, Nodal FR, Schulz AL, King AJ (2010) Adaptation to stimulus statistics in the perception and neural representation of auditory space. Neuron 66:937 – 948.

Dayan P, Abbott LF (2005) Theoretical neuroscience : computational and mathematical modeling of neural systems. Cambridge, MA: MIT Press.

Dodla R, Svirskis G, Rinzel J (2006) Well-Timed, Brief Inhibition Can Promote Spiking: Postinhibitory Facilitation. Journal of Neurophysiology 95:2664–2677.

Eberhard MJB, Schleimer JH, Schreiber S, Ronacher B (2015) A temperature rise reduces trial-to-trial variability of locust auditory neuron responses. Journal of Neurophysiology 114:1424–1437.

Elsner N (1974) Neuroethology of sound production in gomphocerine grasshoppers (Orthoptera: Acrididae). Journal of Comparative Physiology 88:67–102.

Ermentrout B (1996) Type I membranes, phase resetting curves, and synchrony. Neural Computation 8:979–1001.

Faber A (1932) Die Lautäußerungen der Orthopteren II.(Untersuchungen über die biozönotischen, tierpsychologischen und vergleichend-physiologischen Probleme der Orthopterenstridulation. Methodik der Bearbeitung und Auswertung von Stridulationsbeobachtungen. Einzeldarstellungen). Zeitschrift für Morphologie und Ökologie der Tiere 26:1–93.

Faber A (1953) Laut- und Gebärdensprache bei Insekten. Orthoptera (Geradflügler) I. Gesellschaft der Freunde und Mitarbeiter des Staatlichen Museums für Naturkunde in Stuttgart.

Falk G, Gerard RW (1954) Effect of micro-injected salts and ATP on the membrane potential and mechanical response of muscle. Journal of Cellular and Comparative Physiology 43:393–403.

Fenton MB, Faure PA, Ratcliffe JM (2012) Evolution of high duty cycle echolocation in bats. Journal of Experimental Biology 215:2935–2944.

Finck J, Kuntze J, Ronacher B (2016) Chemical cues from females trigger male courtship behaviour in grasshoppers. Journal of Comparative Physiology A pp. 1–9.

Fisch K, Schwalger T, Lindner B, Herz AVM, Benda J (2012) Channel noise from both slow adaptation currents and fast currents is required to explain spike-response variability in a sensory neuron. Journal of Neuroscience 32:17332–17344.

Franke F, Natora M, Boucsein C, Munk MHJ, Obermayer K (2010) An online spike detection and spike classification algorithm capable of instantaneous resolution of overlapping spikes. Journal of Computational Neuroscience 29:127–148.

Franz A, Ronacher B (2002) Temperature dependence of temporal resolution in an insect nervous system. Journal of Comparative Physiology A 188:261–271.

Franzke A, Reinhold K (2012) Limited condition dependence of male acoustic signals in the grasshopper *Chorthippus biguttulus*. Ecology and Evolution 2:1914–1921.

French AS, Kuster JE (1982) The effects of temperature on mechanotransduction in the cockroach tactile spine. Journal of Comparative Physiology A 147:251–258.

Friedel T, Barth FG (1995) The response of interneurons in the spider CNS (*Cupiennius salei* Keyserling) to vibratory courtship signals. Journal of Comparative Physiology A 177:159–171.

Gabbiani F, Krapp HG, Hatsopoulos N, Mo CH, Koch C, Laurent G (2004) Multiplication and stimulus invariance in a looming-sensitive neuron. Journal of Physiology-Paris 98:19–34.

Gabbiani F, Krapp HG, Laurent G (1999) Computation of object approach by a wide-field, motion-sensitive neuron. Journal of Neuroscience 19:1122–1141.

Galtier N, Tourasse N, Gouy M (1999) A Nonhyperthermophilic Common Ancestor to Extant Life Forms. Science 283:220–221.

Garrity PA, Goodman MB, Samuel AD, Sengupta P (2010) Running hot and cold: behavioral strategies, neural circuits, and the molecular machinery for thermotaxis in *C. elegans* and *Drosophila* 24:2365–2382.

Gerhardt HC, Doherty JA (1988) Acoustic communication in the gray treefrog, *Hyla versicolor*: evolutionary and neurobiological implications. Journal of Comparative Physiology A 162:261–278.

Gerhardt HC, Huber F (2002) Acoustic communication in insects and anurans: common problems and diverse solutions. University of Chicago Press.

Gollisch T (2008) Time-warp invariant pattern detection with bursting neurons. New Journal of Physics 10:015012.

Gollisch T, Herz AMV (2005) Disentangling sub-millisecond processes within an auditory transduction chain. PLoS Biology 3:e8.

Gollisch T, Schutze H, Benda J, Herz AVM (2002) Energy integration describes sound-intensity coding in an insect auditory system. Journal of Neuroscience 22:10434–10448.

Gray EG (1960) The fine structure of the insect ear. Philosophical Transactions of the Royal Society of London B 243:75–94.

Gütig R, Sompolinsky H (2009) Time-Warp–Invariant Neuronal Processing. PLoS Biology 7:e1000141.

Hallermann S, de Kock CPJ, Stuart GJ, Kole MHP (2012) State and location dependence of action potential metabolic cost in cortical pyramidal neurons. Nature Neuroscience 15:1007–1014.

Harris KD, Henze DA, Csicsvari J, Hirase H, Buzsáki G (2000) Accuracy of tetrode spike separation as determined by simultaneous intracellular and extracellular measurements. Journal of Neurophysiology 84:401–414.

Hartbauer M, Römer H (2014) From microseconds to seconds and minutes—time computation in insect hearing. Frontiers in Physiology 5.

Hasenstaub A, Otte S, Callaway E, Sejnowski TJ (2010) Metabolic cost as a unifying principle governing neuronal biophysics. Proceedings of the National Academy of Sciences 107:12329–12334.

Hastings JW, Sweeney BM (1957) On the mechanism of temperature independence in a biological clock. Proceedings of the National Academy of Sciences 43:804–811.

Hazel JR, Prosser CL (1974) Molecular mechanisms of temperature compensation in poikilotherms. Physiological Reviews 54:620–677.

Hennig R, Franz A, Stumpner A (2004) Processing of auditory information in insects. Microscopy Research and Technique 63:351–374.

Herz AVM, Gollisch T, Machens CK, Jaeger D (2006) Modeling Single-Neuron Dynamics and Computations: A Balance of Detail and Abstraction. Science 314:80–85.

Hildebrandt KJ (2010) Neural adaptation in the auditory pathway of crickets and grasshoppers. Ph.D. thesis, Humboldt-Universität zu Berlin, Mathematisch-Naturwissenschaftliche Fakultät I.

Hildebrandt KJ, Benda J, Hennig RM (2009) The Origin of Adaptation in the Auditory Pathway of Locusts Is Specific to Cell Type and Function. Journal of Neuroscience 29:2626–2636.

Hildebrandt KJ, Ronacher B, Hennig RM, Benda J (2015) A Neural Mechanism for Time-Window Separation Resolves Ambiguity of Adaptive Coding. PLoS Biology 13.

Hille B (2001) Ion channels of excitable membranes. Sinauer Sunderland, MA.

Hines ML, Carnevale NT (1997) The neuron simulation environment. Neural Computation 9:1179–1209.

Hodgkin AL, Huxley AF (1952) A quantitative description of membrane current and its application to conduction and excitation in nerve. Journal of Physiology 117:500–544.

Hopfield JJ, Brody CD (2000) What is a moment? "Cortical" sensory integration over a brief interval. Proceedings of the National Academy of Sciences 97:13919–13924.

Hopfield JJ, Brody CD (2001) What is a moment? Transient synchrony as a collective mechanism for spatiotemporal integration. Proceedings of the National Academy of Sciences 98:1282–1287.

Horwitz B, Friston K, Taylor J (2000) Neural modeling and functional brain imaging: an overview. Neural Networks 13:829 – 846.

Hubel DH, Wiesel TN (1959) Receptive fields of single neurones in the cat's striate cortex. Journal of Physiology 148:574–591.

Hubel DH, Wiesel TN (1962) Receptive fields, binocular interaction and functional architecture in the cat's visual cortex. Journal of Physiology 160:106–154.

Hudspeth AJ, Choe Y, Mehta AD, Martin P (2000) Putting ion channels to work: mechanoelectrical transduction, adaptation, and amplification by hair cells. Proceedings of the National Academy of Sciences 97:11765–11772.

Huey RB, Stevenson R (1979) Integrating thermal physiology and ecology of ectotherms: a discussion of approaches. American Zoologist 19:357–366.

Hunter I, Korenberg M (1986) The identification of nonlinear biological systems: Wiener and Hammerstein cascade models. Biological Cybernetics 55:135–144.

Hutchinson NA, Koles ZJ, Smith RS (1970) Conduction velocity in myelinated nerve fibres of *Xenopus laevis*. Journal of Physiology 208:279–289.

Izhikevich EM (2007) Dynamical systems in neuroscience: the geometry of excitability and bursting. Cambridge, MA: MIT Press.

Janssen R (1992) Thermal influences on nervous system function. Neuroscience and Biobehavioral Reviews 16:399–413.

Jones G (1999) Scaling of echolocation call parameters in bats. Journal of Experimental Biology 202:3359–3367.

Katz PS, Sakurai A, Clemens S, Davis D (2004) Cycle period of a network oscillator is independent of membrane potential and spiking activity in individual central pattern generator neurons. Journal of Neurophysiology 92:1904–1917.

Kim KJ, Rieke F (2001) Temporal Contrast Adaptation in the Input and Output Signals of Salamander Retinal Ganglion Cells. Journal of Neuroscience 21:287–299.

Kispersky TJ, Caplan JS, Marder E (2012) Increase in sodium conductance decreases firing rate and gain in model neurons. Journal of Neuroscience 32:10995–11004.

Klein M, Afonso B, Vonner AJ, Hernandez-Nunez L, Berck M, Tabone CJ, Kane EA, Pieribone VA, Nitabach MN, Cardona A, Zlatic M, Sprecher SG, Gershow M, Garrity PA, Samuel ADT (2015) Sensory determinants of behavioral dynamics in *Drosophila* thermotaxis. Proceedings of the National Academy of Sciences 112:E220–E229.

Koshland DE (2002) The Seven Pillars of Life. Science 295:2215–2216.

Kostal L, Lansky P, McDonnell MD (2013) Metabolic cost of neuronal information in an empirical stimulus-response model. Biological Cybernetics 107:355–365.

Kostarakos K, Hedwig B (2012) Calling Song Recognition in Female Crickets: Temporal Tuning of Identified Brain Neurons Matches Behavior. Journal of Neuroscience 32:9601–9612.

Krehl L, Soetbeer F (1899) Untersuchungen über die Wärmeökonomie der poikilothermen Wirbelthiere. Archiv für die gesamte Physiologie des Menschen und der Tiere 77:611–638.

Lang F (2000) Acoustic Communication Distances of a Gomphocerine Grasshopper. Bioacoustics 10:233–258.

Laughlin SB, de Ruyter van Steveninck RR, Anderson JC (1998) The metabolic cost of neural information. Nature Neuroscience 1:36–41.

Laughlin SB, Sejnowski TJ (2003) Communication in neuronal networks. Science 301:1870–1874.

Laurent G, Davidowitz H (1994) Encoding of Olfactory Information with Oscillating Neural Assemblies. Science 265:1872–1875.

LeBlanc J, Ward MO, Wittels N (1990) Exploring n-dimensional databases. In: Proceedings of the 1st conference on Visualization'90, pp. 230–237. IEEE Computer Society Press.

Lewicki MS (1998) A review of methods for spike sorting: the detection and classification of neural action potentials. Network: Computation in Neural Systems 9:R53–R78.

Lewis SM, Cratsley CK (2008) Flash Signal Evolution, Mate Choice, and Predation in Fireflies. Annual Review of Entomology 53:293–321.

Loher W (1957) Untersuchungen über den Aufbau und die Entstehung der Gesänge einiger Feldheuschreckenarten und den Einfluss von Lautzeichen auf das Akustische Verhalten. Zeitschrift für vergleichende Physiologie 39:313–356.

MacGregor R (2012) Neural and brain modeling. Elsevier.

Machens CK, Stemmler MB, Prinz P, Krahe R, Ronacher B, Herz AV (2001) Representation of acoustic communication signals by insect auditory receptor neurons. Journal of Neuroscience 21:3215–3227.

Marder E, Bucher D (2001) Central pattern generators and the control of rhythmic movements. Current Biology 11:R986–996.

Marquart V (1985) Local interneurons mediating excitation and inhibition onto ascending neurons in the auditory pathway of grasshoppers. Naturwissenschaften 72:42–44.

McFarland JM, Cui Y, Butts DA (2013) Inferring nonlinear neuronal computation based on physiologically plausible inputs. PLoS Computational Biology 9:e1003143.

McKay CP (2004) What Is Life — and How Do We Search for It in Other Worlds? PLoS Biology 2:e302.

Meier T, Reichert H (1995) The Nervous Systems of Invertebrates: An Evolutionary and Comparative Approach: With a Coda written by T.H. Bullock, chapter Developmental mechanisms, homology and evolution of the insect peripheral nervous system, pp. 249–271. Basel: Birkhäuser Basel.

Meyer J, Hedwig B (1995) The influence of tracheal pressure changes on the responses of the tympanal membrane and auditory receptors in the locust *Locusta migratoria* L. Journal of Experimental Biology 198:1327–1339.

Miles CI (1985) The effects of behaviourally relevant temperatures on mechanosensory neurones of the grasshopper, *Schistocerca americana*. Journal of Experimental Biology 116:121–139.

Mitchell M (1998) An introduction to genetic algorithms. MIT press Cambridge, MA.

Morris MD (1991) Factorial sampling plans for preliminary computational experiments. Technometrics 33:161–174.

Nagel KI, Doupe AJ (2006) Temporal processing and adaptation in the songbird auditory forebrain. Neuron 51:845–859.

Nagel KI, Wilson RI (2011) Biophysical mechanisms underlying olfactory receptor neuron dynamics. Nature Neuroscience 14:208–216.

Nattier R, Robillard T, Amedegnato C, Couloux A, Cruaud C, Desutter-Grandcolas L (2011) Evolution of acoustic communication in the Gomphocerinae (Orthoptera: Caelifera: Acrididae). Zoologica Scripta 40:479–497.

Neuhofer D, Wohlgemuth S, Stumpner A, Ronacher B (2008) Evolutionarily conserved coding properties of auditory neurons across grasshopper species. Proceedings of the Royal Society of London B 275:1965–1974.

Neuweiler G (1990) Auditory adaptations for prey capture in echolocating bats. Physiological Reviews 70:615–641.

Niven JE, Farris SM (2012) Miniaturization of nervous systems and neurons. Current Biology 22:R323–R329.

Niven JE, Laughlin SB (2008) Energy limitation as a selective pressure on the evolution of sensory systems. Journal of Experimental Biology 211:1792–1804.

Nolen TG, Hoy RR (1986) Phonotaxis in flying crickets. Journal of Comparative Physiology A 159:423–439.

Paninski L (2003) Convergence properties of three spike-triggered analysis techniques. Network 14:437–464.

Partridge LD, Connor JA (1978) A mechanism for minimizing temperature effects on repetitive firing frequency. American Journal of Physiology 234:C155–161.

Pearson KG, Heitler WJ, Steeves JD (1980) Triggering of locust jump by multimodal inhibitory interneurons. Journal of Neurophysiology 43:257–278.

Pearson KG, Reye DN, Parsons DW, Bicker G (1985) Flight-initiating interneurons in the locust. Journal of Neurophysiology 53:910–925.

Perdeck A (1958) The isolating value of specific song patterns in two sibling species of grasshoppers (*Chorthippus Brunneus* Thunb. and *C. Biguttulus* L.). Behaviour 12:1–75.

Perge JA, Niven JE, Mugnaini E, Balasubramanian V, Sterling P (2012) Why do axons differ in caliber? Journal of Neuroscience 32:626–638.

Peron S, Gabbiani F (2009) Spike frequency adaptation mediates looming stimulus selectivity in a collision-detecting neuron. Nature Neuroscience 12:318–326.

Petersen RS, Brambilla M, Bale MR, Alenda A, Panzeri S, Montemurro MA, Maravall M (2008) Diverse and Temporally Precise Kinetic Feature Selectivity in the VPm Thalamic Nucleus. Neuron 60:890–903.

Pettersen KH, Einevoll GT (2008) Amplitude variability and extracellular low-pass filtering of neuronal spikes. Biophysical journal 94:784–802.

Pfau HK, Koch UT, Möhl B (1989) Temperature dependence and response characteristics of the isolated wing hinge stretch receptor in the locust. Journal of Comparative Physiology A 165:247–252.

Pillow JW, Simoncelli EP (2006) Dimensionality reduction in neural models: an information-theoretic generalization of spike-triggered average and covariance analysis. Journal of Vision 6:414–428.

Pinault D (2011) Electrophysiological Recording Techniques, chapter The Juxtacellular Recording-Labeling Technique, pp. 41–75. Totowa, NJ: Humana Press.

Pires A, Hoy RR (1992) Temperature coupling in cricket acoustic communication. Journal of Comparative Physiology A 171:79–92.

Prinz AA, Abbott LF, Marder E (2004) The dynamic clamp comes of age. Trends in Neurosciences 27:218–224.

Prinz AA, Billimoria CP, Marder E (2003) Alternative to hand-tuning conductance-based models: Construction and analysis of databases of model neurons. Journal of Neurophysiology 90:3998–4015.

Pulver SR, Pashkovski SL, Hornstein NJ, Garrity PA, Griffith LC (2009) Temporal dynamics of neuronal activation by channelrhodopsin-2 and trpa1 determine behavioral output in drosophila larvae. Journal of Neurophysiology 101:3075–3088.

Rabinowitz N, Willmore B, Schnupp J, King A (2011) Contrast Gain Control in Auditory Cortex. Neuron 70:1178–1191.

Ragge DR (1986) The songs of the western european grasshoppers of the genus Omocestus in relation to their taxonomy (Orthoptera: Acrididae). Bulletin of The British Museum (Natural History) Entomology 53:213–249.

Ragge DR (1987) The songs of the western european grasshoppers of the genus Stenobothrus in relation to their taxonomy (Orthoptera: Acrididae). Bulletin of The British Museum (Natural History), Entomology 55:393–424.

Ramirez JM, Elsen FP, Robertson RM (1999) Long-term effects of prior heat shock on neuronal potassium currents recorded in a novel insect ganglion slice preparation. Journal of Neurophysiology 81:795–802.

Rau F, Clemens J, Naumov V, Hennig RM, Schreiber S (2015) Firing-rate resonances in the peripheral auditory system of the cricket, *Gryllus bimaculatus*. Journal of Comparative Physiology A 201:1075–1090.

Ritchie MG (1990) Are differences in song responsible for assortative mating between subspecies of the grasshopper *Chorthippus parallelus* (Orthoptera: Acrididae)? Animal Behaviour 39:685 – 691.

Robertson RM, Money TG (2012) Temperature and neuronal circuit function: compensation, tuning and tolerance. Current Opinion in Neurobiology 22:724–734.

Robertson RM, Pearson KG (1983) Interneurons in the flight system of the locust: Distribution, connections, and resetting properties. Journal of Comparative Neurology 215:33–50.

Roemschied FA, Eberhard MJ, Schleimer JH, Ronacher B, Schreiber S (2014) Cell-intrinsic mechanisms of temperature compensation in a grasshopper sensory receptor neuron. eLife 3:e02078.

Ronacher B, Franz A, Wohlgemuth S, Hennig RM (2004) Variability of spike trains and the processing of temporal patterns of acoustic signals-problems, constraints, and solutions. Journal of Comparative Physiology A 190:257–277.

Ronacher B, Stumpner A (1988) Filtering of behaviourally relevant temporal parameters of a grasshopper's song by an auditory interneuron. Journal of Comparative Physiology A 163:517–523.

Rothbart MM, Hennig RM (2012) Calling song signals and temporal preference functions in the cricket *Teleogryllus leo*. Journal of Comparative Physiology A 198:817–825.

Rothschild LJ, Mancinelli RL (2001) Life in extreme environments. Nature 409:1092–1101. 10.1038/35059215.

Ruoff P (1992) Introducing temperature-compensation in any reaction kinetic oscillator model. Journal of Interdisciplinary Cycle Research 23:92–99.

Rush ME, Rinzel J (1995) The potassium A-current, low firing rates and rebound excitation in Hodgkin-Huxley models. The Bulletin of Mathematical Biology 57:899–929.

Römer H, Marquart V, Hardt M (1988) Organization of a sensory neuropile in the auditory pathway of two groups of Orthoptera. Journal of Comparative Neurology 275:201–215.

Schmidt-Nielsen K (1997) Animal physiology: adaptation and environment. Cambridge, UK: Cambridge University Press.

Schöneich S, Kostarakos K, Hedwig B (2015) An auditory feature detection circuit for sound pattern recognition. Science Advances 1:e1500325.

Schreiber S, Fellous JM, Tiesinga P, Sejnowski TJ (2004) Influence of ionic conductances on spike timing reliability of cortical neurons for suprathreshold rhythmic inputs. Journal of Neurophysiology 91:194–205.

Schüch W, Barth FG (1990) Vibratory communication in a spider: female responses to synthetic male vibrations. Journal of Comparative Physiology A 166:817–826.

Schul J (1998) Song recognition by temporal cues in a group of closely related bushcricket species (genus *Tettigonia*). Journal of Comparative Physiology A 183:401–410.

Schwartz O, Pillow JW, Rust NC, Simoncelli EP (2006) Spike-triggered neural characterization. Journal of Vision 6:13.

Schwarz G (1978) Estimating the dimension of a model. The Annals of Statistics 6:461–464.

Sengupta B, Stemmler M, Laughlin SB, Niven JE (2010) Action potential energy efficiency varies among neuron types in vertebrates and invertebrates. PLoS Computational Biology 6:e1000840.

Shampine LF, Reichelt MW (1997) The MATLAB ODE suite. SIAM J Sci Comput 18:1–22.

Shimizu I, Barth FG (1996) The effect of temperature on the temporal structure of the vibratory courtship signals of a spider (*Cupiennius salei* Keys.). Journal of Comparative Physiology A 179:363–370.

Simmons P (1990) The effects of temperature on locust ocellar L-neurones and their interconnections. Journal of Comparative Physiology A 166:575–583.

Simoncelli EP, Paninski L, Pillow J, Schwartz O (2004) Characterization of neural responses with stochastic stimuli. The Cognitive Neurosciences 3:327–338.

Slee SJ, Higgs MH, Fairhall AL, Spain WJ (2010) Tonotopic tuning in a sound localization circuit. Journal of Neurophysiology 103:2857–2875.

Smirnakis SM, Berry MJ, Warland DK, Bialek W, Meister M (1997) Adaptation of retinal processing to image contrast and spatial scale. Nature 386:69–73.

Sokoliuk T, Stumpner A, Ronacher B (1989) GABA-like immunoreactivity suggests an inhibitory function of the thoracic low-frequency neuron (TN1) in acridid grasshoppers. Naturwissenschaften 76:223–225.

Stumpner A, Ronacher B (1991) Auditory interneurones in the metathoracic ganglion of the grasshopper *Chorthippus biguttulus*: I. morphological and physiological characterization. Journal of Experimental Biology 158:391–410.

Stumpner A, Ronacher B (1994) Neurophysiological aspects of song pattern recognition and sound localization in grasshoppers. American Zoologist 34:696–705.

Stumpner A, von Helversen D (2001) Evolution and function of auditory systems in insects. Naturwissenschaften 88:159–170.

Stumpner A, von Helversen O (1994) Song production and song recognition in a group of sibling grasshopper species (*Chorthippus dorsatus*, *Ch. dichorus* and *Ch. loratus*: *Orthoptera*, *Acrididae*). Bioacoustics 6:1–23.

Tang LS, Goeritz ML, Caplan JS, Taylor AL, Fisek M, Marder E (2010) Precise temperature compensation of phase in a rhythmic motor pattern. PLoS Biology 8:e1000469.

Tatler B, O'Carroll DC, Laughlin SB (2000) Temperature and the temporal resolving power of fly photoreceptors. Journal of Comparative Physiology A 186:399–407.

Taylor AL, Goaillard JM, Marder E (2009) How multiple conductances determine electrophysiological properties in a multicompartment model. Journal of Neuroscience 29:5573–5586.

Taylor AL, Hickey TJ, Prinz AA, Marder E (2006) Structure and visualization of high-dimensional conductance spaces. Journal of Neurophysiology 96:891–905.

Thompson S, Masukawa L, Prince D (1985) Temperature dependence of intrinsic membrane properties and synaptic potentials in hippocampal CA1 neurons *in vitro*. Journal of Neuroscience 5:817–824.

Traub RD, Wong RK, Miles R, Michelson H (1991) A model of a CA3 hippocampal pyramidal neuron incorporating voltage-clamp data on intrinsic conductances. Journal of Neurophysiology 66:635–650.

Venkatachalam K, Montell C (2007) TRP channels. Annual Review of Biochemistry 76:387.

Vogel A, Hennig RM, Ronacher B (2005) Increase of neuronal response variability at higher processing levels as revealed by simultaneous recordings. Journal of Neurophysiology 93:3548–3559.

Vogel A, Ronacher B (2007) Neural correlations increase between consecutive processing levels in the auditory system of locusts. Journal of Neurophysiology 97:3376–3385.

von Helversen D (1972) Gesang des Männchens und Lautschema des Weibchens bei der Feldheuschrecke *Chorthippus biguttulus* (Orthoptera, Acrididae). Journal of Comparative Physiology 81:381–422.

von Helversen D, von Helversen O (1983) Species recognition and acoustic localization in acridid grasshoppers: A behavioral approach. In: Neuroethology and Behavioral Physiology (Huber F, Markl H, eds.), pp. 95–107. Springer Berlin Heidelberg.

von Helversen D, von Helversen O (1997) Recognition of sex in the acoustic communication of the grasshopper *Chorthippus biguttulus* (Orthoptera, Acrididae). Journal of Comparative Physiology A 180:373–386.

von Helversen O, von Helversen D (1994) Forces driving coevolution of song and song recognition in grasshoppers. Fortschritte der Zoologie pp. 253–284.

Wark B, Lundstrom BN, Fairhall A (2007) Sensory adaptation. Current Opinion in Neurobiology 17:423–429.

Warzecha A, Horstmann W, Egelhaaf M (1999) Temperature-dependence of neuronal performance in the motion pathway of the blowfly *Calliphora erythrocephala*. Journal of Experimental Biology 202:3161–3170.

Wechselberger M, Wright CL, Bishop GA, Boulant JA (2006) Ionic channels and conductance-based models for hypothalamic neuronal thermosensitivity. American Journal of Physiology 291:R518–R529.

Wehr M, Laurent G (1996) Odour encoding by temporal sequences of firing in oscillating neural assemblies. Nature 384:162–166. 10.1038/384162a0.

Weschke G, Ronacher B (2007) Influence of sound pressure level on the processing of amplitude modulations by auditory neurons of the locust. Journal of Comparative Physiology A 194:255–265.

Wicher D, Walther C, Wicher C (2001) Non-synaptic ion channels in insects–basic properties of currents and their modulation in neurons and skeletal muscles. Progress in Neurobiology 64:431–525.

Wirtssohn SK (2015) Stimulus- and context-dependent temporal filtering in the auditory pathway of the locust. Ph.D. thesis, Humboldt-Universität zu Berlin, Lebenswissenschaftliche Fakultät.

Wohlgemuth S, Ronacher B (2007) Auditory discrimination of amplitude modulations based on metric distances of spike trains. Journal of Neurophysiology 97:3082–3092.

Wolf H (1986) Response patterns of two auditory interneurons in a freely moving grasshopper (*Chorthippus biguttulus* L.). Journal of Comparative Physiology A 158:689–696.

Xu GY, Winston JH, Shenoy M, Yin H, Pasricha PJ (2006) Enhanced excitability and suppression of A-type K^+ current of pancreas-specific afferent neurons in a rat model of chronic pancreatitis. American Journal of Physiology 291:G424–G431.

Xu H, Robertson RM (1996) Neural parameters contributing to temperature compensation in the flight CPG of the locust, *Locusta migratoria*. Brain Research 734:213–222.

Yu Y, Hill AP, McCormick DA (2012) Warm body temperature facilitates energy efficient cortical action potentials. PLoS Computational Biology 8:e1002456.